Title
Investigating the role of O-GlcNAcylation in regulating synaptic and cognitive decline with age

Author
Wheatley, Elizabeth Grace

Publication Date
2018

Peer reviewed|Thesis/dissertation

Investigating the role of O-GlcNAcylation in regulating synaptic and cognitive decline with age

by

Elizabeth G. Wheatley

DISSERTATION

Submitted in partial satisfaction of the requirements for the degree of

DOCTOR OF PHILOSOPHY

in

Developmental and Stem Cell Biology

in the

GRADUATE DIVISION

of the

UNIVERSITY OF CALIFORNIA, SAN FRANCISCO

[redacted]

Acknowledgements

I would like to thank my wonderful mentor Saul Villeda for always believing in me, and for teaching me how to be a great scientist. I thank him for giving me the opportunity to pursue aging research, for such meticulous and thorough graduate training, and for generously allowing me creative liberties in designing experiments. Most of all, I thank him for his sincere dedication to the happiness and well being of all of us in his lab. I have grown immensely in my time here at UCSF, and without his support and guidance none of that would have been possible.

I would also like to express my gratitude to the other members of my thesis committee, my chair Barbara Panning, Al Burlingame, and Dena Dubal, for their scientific expertise and support throughout the years. It has been a pleasure and an inspiration to work with a team of such well-rounded and brilliant scientists.

Without our collaborators, this project as a whole would not have been possible. I thank Al Burlingame and Jason Maynard for executing the essential proteomics arm of this project, and for being so dedicated and welcoming to all aspects of our collaboration. I also thank Jun Ding and Eddy Albarran for their enthusiasm to perform electrophysiological studies for us. Lastly, I thank Greg Bieri, who is without a doubt the resident troubleshooting and cloning expert for our lab. Without his expertise, many of the essential tools utilized within this study would not exist.

I have been incredibly fortunate to have worked in such an environment, filled with friends. I thank the members of the Villeda lab for constantly making me laugh, for always helping me, and for making the time we spent together so memorable both in and outside of lab. I thank all of my friends in my graduate program for being such a

wonderful group of people, and for so many priceless memories we've made together over the years. There are so many inspirational people I have met during my time in San Francisco, and I am grateful to know every single one of them.

Most of all, I would like to thank my family. I thank my grandparents, for working incredibly hard over the years to provide for the entire family. I thank Lucy and Bella, for offering me a constant stream of unconditional love and support. I thank my brother Ben, for providing inspiration, support, and advice, and for paving the way with his own victories in graduate school and beyond. Lastly, I thank my parents most of all, for always encouraging me and supporting my career path no matter what. I would not have been able to accomplish any of this without the love and dedication of my family.

Investigating the role of O-GlcNAcylation in regulating synaptic and cognitive decline with age

Elizabeth G. Wheatley

Abstract

Cognitive decline is emblematic of brain aging, ascribed in large part to age-related changes occurring at neuronal synapses. Dynamic post-translational protein modifications – in particular phosphorylation and O-GlcNAcylation – are known regulators of synaptic and cognitive function. However, how the landscape of synaptic PTMs changes with age has yet to be elucidated. In this study, age-dependent changes in phosphorylation and O-GlcNAcylation were characterized using a proteomics-based approach. Analyses implicate age-dependent changes in dynamic PTMs in age-related cognitive decline and vulnerability to neurodegenerative disorders, including Parkinson's and Alzheimer's disease. The functional relevance of age-related changes in PTMs, in particular of O-GlcNAcylation, was also investigated *in vivo*. Mimicking age-related decreased levels of neuronal O-GlcNAc recapitulated features of molecular, synaptic, and cognitive aging in mice, implicating that changes in O-GlcNAc promote brain dysfunction during aging. Moreover, increasing O-GlcNAcylation in the adult hippocampus enhanced cognition, proposing O-GlcNAc as a target for brain rejuvenation. Ultimately, this study proposes dynamic PTMs as novel molecular drivers of brain aging, and provides the foundation for future mechanistic studies to investigate site-specific molecular changes underlying synaptic and cognitive decline with age.

Table of Contents

List of Tables

Chapter 2

List of Figures

Chapter 1

Chapter 2

Chapter 3

Chapter 4

Chapter 1

Investigating neuronal, synaptic, and cognitive impairments in the aging hippocampus

Elizabeth G. Wheatley[1,2], Gregor Bieri[1,3], Saul A. Villeda[1,2,4]

1. Department of Anatomy, University of California San Francisco, San Francisco, California 94143, USA
2. Developmental and Stem Cell Biology Graduate Program, University of California San Francisco, San Francisco, California 94143, USA
3. Neuroscience IDP Program, Stanford University School of Medicine, Stanford, California 94305, USA
4. The Eli and Edythe Broad Center for Regeneration Medicine and Stem Cell Research, San Francisco, California 94143, USA

Author contributions:

E.G.W. and S.A.V. developed concept and designed experiments. E.G.W. collected and analyzed data. E.G.W. performed histological and biochemical studies. E.G.W. and S.A.V. performed cognitive studies. E.G.W. and G.B generated schematics. S.A.V supervised all aspects of this project.

Abstract

Aging elicits significant cognitive impairments governed by the brain region known as the hippocampus. The hippocampus is one of the most extensively characterized regions in the context of aging, due to the presence of stereotypic alterations that occur with age. In this study, molecular, synaptic, and cognitive aspects of hippocampal aging are characterized, in order to demonstrate the facilities, animals, and materials used within the larger scope of this project are suited to characterize the progression or reversal of hallmarks of brain aging.

Introduction

Cognitive impairment is one of the most widespread hallmarks of human aging. Adults over 65 are now the fastest growing age group [1], and as such, it comes as no surprise that incidences of aging-associated impairments have increased dramatically in recent years. While severe forms of cognitive dysfunction like dementia commonly arise due to the onset of neurodegenerative disorders like Alzheimer's disease (AD), many healthy aging individuals still experience impairments in higher-order cognitive functions [2-4]. Among the most common are impairments in spatial and contextual memory, which are governed by a brain region called the hippocampus. Recent work in the scientific community has demonstrated that latent plasticity in the aged mammalian hippocampus can be targeted to reverse cognitive impairments, proposing that brain rejuvenation may be achievable in aging humans [5, 6]. In order to restore cognitive integrity in the elderly, however, it is necessary to further elucidate how the mechanisms that regulate cognition are altered during aging to promote impairments.

The use of model organisms has proven invaluable in the pursuit of mechanisms that regulate learning and memory. In the context of aging, cognitive impairments are conserved across species- ranging from rodents, to non-human primates, to humans. The rodent in particular is utilized extensively for investigating aging of the mammalian hippocampus, due to its adequately sophisticated brain and modest 2-year lifespan. Both the rat and mouse display impaired spatial learning and memory via the Morris and radial arm water mazes [7-9], and Barnes maze [10], and impaired contextual memory via the fear conditioning paradigm [11, 12]. In support of the relevance of these behavioral paradigms, elderly humans display impaired spatial learning and memory in

a virtual-reality based Morris water maze that is analogous to those observed in rodents when compared to young controls [13]. The mammalian hippocampus is a highly attractive platform for investigating the cellular and molecular mechanisms that govern aging and rejuvenation, given it displays such stereotypic impairments in cognition that are conserved between species.

Aging and the mammalian hippocampus

The hippocampus is a complex structure composed of functionally distinct subregions: the dentate gyrus (DG), CA1, CA2, CA3 and subiculum (Figure 1). Information processing in the hippocampus occurs through a mostly unidirectional pathway, via the tri-synaptic neuronal circuit. Projections from neurons in the entorhinal cortex (EC) connect to the DG via the perforant path, which in turn give rise to projections called mossy fibers, terminating within the DG and CA3. Fibers projecting from CA3, called Schaffer collateral projections, innervate the CA1, and the CA1 outputs to the subiculum and the EC [14]. The primary excitatory neurons within the DG and CA1/CA3 are granule cells and pyramidal cells, respectively, and their activity is tightly regulated by a heterogeneous population of inhibitory neurons. Hippocampal neurons also interact with glia cells, microglia (the resident macrophages of the brain) and the neurovasculature, resulting in a complex bi-directional regulation of cellular functionality.

The hippocampus as whole is a particularly sensitive brain region to the effects of aging. Although it was initially believed that age-related impairments in cognition were caused by widespread cell death, particularly the death of neurons, modern advances in post-mortem tissue processing have clarified there is no significant cell loss in the

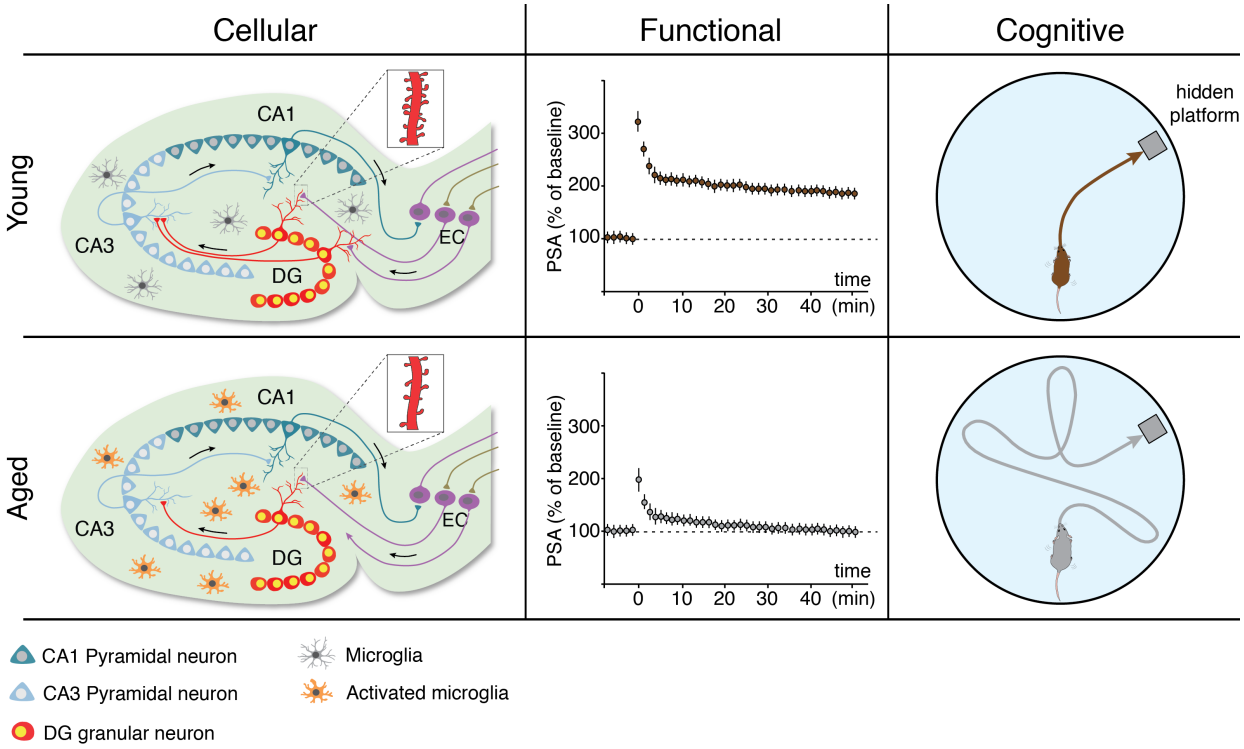

Figure 1. Hallmarks of hippocampal aging. Schematic illustration depicting alterations in cellular, functional and cognitive processes that occur with increased age in the adult hippocampal brain region. Cellular changes include decreased synaptic spine density on mature neurons, and increased microglial activation, resulting in impaired excitatory neuronal function and decreased cognitive capabilities, such as capacity for spatial learning and memory. Hippocampal sub-regions depicted are the CA1, CA3, dentate gyrus (DG), and entorhinal cortex (EC). Functional schematic depicts population spike amplitude (PSA) from electrophysiological recordings, and cognitive task depicted is the radial arm water maze. Schematic is adapted from Fan et al., *Annu Rev Neurosci*, 2017 Jul 25;40:251-272.

hippocampus of humans, non-human primates, or rodents [15, 16]. Despite this preservation of cell number, aging elicits significant changes in the structure and function of different cell types, especially neurons. Age-related structural changes are somewhat subtle in hippocampal neurons, and are primarily localized to neuronal synapses [17, 18]. In particular, aging elicits changes in synaptic composition, reduced synaptic density, and impaired synaptic plasticity [19-21]- the activity-dependent change in the strength of synaptic connections between neurons. Alongside these cellular changes, electrophysiological recordings performed on excitatory neurons in the hippocampal circuitry reveal a reliable decline in excitatory synaptic function with age [22, 23]. Collectively, these cellular alterations and synaptic impairments manifest as declines in hippocampal-dependent cognition, such as impaired performance in a spatial memory task (summarized in Figure 1).

Although hallmarks of hippocampal aging have been well established by the field, the progression of cellular and cognitive phenotypes is impacted by variables such as rodent background strain, housing, diet, enrichment, and behavioral facility. It is of significant importance therefore to validate the development of stereotypic cellular and cognitive changes in the context of a cognitive aging study.

Results

In order to establish a valid reference point for characterizing hallmarks of hippocampal aging, molecular, structural, and cognitive changes were characterized in young (3 month old) and aged (18-20 month old) wild type C57BL/6 mice.

The gross architecture of the aging hippocampus was profiled using a Cresyl violet stain for Nissl bodies, which are granules of rough endoplasmic reticulum enriched in neurons. The mean intensity of Nissl body staining was measured as a gauge for widespread changes in neuronal cell number. Consistent with previous reports, no widespread cell loss was observed in the CA1 or DG sub-regions in aged versus young hippocampal sections (Figure 2A,B). Neuronal molecular hallmarks were then characterized using diaminobenzadine (DAB) immunohistochemical staining. Phosphorylation of the transcription factor Creb at site Ser133 (pCreb) promotes immediate early gene (IEG) expression, synaptic plasticity, and learning and memory [24]. Mean intensity of neuronal pCreb was quantified in young and aged hippocampal brain sections (Figure 2C,D). In addition, cFos, an IEG downstream of pCreb and a marker of neuronal activity [25], was characterized as well (Figure 2E,F). Consistent with independent reports of hippocampal aging [5, 6], neuronal pCreb and cFos-positive neurons both declined with age in the CA1 and DG sub-regions (Figure 2C-F).

Neuronal structural changes were then profiled using a Golgi stain, which labels the entire cell body, processes, and synaptic structures of individual sparsely distributed neurons. The post-synaptic structural components of neurons, called dendritic spines, can be readily quantified using Golgi staining. The density of tertiary dendritic spines (spines per μm) was quantified on both CA1 pyramidal and DG granular neurons, and an age-dependent decrease in neuronal spine density was observed in both hippocampal sub-regions (Figure 3A,B).

Lastly, in a larger cohort of young and aged mice, two forms of hippocampal-dependent cognition were characterized. Spatial learning and memory was assessed by

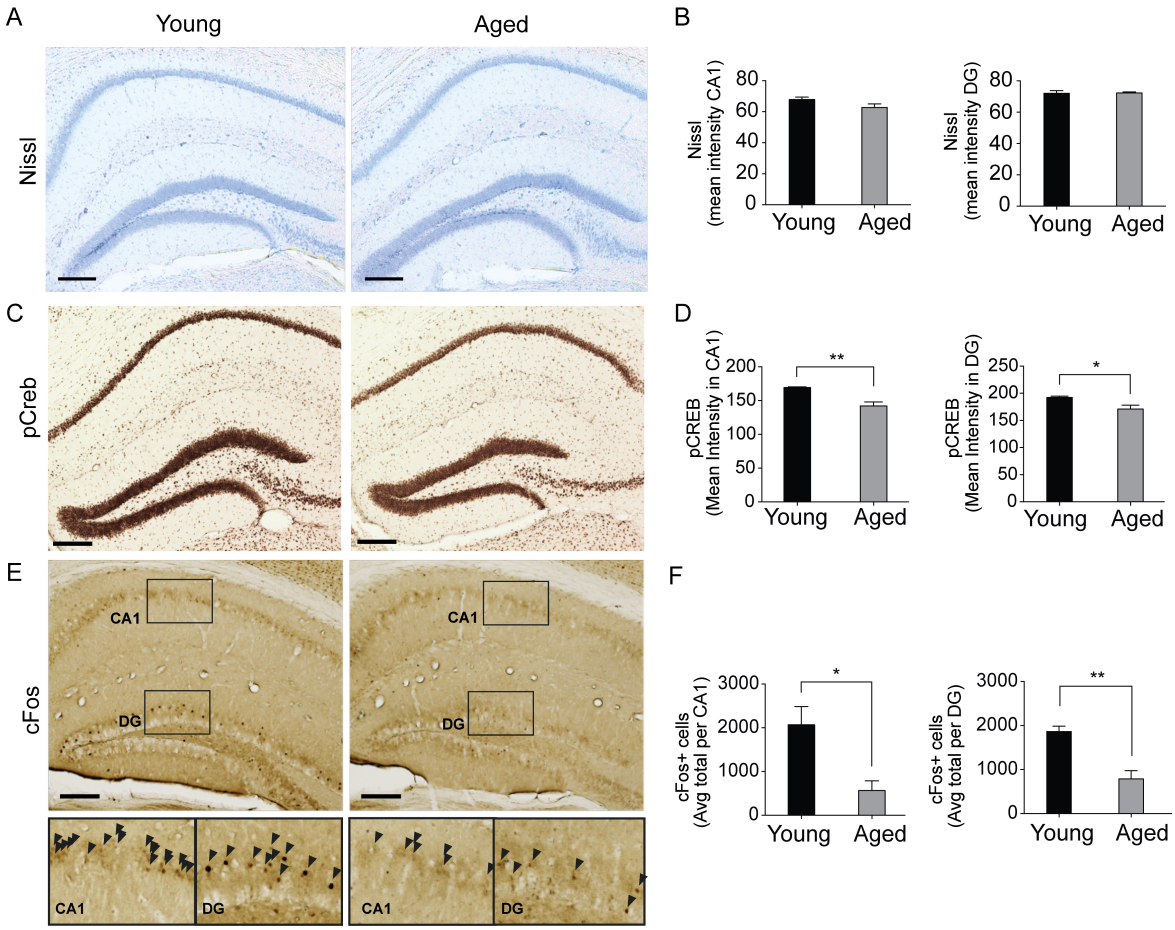

Figure 2. Hippocampal aging elicits a decline in neuronal activity but no widespread cell loss. (A) Representative field of Nissl stain in the hippocampus of young (3 month old) and aged (18 month old) mice, with quantification of mean intensity in DG and CA1 regions shown in (B). (C) Representative field of pCreb immunostain in young and aged mice with quantification of mean intensity in DG and CA1 regions shown in (D). (E) Representative field of cFos immunostain in young and aged mice with quantification of cFos-positive cells in the DG or CA1 region shown in (F). Data represented as mean ± SEM *P<0.05; **P<0.01; t-test (B,D,F). Scale bars = 200 μm, *n* = 3 mice per group.

the radial arm water maze (RAWM) (Figure 4A,B), and contextual memory was assessed using the fear-conditioning paradigm (Figure 4F). Results from RAWM revealed that while young and aged mice are able to learn the task at a similar rate during the training phase (Figure 4C), aged mice exhibit a modest impairment in short-term spatial memory (Figure 4D), and significant impairments in longer-term spatial memory (Figure 4C,E). Results from the fear conditioning behavioral paradigm revealed that while young and aged mice exhibit no differences in baseline freezing, aged mice freeze less during the contextual testing phase, confirming an impairment in hippocampal memory (Figure 4G). Additionally, no difference was observed in cued freezing behavior between young and aged mice (Figure 4G). Cued fear memory is more strongly dependent on a brain region called the amygdala, which is less sensitive to the effects of aging [11, 17].

Discussion

Characteristic hallmarks of aging were profiled in cohorts of young and aged wild type mice in-house, in order to elucidate the timeframe under which housing and handling would permit aging-related impairments. Consistent with previous reports, aging did not drive significant neuronal cell loss in the hippocampus, but did elicit reduced pCreb and c-Fos expression, two molecular changes associated with impaired synaptic plasticity. Consistent with this finding, aging elicited a reduction in dendritic spine density in CA1 pyramidal and DG granular neurons of the hippocampus, suggesting fewer synaptic connections exist in the circuitry of the aged hippocampus. Synaptic signaling is essential for regulating learning and memory, and impairments in plasticity and structure are highly suggestive of cognitive impairments. Indeed, aged mice demonstrated

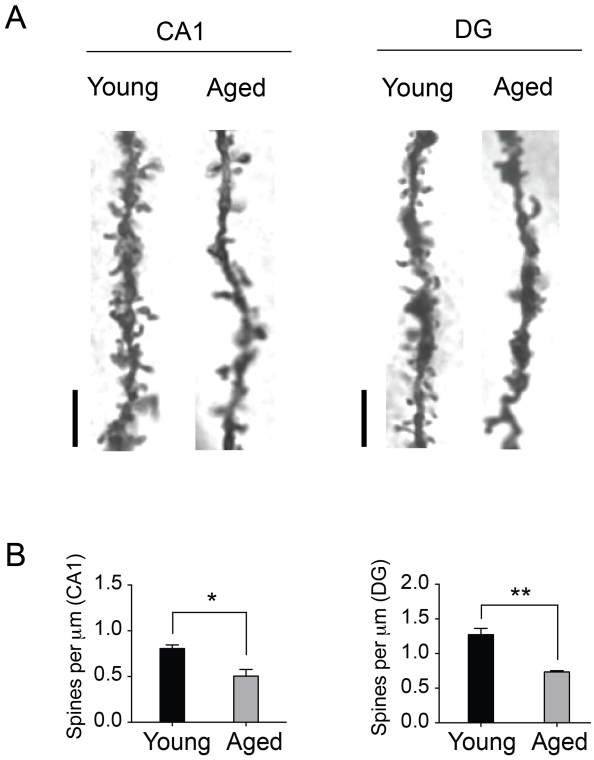

Figure 3. Aging elicits a reduction in hippocampal neuron dendritic spine density. (A) Representative field of Golgi stain from DG granule cell neurons and CA1 pyramidal neurons in young (3 month old) versus aged (24 month old) mice. (B) Quantification of spine number from tertiary dendrites of DG granule cell neurons or CA1 pyramidal neurons in young or aged mice; 4 neurons were quantified per sub-region, per mouse; *n* = 4 mice per group. Data represented as mean ± SEM *P<0.05; **P<0.01; t-test.

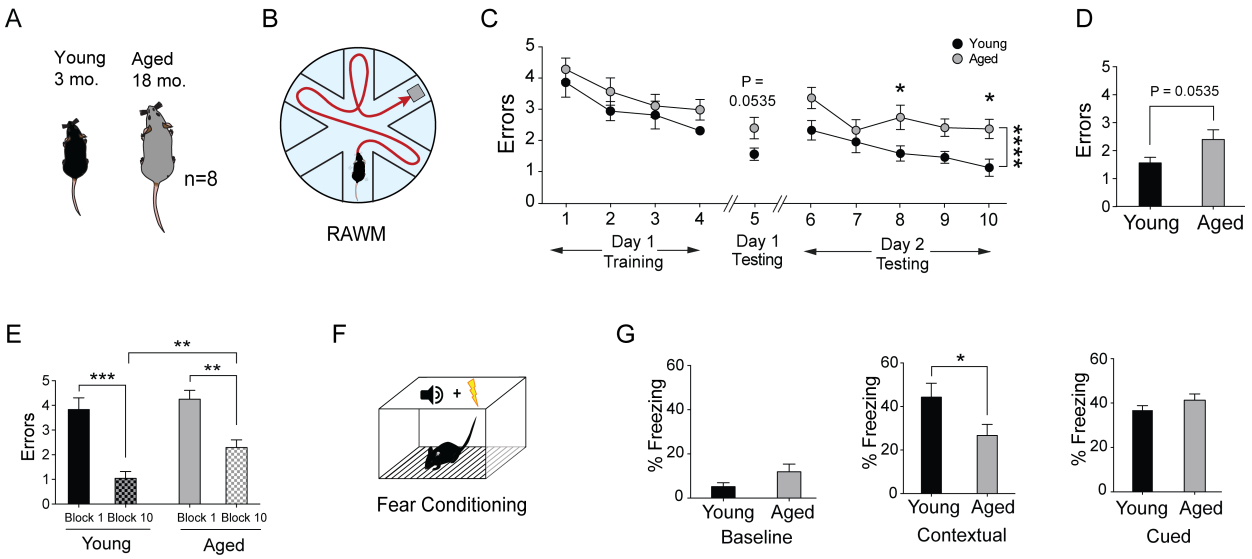

Figure 4. Aging elicits impairments in hippocampal-dependent spatial and contextual memory. (A) Hippocampal-dependent learning and memory was assessed in young (3 month old) and aged (18–20 month old) mice using two independent paradigms. (B) Radial arm water maze (RAWM) was used to assess spatial learning and memory. (C-E) Quantification of the number of entry errors during RAWM training and testing, (D) short-term memory testing, and (E) long-term learning and memory testing. (F) Fear conditioning was used to assess contextual fear memory. (G) Baseline, hippocampal-dependent contextual, and amygdala-dependent cued freezing behavior was quantified in young and aged mice using FreezeScan software. *n* = 8 mice per group. Data represented as mean ± SEM; *P<0.05; **P<0.01; ***P<0.001; repeated measures ANOVA, Bonferroni post-hoc test (C); t-test (D,E,G).

impairments, specifically in hippocampal-dependent spatial and contextual memory when compared to young controls. Collectively, these data establish a reference point for hippocampal aging and support the validity of the techniques and paradigms utilized within the present studies.

Materials and Methods

Animal Models. All mouse handling and use was in accordance with institutional and ethical guidelines approved by the University of California San Francisco IACUC. The following mouse lines were used: C57BL/6 young mice (The Jackson Laboratory), C57BL/6 young and aged mice (National Institutes of Aging; Taconic Biosciences). All studies were done in male mice. The numbers of mice used to result in statistically significant differences were calculated using standard power calculations with $\alpha = 0.05$ and a power of 0.8. We used an online tool (http://www.stat.uiowa.edu/~rlenth/Power/index.html) to calculate power and samples size based on experience with the respective tests, variability of the assays and inter-individual differences within groups. Mice were housed under specific pathogen-free conditions under a 12 h light-dark cycle. All experiments were randomized and blinded by an independent researcher. Researchers remained blinded throughout histological, molecular, and behavioral assessments. Groups were un-blinded at the end of each experiment upon statistical analysis.

Nissl Staining. Sections were cut to 40µm and mounted on superfrost plus microscope slides (ThermoFisher) and allowed to dry overnight. Slides were then soaked in 100% ethanol 3x2min each, and then immersed in cresyl violet working solution for 10 min. Slides were then dipped in 95% ethanol, soaked in 100% ethanol 2x2min, then in Citrasolv 2x2min before being cover slipped with Entellan. Mean intensity was quantified using FIJI software (Version 1.0).

Immunohistochemistry. Tissue processing and immunohistochemistry was performed on free-floating sections following standard published techniques [26]. Mice were anesthetized with ketamine, transcardially perfused with 0.9% saline, and brains removed and fixed in phosphate-buffered 4% paraformaldehyde for 48h before cryoprotection with 30% sucrose. Free floating coronal sections (40 µm) were incubated overnight with either rabbit anti-phospho-Creb (Ser133) (1:2,500; CST) or rabbit anti-c-Fos (Ab-5) (4-17) (1:10,000; Calbiochem) primary antibodies, and staining was revealed using biotinylated secondary antibodies and the ABC kit (Vector) with Diaminobenzidine (DAB, Sigma-Aldrich). Sections were mounted in phosphate buffer on superfrost plus microscope slides (ThermoFisher), allowed to dry overnight, briefly soaked in Citrasolv and cover slipped with Entellan. Mean intensity for phospho-Creb and individual cell number for c-Fos were quantified using FIJI software (Version 1.0).

Golgi Staining. After brain removal, hemispheres were immersed in 10 ml of A+B solution from FD Rapid GolgiStain™ Kit, which was prepared 24 hours prior. Solution was then changed after the initial 12 hours, and left for 10 days at room temperature in the dark. Brains were then transferred to solution C, which was changed after the initial 24 hours, and then left for 3 days at room temperature in the dark. Brains were cut into 100 µm sections using a vibratome and were mounted onto slides coated with 0.3% gelatin in solution C. Slides were then air-dried for 24 hours in the dark. Slides were immersed into Milli-Q H_2O, 2 x 4 min with gentle shaking, then transferred to a developing solution (Solution D, E, and Milli-Q H_2O) for 10 min. Slides were then rinsed

2x4 min in Milli-Q H_2O, dehydrated through graded ethanol, immersed in Xylenes 3x4 min, and then coverslipped using Permount. All slides were then blinded and neurons imaged using a 63X oil immersion objective. Tertiary dendritic spine density was quantified using FIJI software (Version 1.0) for dendritic tracing and spine count, and results were un-blinded just prior to statistical analyses.

Radial Arm Water Maze. Paradigm followed previously described protocol [27]. The goal arm location containing a platform remains constant throughout the training and testing phase, while the start arm is changed during each trial. Entry into an incorrect arm is scored as an error, and errors are averaged over training blocks (three consecutive trials). On day one during the training phase, mice are trained for 15 trials, with trials alternating between a visible and hidden platform. Every 3 trials are counted as one block of training. Prior to the final 3 trials of day 1 (block 5), the mice are given an extended break, and short-term memory is then tested using three consecutive hidden platform trials. On subsequent days during the testing phase, mice are tested for 15 trials per day with a hidden platform. All behavior is performed double blinded.

Contextual Fear Conditioning. Paradigm follows previously published techniques [28]. Mice learned to associate the environmental context (fear conditioning chamber) with an aversive stimulus (mild foot shock; unconditioned stimulus, US) enabling testing for hippocampal-dependent contextual fear conditioning. The mild foot shock was paired with a light and tone cue (conditioned stimulus, CS) in order to also assess amygdala-dependent cued fear conditioning. Conditioned fear was displayed as freezing behavior.

Specific training parameters are as follows: tone duration is 30 seconds; level is 70 dB, 2 kHz; shock duration is 2 seconds; intensity is 0.6 mA. On day 1 each mouse was placed in a fear-conditioning chamber and allowed to explore for 2 minutes before delivery of a 30-second tone (70 dB) ending with a 2-second foot shock (0.6mA). Two minutes later, a second CS-US pair was delivered. On day 2 each mouse was first place in the fear- conditioning chamber containing the same exact context, but with no administration of a CS or foot shock. Freezing was analyzed for 1-3 minutes. One hour later, the mice were placed in a new context containing a different odor, cleaning solution, floor texture, chamber walls and shape. Animals were allowed to explore for 2 minutes before being re-exposed to the CS. Freezing was analyzed for 1-3 minutes. Freezing was measured using a FreezeScan video tracking system and software (Cleversys, Inc). All behavior is performed double blinded.

Data and statistical analysis. Graphed data are expressed as mean ± SEM. Statistical analysis was performed with Prism 5.0 software (GraphPad Software). Means between two groups were compared with two-tailed, unpaired Student's t-test. Comparisons of means from multiple groups with each other or against one control group were analyzed with 2-way ANOVA and Bonferroni post hoc tests. All histology, electrophysiology and behavior experiments conducted were done in a randomized and blinded fashion. For each experiment, the overall size of the experimental groups corresponded to distinct animals. Unique samples were not measured repeatedly within the same characterization of a given cohort.

References

1. Klenk, J., et al., *Changes in life expectancy 1950-2010: contributions from age- and disease-specific mortality in selected countries.* Popul Health Metr, 2016. **14**: p. 20.
2. Hedden, T. and J.D. Gabrieli, *Insights into the ageing mind: a view from cognitive neuroscience.* Nat Rev Neurosci, 2004. **5**(2): p. 87-96.
3. Hertzog, C., et al., *Latent change models of adult cognition: are changes in processing speed and working memory associated with changes in episodic memory?* Psychol Aging, 2003. **18**(4): p. 755-69.
4. Oberauer, K., M. Wendland, and R. Kliegl, *Age differences in working memory--the roles of storage and selective access.* Mem Cognit, 2003. **31**(4): p. 563-9.
5. Villeda, S.A., et al., *Young blood reverses age-related impairments in cognitive function and synaptic plasticity in mice.* Nat Med, 2014.
6. Pigino, G., et al., *Disruption of fast axonal transport is a pathogenic mechanism for intraneuronal amyloid beta.* Proc Natl Acad Sci U S A, 2009. **106**(14): p. 5907-12.
7. Gallagher, M., R. Burwell, and M. Burchinal, *Severity of spatial learning impairment in aging: development of a learning index for performance in the Morris water maze.* Behav Neurosci, 1993. **107**(4): p. 618-26.
8. de Fiebre, N.C., et al., *Spatial learning and psychomotor performance of C57BL/6 mice: age sensitivity and reliability of individual differences.* Age (Dordr), 2006. **28**(3): p. 235-53.

9. Villeda, S.A., et al., *The ageing systemic milieu negatively regulates neurogenesis and cognitive function.* Nature, 2011. **477**(7362): p. 90-4.

10. Lee, G., et al., *Casein kinase II-mediated phosphorylation regulates alpha-synuclein/synphilin-1 interaction and inclusion body formation.* J Biol Chem, 2004. **279**(8): p. 6834-9.

11. Moyer, J.R., Jr. and T.H. Brown, *Impaired trace and contextual fear conditioning in aged rats.* Behav Neurosci, 2006. **120**(3): p. 612-24.

12. Kaczorowski, C.C. and J.F. Disterhoft, *Memory deficits are associated with impaired ability to modulate neuronal excitability in middle-aged mice.* Learn Mem, 2009. **16**(6): p. 362-6.

13. Driscoll, I., et al., *The aging hippocampus: cognitive, biochemical and structural findings.* Cereb Cortex, 2003. **13**(12): p. 1344-51.

14. Pei, J.J., et al., *Distribution of active glycogen synthase kinase 3beta (GSK-3beta) in brains staged for Alzheimer disease neurofibrillary changes.* J Neuropathol Exp Neurol, 1999. **58**(9): p. 1010-9.

15. West, M.J., et al., *Differences in the pattern of hippocampal neuronal loss in normal ageing and Alzheimer's disease.* Lancet, 1994. **344**(8925): p. 769-72.

16. Rapp, P.R. and M. Gallagher, *Preserved neuron number in the hippocampus of aged rats with spatial learning deficits.* Proc Natl Acad Sci U S A, 1996. **93**(18): p. 9926-30.

17. von Bohlen und Halbach, O., et al., *Age-related alterations in hippocampal spines and deficiencies in spatial memory in mice.* J Neurosci Res, 2006. **83**(4): p. 525-31.

18. Nicholson, D.A., et al., *Reduction in size of perforated postsynaptic densities in hippocampal axospinous synapses and age-related spatial learning impairments.* J Neurosci, 2004. **24**(35): p. 7648-53.

19. Sato, Y., et al., *Comparison of hippocampal synaptosome proteins in young-adult and aged rats.* Neurosci Lett, 2005. **382**(1-2): p. 22-6.

20. Geinisman, Y., *Structural synaptic modifications associated with hippocampal LTP and behavioral learning.* Cereb Cortex, 2000. **10**(10): p. 952-62.

21. Geinisman, Y., L. de Toledo-Morrell, and F. Morrell, *Loss of perforated synapses in the dentate gyrus: morphological substrate of memory deficit in aged rats.* Proc Natl Acad Sci U S A, 1986. **83**(9): p. 3027-31.

22. Barnes, C.A., G. Rao, and F.P. Houston, *LTP induction threshold change in old rats at the perforant path--granule cell synapse.* Neurobiol Aging, 2000. **21**(5): p. 613-20.

23. Rosenzweig, E.S. and C.A. Barnes, *Impact of aging on hippocampal function: plasticity, network dynamics, and cognition.* Prog Neurobiol, 2003. **69**(3): p. 143-79.

24. Sakamoto, K., K. Karelina, and K. Obrietan, *CREB: a multifaceted regulator of neuronal plasticity and protection.* J Neurochem, 2011. **116**(1): p. 1-9.

25. Pavlopoulos, E., et al., *Molecular mechanism for age-related memory loss: the histone-binding protein RbAp48.* Sci Transl Med, 2013. **5**(200): p. 200ra115.

26. Luo, J., et al., *Glia-dependent TGF-beta signaling, acting independently of the TH17 pathway, is critical for initiation of murine autoimmune encephalomyelitis.* J Clin Invest, 2007. **117**(11): p. 3306-15.

27. Alamed, J., et al., *Two-day radial-arm water maze learning and memory task; robust resolution of amyloid-related memory deficits in transgenic mice.* Nat Protoc, 2006. **1**(4): p. 1671-9.

28. Raber, J., et al., *Irradiation enhances hippocampus-dependent cognition in mice deficient in extracellular superoxide dismutase.* Hippocampus, 2011. **21**(1): p. 72-80.

Chapter 2

Proteomic analysis of the dynamic post-translational protein modifications phosphorylation and O-GlcNAcylation at the aging synapse

Elizabeth G. Wheatley[1,2], Jason C. Maynard[3], Shreya Chand[3], Alma L. Burlingame[3], Saul A. Villeda[1,2,4,5]

1. Department of Anatomy, University of California San Francisco, San Francisco, California 94143, USA
2. Developmental and Stem Cell Biology Graduate Program, University of California San Francisco, San Francisco, California 94143, USA
3. Mass Spectrometry Facility and Department of Pharmaceutical Chemistry, University of California, San Francisco, California 94158, USA
4. Department of Physical Therapy and Rehabilitation Science, University of California San Francisco, San Francisco, California 94143, USA
5. The Eli and Edythe Broad Center for Regeneration Medicine and Stem Cell Research, San Francisco, California 94143, USA

Author contributions:

E.G.W. and S.A.V. developed concept and designed experiments. E.G.W. collected and analyzed data. J.C.M, and S.C. performed mass spectrometry studies. J.C.M. and E.G.W. analyzed mass spectrometry results. E.G.W. performed histological and biochemical studies. A.L.B. provided scientific and technical expertise. E.G.W. generated schematics. S.A.V supervised all aspects of this project.

Abstract

Cognitive decline is a prominent hallmark of brain aging, attributed in large part to age-related changes at the neuronal synapse. Numerous synaptic properties are regulated by dynamic post-translational modifications (PTMs), like phosphorylation and O-GlcNAcylation. However how this landscape changes with age, and its functional significance, has yet to be elucidated. Here, a proteomics study describing the aging synaptic phosphoproteome and O-GlcNAcome is reported. These analyses highlight the relevance of this resource to age-related cognitive decline and vulnerability to neurodegenerative disorders, including Parkinson's and Alzheimer's diseases. Ultimately, these findings propose dynamic PTMs as novel molecular drivers of brain aging, and provide the foundation for future mechanistic studies to investigate site-specific molecular changes underlying synaptic and cognitive impairments during aging.

Introduction

It is a well-appreciated notion that communication between neurons is a fundamental component of learning and memory regulation [1]. Learning elicits lasting alterations in synaptic plasticity that involve a wide array of cellular changes, many of which are localized to the synapse itself. A neuronal synapse is the meeting point of the pre-synaptic terminal (axonal bouton) of one neuron, and the post-synaptic terminal (dendritic spine) of another neuron, across which a signal is transduced in response to a stimulus such as a learning event (Figure 1).

Signal transduction at synaptic connections is a complex and highly regulated process, initiated when an action potential reaches the axonal terminal and triggers sufficient influx of calcium into the cell. Pre-synaptic vesicles move from a reserve pool to a readily releasable pool, fuse with the pre-synaptic plasma membrane, and exocytose specialized molecules called neurotransmitters into the synaptic cleft. When glutamate, a major excitatory neurotransmitter of the central nervous system, crosses the synaptic cleft, it selectively binds to post-synaptic receptors such as N-methyl-D-aspartate receptor (NMDAR) and α-amino-3-hydroxy-5-methyl-4-isoxazolepropionic acid receptor (AMPAR). In addition to promoting the propagation of another action potential, activation of these post-synaptic receptors promotes numerous synaptic alterations, including trafficking of additional receptors to the cell surface, synaptic structural changes, and the activation of local signaling cascades (summarized in Figure 1). Neurons are each capable of forming thousands of synaptic connections with neighboring cells, establishing complex and highly organized neuronal networks, such as the tri-synaptic circuit in the hippocampus.

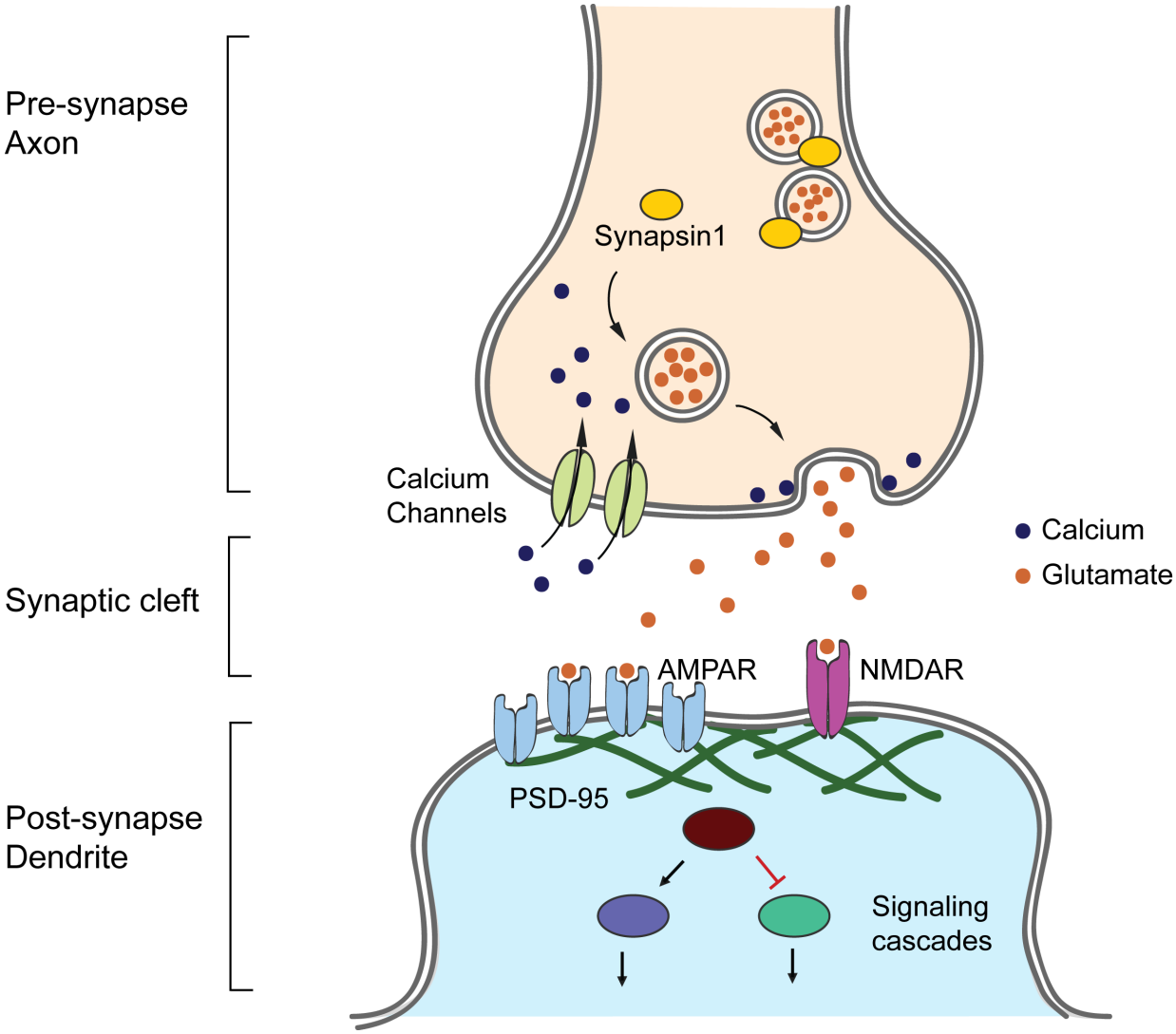

Figure 1. Schematic representation of a glutamatergic neuronal synapse. A Neuronal synapse is comprised of a pre-synaptic axonal terminal, a synaptic cleft, and a post-synaptic dendritic terminal. An action potential triggers calcium influx at the pre-synapse, which promotes the mobilization of pre-synaptic vesicles, a process that involves pre-synaptic vesicle regulating proteins like Synapsin1. Vesicles fuse with the membrane and exocytose neurotransmitters like glutamate into the synaptic cleft. Glutamate binds to post-synaptic receptors like AMPAR and NMDAR, which are tethered to the surface by scaffolding proteins like PSD-95. Binding of glutamate elicits numerous changes, including receptor trafficking to the surface, influx of ions into the post-synapse, structural changes, and the activation of local signaling cascades.

With age, a diverse array of synaptic features and functions are impacted. Calcium homeostasis is disrupted in excitatory neurons of the aged hippocampal circuit [2]. Glutamate receptor subunit expression profiles shift during aging, and there is a proposed decrease in receptor function and trafficking during aging as well [3-5]. Synaptic structure and density are negatively impacted in the aging hippocampus [6-8] (Chapter 1, Figure 3), and learning-induced synaptic remodeling is impaired in the prefrontal cortex as well [9]. At the molecular level, the composition of the synaptic protein fraction (synaptosome) has been characterized during aging using shotgun proteomics studies. These studies have characterized differential expression of pre-synaptic vesicle release proteins, signaling proteins mediating phosphatase activity, and cytoskeletal proteins involved in structural remodeling [10-12]. In addition, aging elicits reduced activity of kinases required for signaling cascades that promote plasticity [13, 14]. Collectively, this work demonstrates that extensive changes in synaptic features and functions have been characterized during aging. Despite these characterizations, however, the mechanisms that functionally regulate age-related synaptic and cognitive impairments have not been fully elucidated.

Dynamic post-translational modifications and synaptic function

Proteins at the pre- and post-synapse contain post-translational protein modifications (PTMs), in particular dynamic PTMs like phosphorylation and O-linked N-acetylglucosaminylation (O-GlcNAcylation) [15]. Phosphorylation involves the reversible addition of a phosphate molecule onto serine, threonine, or tyrosine residues of proteins. Phosphate modifications are added to proteins by enzymes called kinases,

and removed by enzymes called phosphatases, of which there are hundreds [16] (Figure 2A). O-GlcNAcylation is a uniquely dynamic form of glycosylation involving the addition of a single sugar molecule, GlcNAc, onto serine and threonine residues of proteins. Unlike phosphorylation, however, O-GlcNAcylation is added to proteins by a single enzyme, O-GlcNAc transferase (Ogt) and is removed by a single enzyme called O-GlcNAcase (Oga) (Figure 2B). Intriguingly, protein phosphorylation and O-GlcNAcylation regulate nearly every aspect of synaptic function, including features sensitive to aging like pre-synaptic vesicle dynamics, post-synaptic glutamate receptor trafficking, and structural remodeling [17-20].

In support of this, a collection of literature attributes roles for these dynamic PTMs in regulating aspects of synaptic function and aging. Biochemical analysis of hippocampal tissue from learning-impaired aged rats has linked decreased phosphorylation of the AMPA receptor subunit GluR1 to cognitive impairments [5]. Conversely, pharmacological activation of the kinases PKA and PKC, which employ phosphorylation to mediate excitatory synaptic function, rescues synaptic impairments in aged Aplysia neurons [14]. O-GlcNAcylation has recently been demonstrated to regulate excitatory synapse maturation [21] and synaptic plasticity [22]. More broadly, decreased neuronal O-GlcNAcylation levels have been implicated in neurodegeneration [23, 24], and dementia-related diseases of aging [23]. Although there are emerging roles for dynamic PTMs in conditions of age-related synaptic decline, how the landscape of dynamic PTMs changes with age at the synapse has never been characterized.

To address this gap in knowledge, a proteomics study employing isobaric labeling using tandem mass tagging followed by tandem mass spectrometry was performed. This

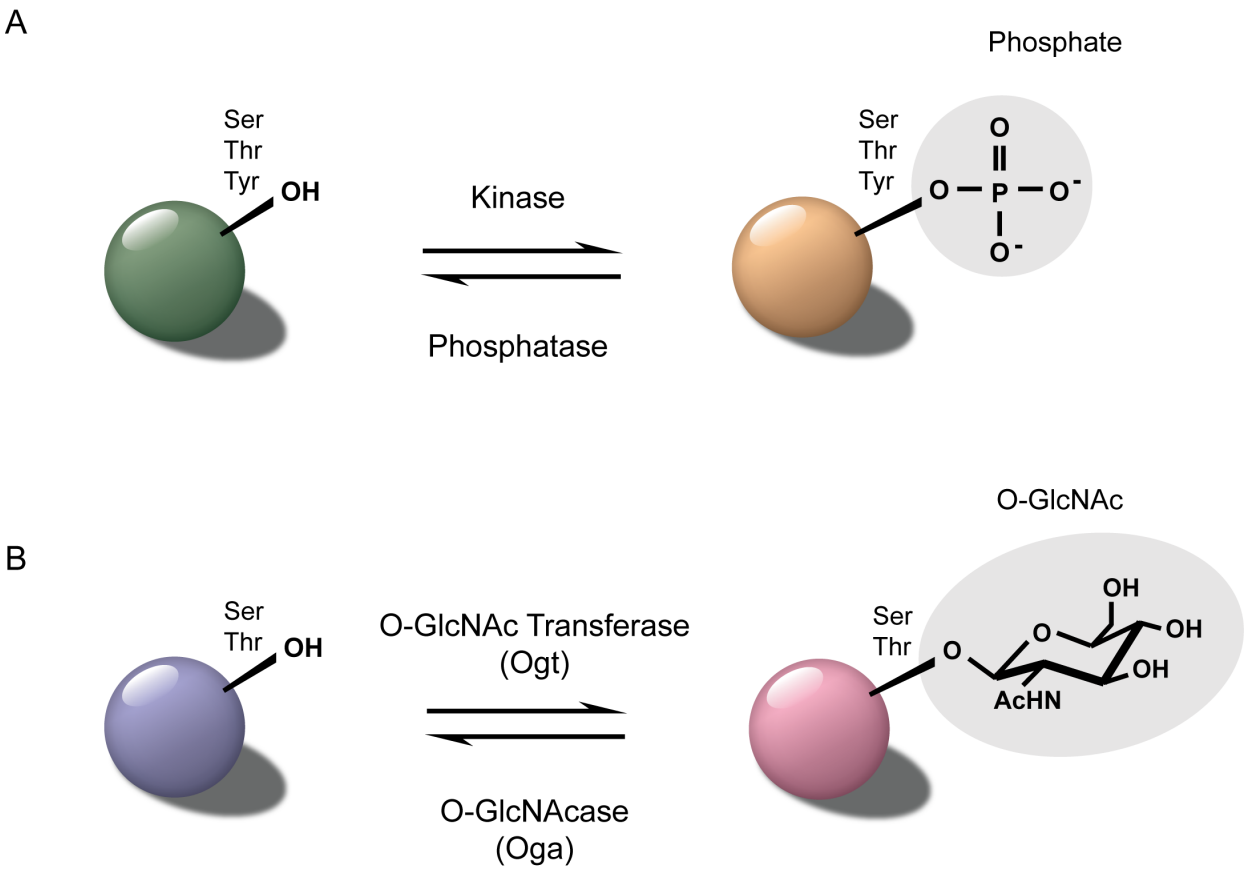

Figure 2. Phosphorylation and O-GlcNAcylation are dynamic reversible forms of post-translational protein modification. (A) Protein phosphorylation. Phosphate groups are added to the hydroxyl group on side chains of serine (Ser), threonine (Thr), or tyrosine (Tyr) amino acids by enzymes called kinases, and are removed by enzymes called phosphatases. (B) Protein O-GlcNAcylation. O-GlcNAc molecules are added to the hydroxyl group on side chains of serine (Ser), or threonine (Thr) amino acids by a single enzyme called Ogt, and removed by a single enzyme called Oga.

study provides the first relative quantitative assessment of site-specific synaptic PTMs in the young and aged mammalian synaptosome.

Results

Relative quantitation of dynamic PTM abundance on young and aged synaptic proteins using LC-MS/MS

To strike a balance between obtaining sufficient staring material, and profiling brain regions most relevant to age-related impairments, hippocampal and cortical tissues were sub-dissected and pooled from a cohort of either young (3 month old) or aged (18-20 month old) wild type mice (Figure 3A). Synaptosomes were isolated from fresh brain tissue using dounce homogenization, centrifugation, and separation on a sucrose gradient outlined in a previously published protocol [15] (Figure 3A). Western blot analysis was performed to confirm synaptosomes were free of gross contamination by nuclear markers Histone H3 and LaminB, and that they contained both pre- and post-synaptic fractions by measuring Synapsin1 and PSD-95 (Figure 3B). Synaptic proteins were then prepared for mass spectrometry analysis, by reducing and alkylating cysteine side chains, followed by a trypsin digest to generate peptides (Figure 3C).

Peptides from each replicate were then separated into O-GlcNAc modified, phosphorylated, and unmodified samples. O-GlcNAcylated peptides were enriched for using lectin weak affinity chromatography (LWAC), and flow through was collected for subsequent enrichment of phosphorylated peptides using a TiO_2–based approach (Figure 4A). Peptides were then isobarically labeled by using a 6-plex tandem mass

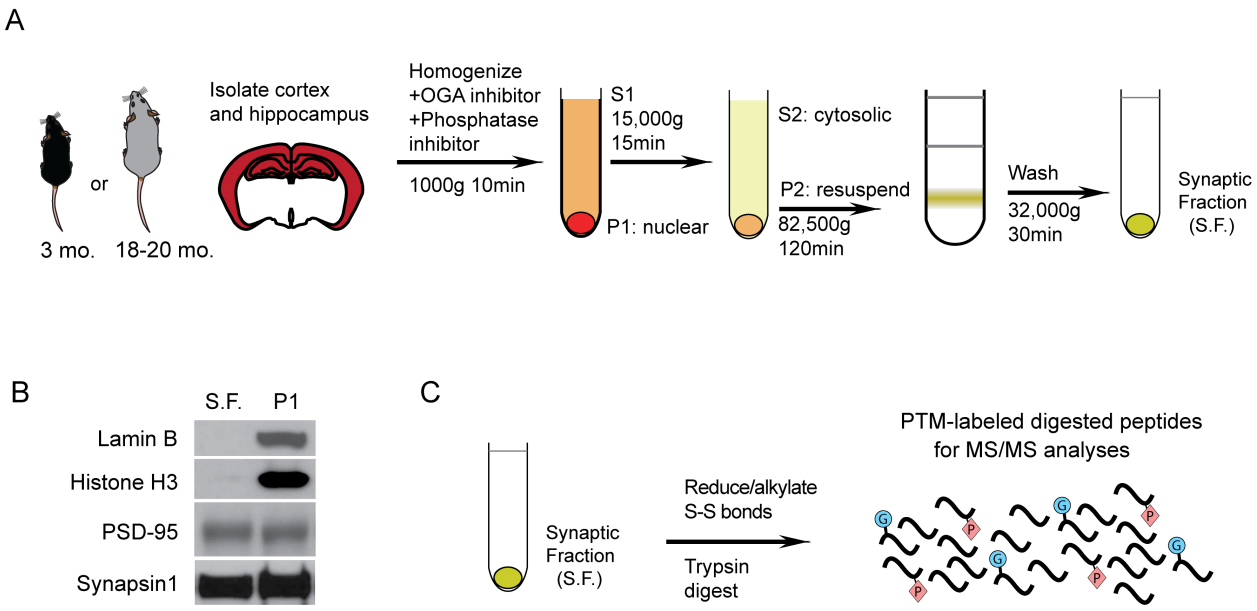

Figure 3. Schematic for isolation of synaptic fractions from young and aged mice. (A) Schematic depicting enrichment paradigm of synaptic fractions (synaptosomes) from hippocampal and cortical brain tissue of young (3 month old) and aged (18–20 month old) mice, *n* = 16–18 mice per age group. (B) Representative western blot analyses of synaptic (S.F.) and nuclear (P1) fractions, taken from a small aliquot of each sample. Lamin B and Histone H3 are nuclear markers, and PSD-95 and Synapsin1 are synaptic markers. (C) Proteins in synaptic fractions were prepared for mass spectrometry analyses by reduction and alkylation of cysteine side chain disulfide bonds, and trypsin digest to generate peptides.

tagging approach (TMT), such that distinct replicates from either age group were labeled with a tag containing a uniquely weighted balancer group (Figure 4B). Samples were then pooled together and profiled using a liquid chromatography tandem mass spectrometry (LC-MS/MS)-based approach. The relative abundance of dynamic PTMs were quantified using the peak intensities of the TMT fragment ions, and total protein abundance was also accounted for in order to specifically detect changes in PTM abundance above changes in protein expression. Higher energy collision dissociation (HCD) was employed for robust peptide identification and relative quantitation of TMT ions in all samples, as well as site-specific assignment of phosphorylation. O-GlcNAc is a particularly labile PTM and poses challenges for site-specific detection using HCD. Thus, to increase the resolution of O-GlcNAc site assignment electron-transfer dissociation (ETD) was also employed for O-GlcNAcylated peptides (Figure 4C).

A total of 3,276 proteins were detected in the synaptosome, of which 0.67% increased and 1.37% decreased in abundance with age. Gene ontology (GO) terms for all proteins detected in the synaptosome were assessed using the ConsensusPathDB platform [25]. Compared against the entire mouse genome, the synaptosome contained overrepresented processes, functions, cellular components, and pathways consistent with synaptic structure and function (Figure 5A-D), indicating the fractions analyzed were significantly enriched for synaptic components.

The overall distribution and abundance of phosphorylation and O-GlcNAcylation in the synaptosome was then assessed. A total of 7,621 unambiguous phosphorylation sites (phosphosites) were detected on 6,629 phosphorylated peptides (phosphopeptides) from

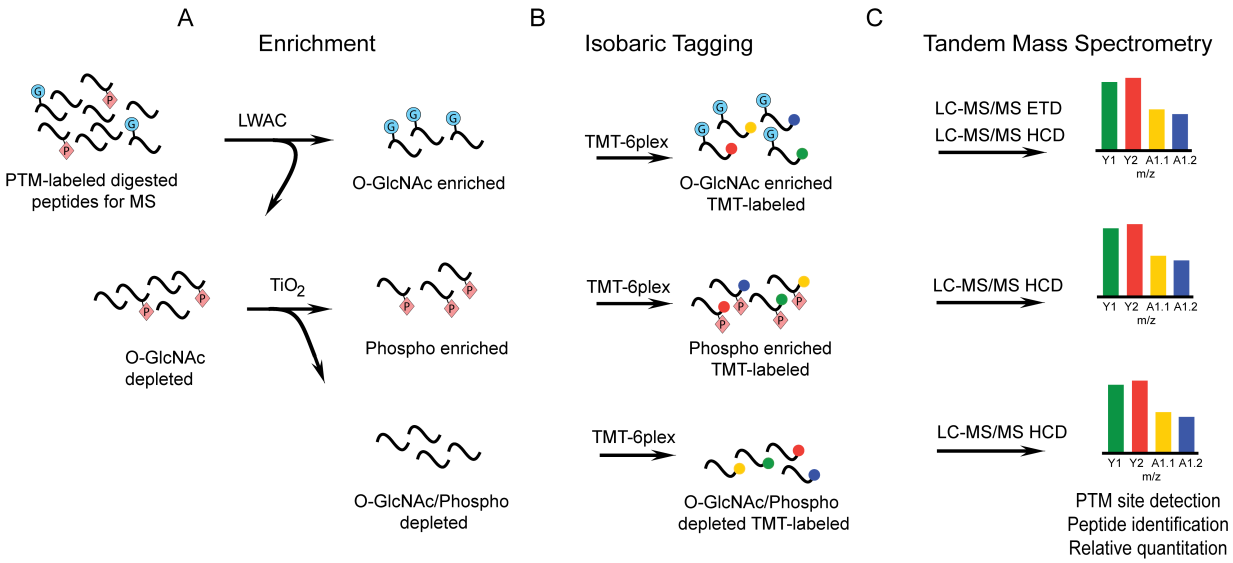

Figure 4. Tandem mass spectrometry-based characterization of age-related changes in synaptic phosphorylation and O-GlcNAcylation. Schematic depiction of liquid chromatography tandem mass spectrometry (LC-MS/MS) paradigm using to measure relative quantitative abundance of dynamic post-translational modifications (PTMs) in the aging synaptosome. (A) O-GlcNAcylated peptides were enriched for using lectin weak affinity chromatography (LWAC), and phosphorylated peptides enriched for using TiO_2–based treatment. (B) 6-plex tandem mass tagging (TMT) was employed to allow for relative quantitation of PTM abundance. (C) Site-specific O-GlcNAcylation was measured using electron-transfer dissociation (ETD). Site-specific phosphorylation, peptide identification, and relative quantitation of TMT ions was achieved using higher-energy collision dissociation (HCD).

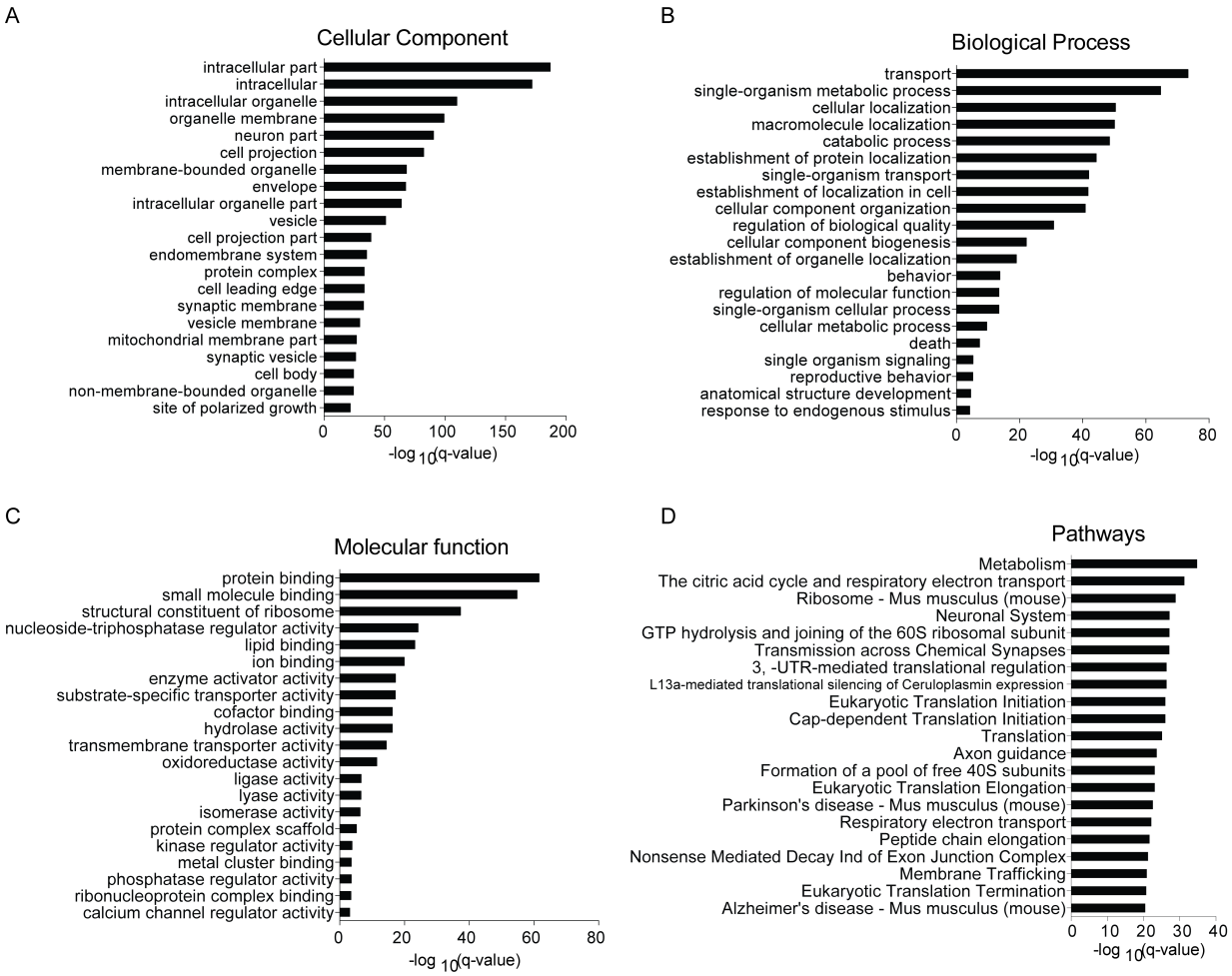

Figure 5. Gene Ontology Analyses of the Synaptosome. (A) Gene ontology (GO) cellular component overrepresentation analysis of all proteins detected in the synaptosome dataset. Calculations were done using ConsensusPathDB with the mouse genome as the reference dataset, using false discovery rate (FDR) correction and a cutoff of $P<0.01$. (B) GO biological process overrepresentation analysis performed as described in (A). (C) GO molecular function overrepresentation analysis performed as described in (A). (D) GO pathway overrepresentation analysis performed as described in (A).

1,978 distinct proteins (phosphoproteins) (Figure 6A). A total of 197 unambiguous O-GlcNAc sites were detected, on a total of 586 peptides from 175 proteins (Figure 6A). Additionally, 56.84% of all proteins were phosphorylated, 1.89% were O-GlcNAcylated, and 3.51% were both phosphorylated and O-GlcNAcylated (Figure 6B). These findings are within the normal range that has been reported for the relative abundance of phosphorylation versus O-GlcNAcylation [15].

Of proteins bearing unambiguous phosphorylation sites, 23.41% had increased phosphorylation, 28.97% had decreased phosphorylation, and 16.98% had two or more distinct sites that increased and decreased their phosphorylation with age (Figure 6B). Of proteins bearing O-GlcNAcylation sites, 12.00% had increased O-GlcNAcylation, 8.57% had decreased O-GlcNAcylation, and 1.14% had two or more distinct sites that increased and decreased their O-GlcNAcylation with age (Figure 6B). Together these initial analyses demonstrate that widespread and bi-directional alterations in phosphorylation and O-GlcNAcylation occur with age at the synapse.

Characterization of the aging synaptic phosphoproteome.

To begin the investigation of dynamic PTMs at the aging synapse, proteins with age-dependent changes in phosphorylation were characterized. Since protein phosphorylation can elicit activation, repression, or a host of other protein behaviors, both loss and gain of phosphorylation were considered important. Thus, all synaptic proteins upon which age-dependent changes in phosphorylation was detected were collectively termed: the aging synaptic phosphoproteome. More specifically, proteins with peptides containing up to two unambiguous phosphorylation sites that had an age–dependent

A

Species	Count
Proteins	3,276
Phosphoproteins	1,978
Phosphopeptides	6,629
Unambiguous Phosphosites	7,261
O-GlcNAcylated proteins	175
O-GlcNAcylated peptides	586
Unambiguous O-GlcNAc sites	197

B

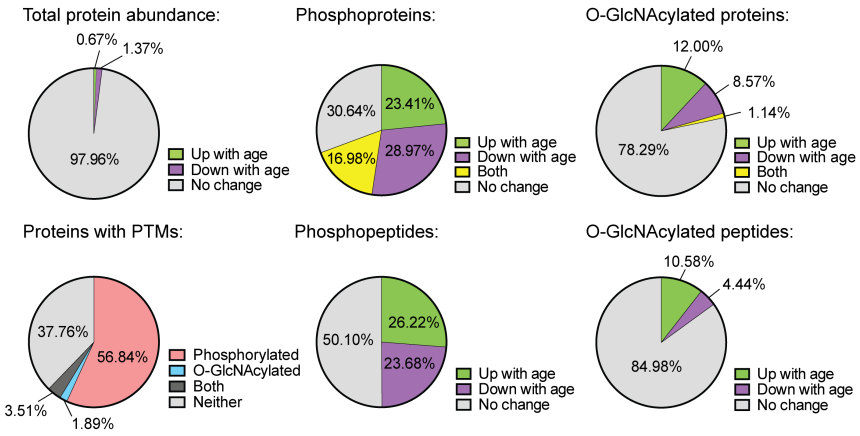

Figure 6. Summary of relative quantitative changes in the aging synaptic phosphoproteome and O-GlcNAcome. (A) Table depicting the total number of detected proteins, PTM-modified proteins, PTM-modified peptides, and unambiguous PTM sites in the synaptosome. (B) Pie charts representing changes in total protein abundance, the distribution of PTM modifications, and age-dependent changes in proteins and peptides with phosphorylation and O-GlcNAcylation.

change of at least 1.4-fold were included. A curated list of selected proteins, peptides, phosphorylation sites, and their direction and magnitude of change with age, is provided in Table 1.

Over 7,000 phosphorylation modifications were resolved to site-specificity using HCD, which also produced robust fragmentation of the peptide backbones, and cleavage of TMT ions. A representative spectrum of a peptide from the NMDA receptor subunit 2B (Grin2B/NR2B) is provided, wherein a phosphorylation site is detected at Serine residue 1303 (Figure 7A). For this site, a relative 1.73-fold increase in phosphorylation with age was quantified using TMT reporter ions (Figure 7B). A representative schematic of the entire Grin2b protein is shown to depict the distribution of unambiguous phosphorylation sites that were detected over different regions of the protein, as well as their relative changes with age (Figure 7C). Many un-reported novel sites, as well as previously reported sites, were characterized across proteins in the phosphoproteome.

Synaptic proteins with age-dependent changes in phosphorylation are involved in broad neuronal functions.

To gain broad insight into how age-dependent changes in phosphorylation may influence synaptic functions or pathways, the aging synaptic phosphoproteome was analyzed using motif-x [26, 27], ConsensusPathDB [25], PANTHERdb [28], and STRING [29] platforms.

Motif analysis of the phosphoproteome was performed using motif-x, on sequences that were 11 amino acids in length, with the central residue as an unambiguous phosphorylation site that changed with age. Peptides were separated based on phosphorylated residue and direction of change with age, and a significance

Acc#	Gene	Protein Name	Peptide	Modification Site	Change with Age	Fold Change Aged/Young
P11798	Camk2a	Calcium/calmodulin-dependent protein kinase type II subunit alpha	MLTINP**S**KR	Oxidation@251;Phospho@257=54	down	0.51800544
			ML**T**INPSKR	Phospho@253=57	down	0.31369255
			MLTINP**S**KR	Phospho@257=40	down	0.44686841
			ITAAEALKHPWI**S**HR	Phospho@272=74	down	0.28974422
			RITAAEALKHPWI**S**HR	Phospho@272=71	down	0.48424436
			GAILTTMLATRNF**S**GGK	Phospho@314=21	down	0.34518604
P23818	Gria1	Glutamate receptor 1	GFCLIPQQSINEAIR	Phospho@849	down	0.59063027
P23819	Gria2	Glutamate receptor 2	NAQNINPSSSQN**S**QNFATYK	Phospho@863=22	up	1.55874861
			EGYNVYGIE**S**VKI	Phospho@880=54	down	0.64401157
P35438	Grin1	Glutamate receptor ionotropic, NMDA 1	AITSTLAS**S**FK	Phospho@890=7	down	0.55371949
P35436	Grin2A	Glutamate receptor ionotropic, NMDA 2A	SPDFNLTG**S**QSNMLK	Phospho@890=18	down	0.65174058
			KKSPDFNLTG**S**QSNMLK	Phospho@890=11	down	0.68983121
			G**S**LIVDMVSDK	Phospho@929=79	down	0.69253675
			SMESLRQD**S**LNQNPVSQR	Oxidation@1018;Phospho@1025=39	up	2.19749081
			QH**S**YDNILDKPR	Phospho@1291=42	up	1.44543903
			KMP**S**IESDV	Phospho@1459=6	down	0.65620161
Q01097	Grin2B	Glutamate receptor ionotropic, NMDA 2B	NMANLSGVNG**S**PQSALDFIR	Phospho@917=12	down	0.67037919
			HSQL**S**DLYGK	Phospho@1036=23	down	0.64554827
			HSQLSDLYGKF**S**FK	Phospho@1043=33	down	0.6671011
			AGNLYDI**S**EDNSLQELDQPAAPVAVSSNASTTK	Phospho@1255=8	up	1.75716191
			RQH**S**YDTFVDLQK	Phospho@1303=22	up	1.45865488
			RQH**S**YDTFVDLQKEEAALAPR	Phospho@1303=24	up	1.79815836
			QH**S**YDTFVDLQKEEAALAPR	Phospho@1303=31	up	1.58350557
Q03391	Grin2D	Glutamate receptor ionotropic, NMDA 2D	RG**S**AHFSSLESEV	Phospho@1313=34	up	2.19108803
P97772	Grm1	Metabotropic glutamate receptor 1	SN**T**FLNIFR	Phospho@871=18	down	0.54738208
Q68EF4	Grm4	Metabotropic glutamate receptor 4	AVVTAATM**S**NKFTQK	Phospho@870=23	down	0.58724556
Q3UVX5	Grm5	Metabotropic glutamate receptor 5	S**S**SLVNLWK	Phospho@859=8	down	0.5674682
			SS**S**LVNLWK	Phospho@860=11	down	0.50760131
			DSVDSGSTTPNSPVSESALC	Phospho@1185=10	up	1.96640918
P42859	Htt	Huntingtin	DA**S**GWFDVLQK	Phospho@1368	down	0.51023776
			SLNPQKSGEEEDSGSAAQLGMC	Phospho@1853=28	up	1.75478542
			SLNPQKSGEEEDSGSAAQLGMC	Phospho@1853=11;Oxidation@1867	up	2.2520241
A2CG49	Kalrn	Kalirin	SFDLGSPKPGDETTPQGD**S**ADEK	Phospho@1789=24	up	1.84956211
			DILGNKV**S**VK	Phospho@2409	down	0.61531374
P63085	Mapk1	Mitogen-activated protein kinase 1	VADPDHDHTGFLTE**Y**VATR	Phospho@185=17	up	1.53278862
P46460	Nsf	Vesicle-fusing ATPase	Q**S**IINPDWNFEK	Phospho@207	down	0.62630135
			TKENRQ**S**IINPDWNFEK	Phospho@207=7	up	1.51477997
			KFLALMREEGA**S**PLDFD	Phospho@739	down	0.67279587
O88643	Pak1	Serine/threonine-protein kinase PAK 1	FYR**S**ILPGDKTNK	Phospho@57=20	down	0.68628447
			KNPQAVLDVLEFYN**S**K	Phospho@133=39	down	0.66970911
			YM**S**FTDK	Phospho@144=15	down	0.5258299
			YM**S**FTDK	Oxidation@143;Phospho@144=14	down	0.64860989
			DVATSPI**S**PTENNTTPPDALTR	Phospho@223=6	up	1.56587232
Q8BLE7	Slc17a6	Vesicular glutamate transporter 2	**S**LGQIYR	Phospho@23=63	down	0.62002144
P43006	Slc1a2	Excitatory amino acid transporter 2	DVEMGN**S**VIEENEMK	Oxidation@509=95;Phospho@512	up	1.91297041
			DVEMGN**S**VIEENEMK	Oxidation@509;Phospho@512;Oxidation@519	up	2.13787458
			NRDVEMGN**S**VIEENEMK	Oxidation@509=56;Phospho@512	up	3.13368896
			NRDVEMGN**S**VIEENEMK	Oxidation@509;Phospho@512;Oxidation@519	up	3.71759882
			KP**Y**QLIAQDNEPEKPVADSETK	Phospho@523=109	up	2.27749357
			ESNSNQC	Phospho@537=25	up	2.18183727
			ESNSNQC	Phospho@542=58	up	2.24186845
			SADC	Phospho@558=17	up	2.06337513
			SADC	Phospho@562=19	up	1.70604345
O88935	Syn1	Synapsin-1	ASTAAPVASPAAP**S**PGSSGGGGFFSSLSNAVK	Phospho@67=7	down	0.66718764
			QTTAAAAA**T**FSEQVGGGSGGAGR	Phospho@94=14	up	1.79073115
			QTTAAAAATFSEQVGGG**S**GGAGR	Phospho@103=39	up	1.71815263
			SLKPDFVLIR	Phospho@177	down	0.67476813
			QPQRDA**S**PGRGSHSQSSSPGALTLGR	Phospho@427=13	up	1.84666045
			DA**S**PGRGSHSQSSSPGALTLGR	Phospho@427=10	up	2.39609568
			DASPGRG**S**HSQSSSPGALTLGR	Phospho@432=7	up	2.00515188
			QGPPLQQRPPPQGQQHL**S**GLGPPAGSPLPQR	Phospho@494=55	up	1.80057628
			LPSPTAAPQQSA**S**QATPVTQGQGR	Phospho@520=22	up	1.93996371
			QSRPVAGGPGAPPAARPPA**S**PSPQR	Phospho@551=7	up	1.96874781
			QSRPVAGGPGAPPAARPPASP**S**PQR	Phospho@553=10	up	2.37028899
			QASI**S**GPAPTK	Phospho@568=10	down	0.68733385
			SQ**S**LTNAFNLPEPAPPRPSLSQDEVK	Phospho@666=8	up	1.57965952

Table 1. Age-dependent changes in phosphorylation sites of synaptic proteins. This table contains a hand-curated list of proteins with age-dependent changes in phosphorylation. All modification sites are unambiguous. Phosphorylated residues are bolded and underlined in the peptide column. Fold change is depicted as aged/young, such that values > 1 indicate increased phosphorylation with age and < 1 indicate decreased phosphorylation with age. All N-termini of peptides and lysine residues are TMT-labeled and all cysteine residues are carbamidomethylated.

A

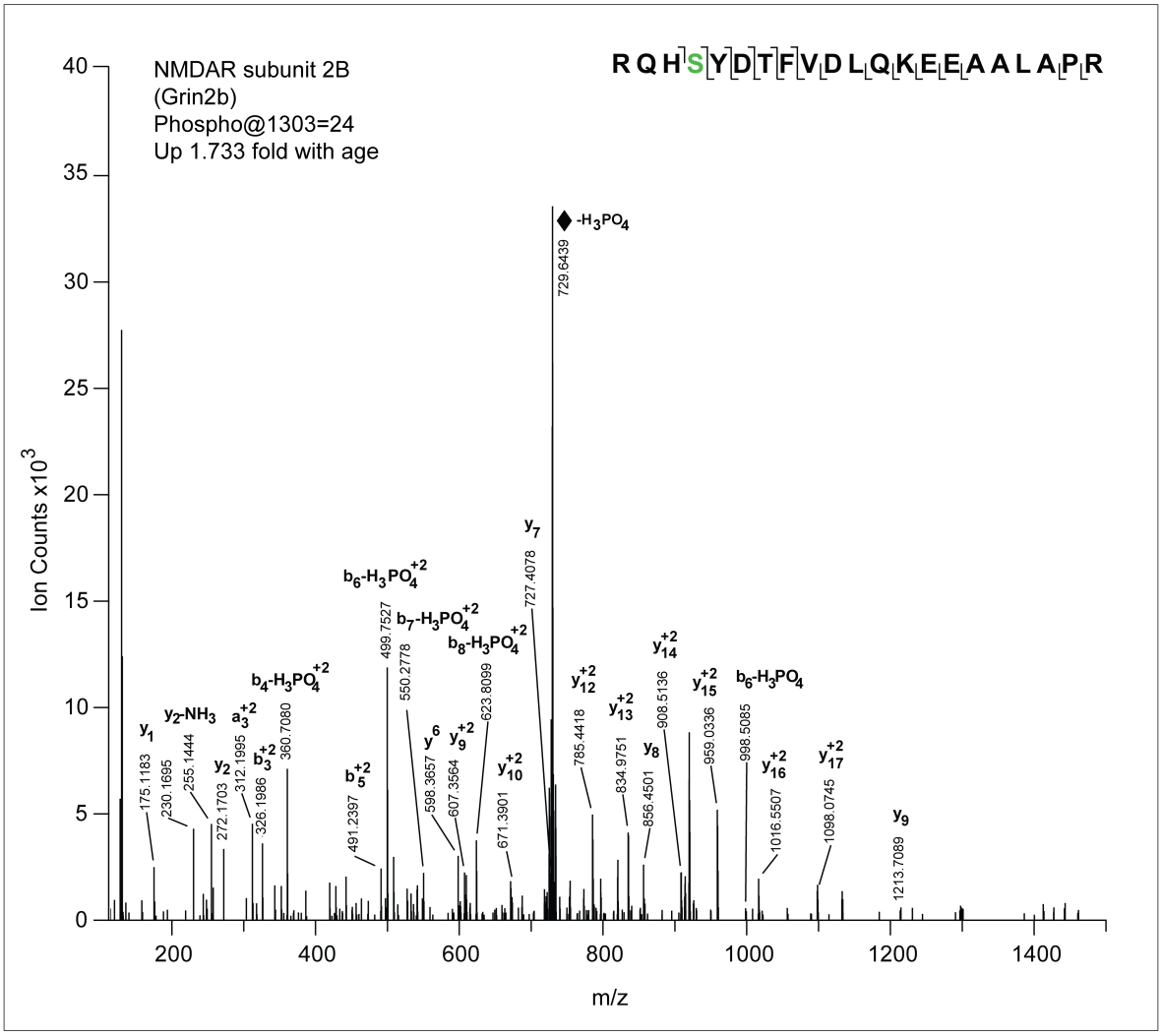
NMDAR subunit 2B
(Grin2b)
Phospho@1303=24
Up 1.733 fold with age
R Q H S Y D T F V D L Q K E E A A L A P R
Ion Counts x10^3
m/z
-H3PO4
729.6439
y7
727.4078
b6-H3PO4+2
499.7527
b7-H3PO4+2
550.2778
b8-H3PO4+2
623.8099
b4-H3PO4+2
360.7080
y14+2
908.5136
y12+2
785.4418
y13+2
834.9751
y15+2
959.0336
b6-H3PO4
998.5085
y16+2
1016.5507
y17+2
1098.0745
y9
1213.7089
y1
175.1183
y2-NH3
230.1695
a3+2
255.1444
y2
272.1703
b3+2
312.1995
326.1986
b5+2
491.2397
y6
598.3657
y9+2
607.3564
y10+2
671.3901
y8
856.4501

B

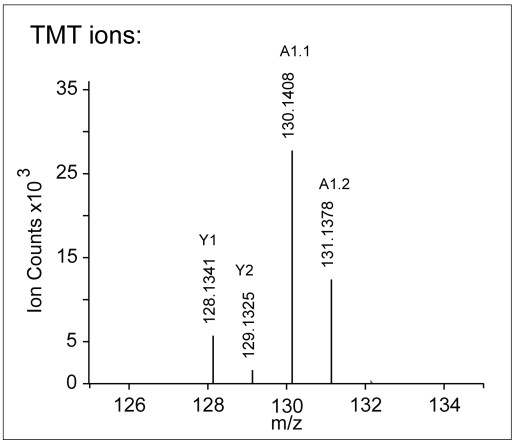
TMT ions:
Ion Counts x10^3
m/z
A1.1
130.1408
A1.2
131.1378
Y1
128.1341
Y2
129.1325

C

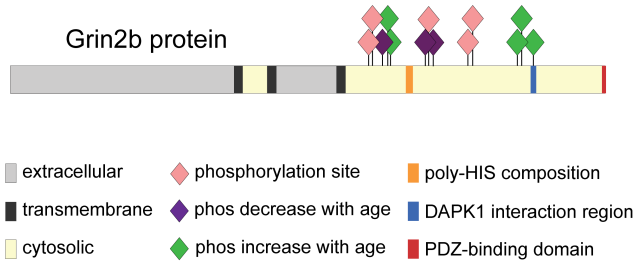
Grin2b protein
extracellular
transmembrane
cytosolic
phosphorylation site
phos decrease with age
phos increase with age
poly-HIS composition
DAPK1 interaction region
PDZ-binding domain

Figure 7. Representative site-specific identification and relative quantitation of synaptic protein phosphorylation. (A) Representative HCD spectra identifies a phosphorylation site on the serine in the fourth position of the Grin2b peptide RQH**S**YDTFVDLQKEEAALAPR. The phosphorylated Ser1303 residue is shown in green. (B) TMT-6plex reporter ions used for relative quantitation. (C) Representative distribution of unambiguous phosphorylation sites and their change with age that were detected on the Grin2b protein. Some compositional features for Grin2b that are reported on UniProt have also been included.

cutoff of 0.000001 was employed (see methods for more details). Motif analysis identified 8 motifs with age-dependent increases in phosphorylation (Figure 8A), and 11 motifs with age-dependent decreases in phosphorylation (Figure 8B). Potential kinases were assigned to these motifs based on a curated list compiled from the literature (Table 2) [30]. Age-dependent increases in phosphorylation were detected on motifs consistent with casein kinase II (CK2) substrate motifs such as pSXX[E/D] and pS[D/E][D/E][D/E], where pS is a phosphorylated serine and X is any amino acid (Figure 8A; Table 2) [30]. Age-dependent decreases in phosphorylation were also detected on motifs consistent with CDK3, PKA, and PKC (Figure 8A; Table2) [30]. Alterations in motifs targeted by these kinases are suggestive of alterations in their function, with CK2 activity proposed to increase, and CDK3, PKA, and PKC activity proposed to decrease at the synapse with age.

The aging synaptic phosphoproteome was next analyzed using ConsensusPathDB to profile overrepresentation of GO terms and pathways. Using the entire detected synaptosome proteome as a background dataset, GO analyses of the phosphoproteome identified biological processes indicative of neurogenic functions that are sensitive to aging, such as neurogenesis (Figure 9A). Overrepresented cellular components included both axonal and dendritic structures, demonstrating that age-related changes in phosphorylation occur at both the pre- and post-synapse (Figure 9B). Molecular functions contained various kinase and other enzymatic activity terms, consistent with the notion that phosphorylation is a broad regulator of kinase and enzymatic activity (Figure 9C). From a total of 23 overrepresented pathways, neuronal system, PodNet network, and calcium signaling were most significant (Figure 9D). While

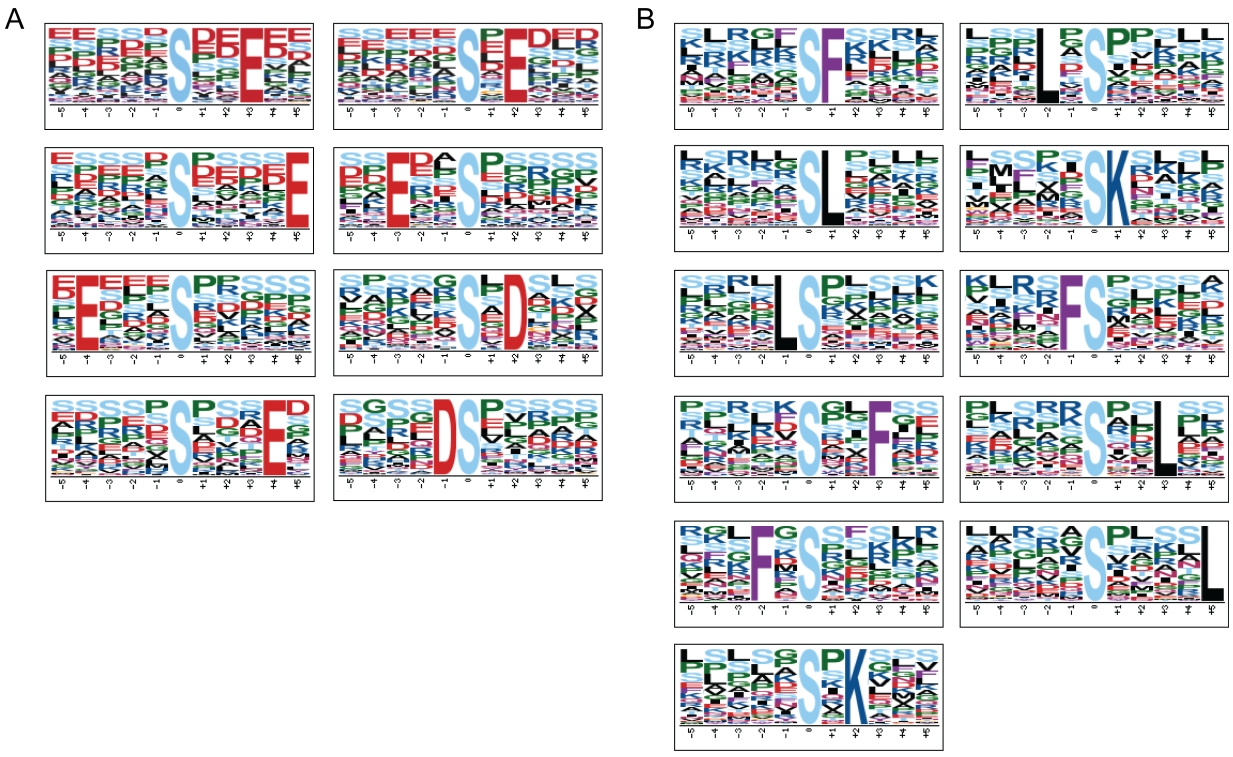

Figure 8. Position weight matrices of motifs with age-dependent changes in phosphorylation. Graphic sequence logos of position weight matrices (PMWs) depicting (A) motifs with phosphorylation sites that increased at the synapse with age and (B) motifs with phosphorylation sites that decreased at the synapse with age. The height of each amino acid letter corresponds to how tightly the residue is conserved within the enriched motif. PMWs were calculated using the motif-x platform.

Motifs with age-dependent increased phosphorylation

Motif	Motif Score	Foreground Matches	Foreground Size	Background Matches	Background Size	Fold Increase	Potential Kinases
.....S..E..	16	396	2604	1011	10314	1.55	CK2
.....S....E	13.68	271	2208	711	9303	1.61	CK2
.....S.E...	12.44	263	1937	742	8592	1.57	CK2
.E...S.....	9.36	201	1674	604	7850	1.56	CK2
.....S...E.	8.26	141	1473	418	7246	1.66	
..E..S.....	7.14	130	1332	411	6828	1.62	CK1; CK2
.....S.D...	6.47	148	1202	520	6417	1.52	
....DS.....	6.58	111	1054	377	5897	1.65	

Motifs with age-dependent decreased phosphorylation

Motif	Motif Score	Foreground Matches	Foreground Size	Background Matches	Background Size	Fold Increase	Potential Kinases
.....SF....	13.98	162	2266	384	10314	1.92	PKCs; Akt
.....SL....	12.48	362	2104	1175	9930	1.45	Akt; p70 Ribosomal S6 kinase
....LS.....	11	265	1742	879	8755	1.52	CDK4
.....S..F..	11.1	90	1477	217	7876	2.21	
...F.S.....	9.36	76	1387	191	7659	2.2	
.....S.K...	8.94	113	1311	352	7468	1.83	PKC; PKA
...L.S.....	8.82	160	1198	586	7116	1.62	ERK1
.....SK....	8.3	84	1038	267	6530	1.98	
....FS.....	7.74	73	954	236	6263	2.03	
.....S..L..	6.81	111	881	458	6027	1.66	
.....S....L	6.86	107	770	462	5569	1.68	

Table 2. Motifs with age-dependent changes in phosphorylation and associated kinases. Kinases were matched with enriched motifs based on previously reported literature [30]. Motif score, fold increase, and all other parameters were calculated using the motif-x platform. See methods for more details.

A

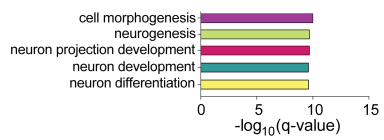
Biological Process
cell morphogenesis
neurogenesis
neuron projection development
neuron development
neuron differentiation
0
5
10
15
-log10(q-value)

B

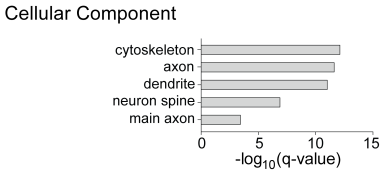
Cellular Component
cytoskeleton
axon
dendrite
neuron spine
main axon
0
5
10
15
-log10(q-value)

C

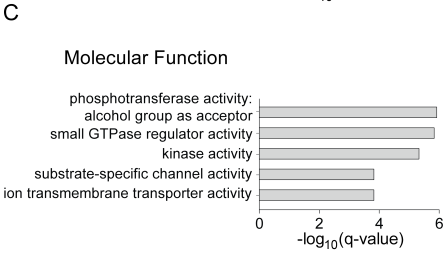
Molecular Function
phosphotransferase activity:
alcohol group as acceptor
small GTPase regulator activity
kinase activity
substrate-specific channel activity
ion transmembrane transporter activity
0
2
4
6
-log10(q-value)

D

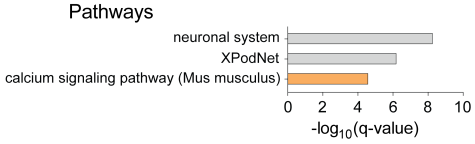
Pathways
neuronal system
XPodNet
calcium signaling pathway (Mus musculus)
0
2
4
6
8
10
-log10(q-value)

E

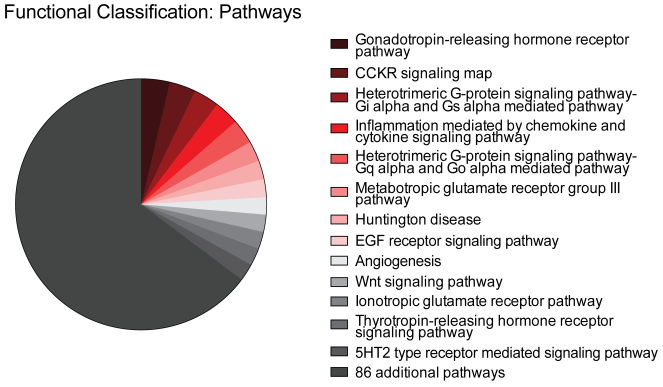
Functional Classification: Pathways
Gonadotropin-releasing hormone receptor pathway
CCKR signaling map
Heterotrimeric G-protein signaling pathway-Gi alpha and Gs alpha mediated pathway
Inflammation mediated by chemokine and cytokine signaling pathway
Heterotrimeric G-protein signaling pathway-Gq alpha and Go alpha mediated pathway
Metabotropic glutamate receptor group III pathway
Huntington disease
EGF receptor signaling pathway
Angiogenesis
Wnt signaling pathway
Ionotropic glutamate receptor pathway
Thyrotropin-releasing hormone receptor signaling pathway
5HT2 type receptor mediated signaling pathway
86 additional pathways

F

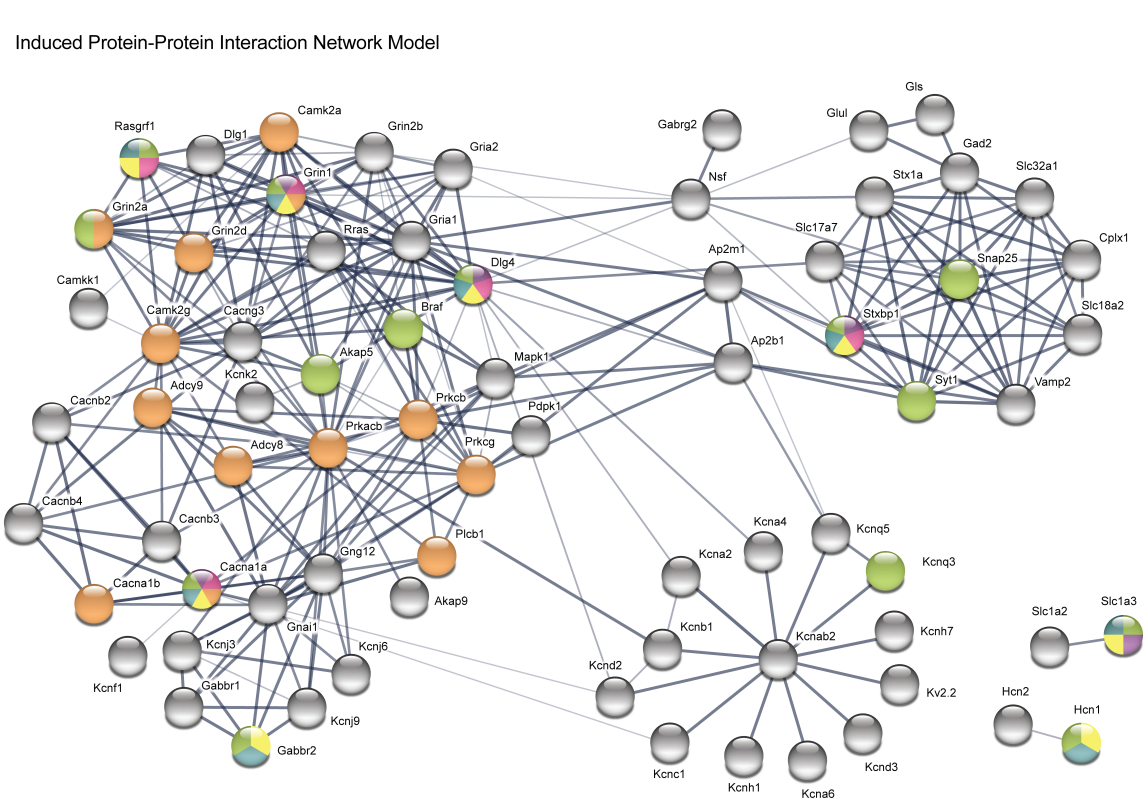
Induced Protein-Protein Interaction Network Model
Rasgrf1
Dlg1
Camk2a
Grin2b
Gria2
Grin1
Grin2a
Grin2d
Rras
Gria1
Dlg4
Camkk1
Camk2g
Cacng3
Braf
Akap5
Kcnk2
Mapk1
Adcy9
Cacnb2
Prkcb
Pdpk1
Prkacb
Adcy8
Prkcg
Cacnb4
Cacnb3
Plcb1
Gng12
Cacna1a
Cacna1b
Akap9
Gnai1
Kcnj3
Kcnj6
Kcnf1
Gabbr1
Kcnj9
Gabbr2
Gabrg2
Nsf
Gls
Glul
Gad2
Slc32a1
Stx1a
Slc17a7
Cplx1
Ap2m1
Snap25
Stxbp1
Slc18a2
Ap2b1
Syt1
Vamp2
Kcna4
Kcnq5
Kcna2
Kcnq3
Kcnb1
Kcnab2
Kcnh7
Kcnd2
Kv2.2
Kcnc1
Kcnh1
Kcna6
Kcnd3
Slc1a2
Slc1a3
Hcn2
Hcn1

Figure 9. Synaptic proteins with age-dependent changes in phosphorylation are involved in a broad array of neuronal functions. (A-D) Gene ontology (GO) overrepresentation analyses of proteins with age-dependent alterations in phosphorylation. Calculations were done using ConsensusPathDB with the total set of proteins detected as the reference dataset, using false discovery rate (FDR) correction. Top five GO terms for each category, and top three pathways are shown. (E) Functional classification of proteins with age-dependent alterations in unambiguous phosphorylation was used to represent pathway distribution; performed using PANTHERdb. (F) Protein-protein interaction networks generated using STRING analysis of differentially phosphorylated proteins. A representative network is shown using proteins from the most overrepresented pathway as input. Line thickness denotes relative interaction strength. Nodes are color coded according to their association with GO terms in (A) and (D).

PodNet is a distinct network compiled using literature to describe protein-protein interactions in the podocyte cells of the kidney [31], many categorized genes are attributed dual roles in neuronal and synaptic function. In addition, functional classification of the aging synaptic phosphoproteome was assessed using PANTHERdb, and detected a wide distribution over 99 unique pathways, with enrichments in Gonadotropin-releasing hormone receptor pathway (GnRH), several G-protein signaling pathways, and metabotropic and ionotropic glutamate receptor pathways (Figure 9E).

Induced protein-protein interaction network modeling was also performed using the STRING platform. The most significantly overrepresented pathway (neuronal system) was used as the input dataset for STRING modeling, due to the overall size of the phosphoproteome. The protein interaction network depicts proteins (nodes) and their physical interactions with one another (lines connecting nodes). A highly dense and interconnected network was generated, indicating that synaptic proteins with age-dependent changes in phosphorylation undergo a large number of interactions with one another (Figure 9F). Proteins in the induced network were color coded according to their association with biological processes, such as neurogenesis (green) and calcium signaling (orange) (Figure 9A,D). A number of proteins in the network are associated with various processes, and are highly connected to other proteins, suggesting if changes in phosphorylation affect the functions of these proteins, neuronal processes like calcium signaling may be strongly impacted by age-dependent changes in phosphorylation. Furthermore, a few highly connected nodes, such as the NMDA receptor subunit Grin1, the calcium voltage gated channel subunit Cacna1a, and *Dlg4*, the gene which encodes PSD-95, were associated with multiple overrepresented processes and pathways from

GO analyses (Figure 9F). These nodes represent candidates that may elicit the greatest functional impact due to age-dependent changes in synaptic phosphorylation, as they are involved in numerous pathways. Together, these data implicate involvement of the aging synaptic phosphoproteome in broad neuronal functions, some of which are indeed sensitive to aging.

Characterization of the aging synaptic O-GlcNAcome.

To continue the investigation of dynamic PTMs at the aging synapse, proteins with age-dependent changes in O-GlcNAcylation were characterized. Much like phosphorylation, O-GlcNAcylation elicits a wide array of protein behaviors. Thus, both loss and gain of O-GlcNAcylation were also considered to be important. Similarly, all synaptic proteins upon which age-dependent changes in O-GlcNAcylation was detected were collectively termed: the aging synaptic O-GlcNAcome. More specifically, the aging synaptic O-GlcNAcome refers to proteins exhibiting any age-dependent change in O-GlcNAcylation of at least 1.4-fold. A curated list of selected proteins, peptides, O-GlcNAcylation sites, and their direction and magnitude of change with age, is provided in Table 3.

O-GlcNAc is a particularly labile PTM, and poses challenges for site-specific detection using HCD. Thus, to increase the resolution of O-GlcNAc site assignment, electron-transfer dissociation (ETD) was employed on O-GlcNAcylated peptides. Using a combination of HCD and ETD, 586 O-GlcNAcylated peptides were detected, on which 197 modifications were resolved to site-specificity (Figure 6A). A representative ETD spectrum used to resolve an unambiguous O-GlcNAcylation site on a peptide from the Ras/Rap GTP-ase activating protein (Syngap1) is provided, wherein an O-GlcNAc site is

Acc #	Gene	Protein Name	Dissoc Type	Start	Peptide	# of Mods	Modification Sites	Change in O-GlcNAc with Age	Fold Change A/Y
P62484	Abi2	Abl interactor 2	ETD	293	HTPP**T**IGGSLPYR	1	HexNAc@297=6	up	1.433
Q69ZX8	Ablim3	Actin-binding LIM protein 3	ETD	371	ASSPGYIDSP**TYS**R	1	HexNAc@381|383	up	1.42
Q9JKV1	Adrm1	Proteasomal ubiquitin receptor ADRM1	ETD	211	SQ**S**AAVTPSSSTSSAR	1	HexNAc@213=7	down	0.6
Q80WC7	Agfg2	Arf-GAP domain and FG repeat-containing protein 2	HCD	178	**T**LLGDPVP**SLS**DPA**STSS**QPG**S**Q**S**QAR	1	HexNAc@178|186|188|192|193|194|195|199|201	up	1.862
			ETD	178	TLLGDPVPSLSDPA**STSS**QPGSQSQAR	1	HexNAc@192|193|194|195	up	1.464
Q9DBG3	Ap2b1	AP-2 complex subunit beta	HCD	905	IQPGNPNY**TLS**LK	1	HexNAc@913|915	down	0.657
P50516	Atp6v1a	V-type proton ATPase catalytic subunit A	HCD	257	**T**VI**S**Q**S**L**S**K	1	HexNAc@257|260|262|264	down	0.696
O35927	Ctnnd2	Catenin delta-2	HCD	307	**SYSTSS**PINIVV**SS**AGL**S**PIR	2	HexNAc@307|309|310|311|312|319|320|324;HexNAc@319|320	up	1.387
Q9D415	Dlgap1	Disks large-associated protein 1	ETD	519	SSSPPR**TT**TTVR	2	HexNAc@525=7;HexNAc@526=7	up	1.526
Q05BC3	Eml1	Echinoderm microtubule-associated protein-like 1	HCD	119	KEVVVPV**T**K	1	HexNAc@126	down	0.717
Q9Z2H5	Epb41l1	Band 4.1-like protein 1	ETD	763	GAAAMIPGPQ**T**VATEIR	1	HexNAc@773=8	up	1.379
Q14CH0	Fam171b	Protein FAM171B	ETD	601	EEDIVLEGQQSLP**S**Q**TS**DWSR	1	HexNAc@614|616|617	down	0.721
Q3UNH4	Gprin1	G protein-regulated inducer of neurite outgrowth 1	HCD	263	TELVSSVTVAPVTSENVNPVCSGGAGPAAVGNSETLSSVK	1	HexNAc@263|267|268|270|275|276|284|295|297|299|300	down	0.699
Q01097	Grin2b	Glutamate receptor ionotropic, NMDA 2B	ETD	1021	KPLDIGLP**SS**K	1	HexNAc@1029|1030	down	0.676
Q6RHR9	Magi1	Membrane-associated guanylate kinase	ETD	1088	IATIT**TT**HAPSQQGTQETR	1	HexNAc@1093|1094	up	2.022
Q7TSJ2	Map6	Microtubule-associated protein 6	HCD	78	A**T**GPAPGP**S**VDR	1	HexNAc@79|86	up	1.437
			ETD	420	EEVAS**T**VSSSYR	1	HexNAc@425=7	up	1.649
P08551	Nefl	Neurofilament light polypeptide	HCD	24	VH**ISS**VR	1	HexNAc@27|28	up	1.954
Q68FH0	Pkp4	Plakophilin-4	ETD	218	AQSPSYV**T**STGVSPSR	1	HexNAc@225=14	up	1.429
			HCD	218	AQSPSYV**TS**TGVSPSR	1	HexNAc@225|227	up	1.457
			HCD	218	AQSPSYVT**ST**GVSPSR	1	HexNAc@226|227	up	1.457
Q8BSS9	Ppfia2	Liprin-alpha-2	ETD	547	THID**TS**TELR	1	HexNAc@551|552	down	0.697
			ETD	1247	LDNSTVRTYSC	1	HexNAc@1254=17	up	1.426
P60469	Ppfia3	Liprin-alpha-3	HCD	499	GRPPSSY**S**R	1	HexNAc@506=7	up	2.342
Q8R361	Rab11fip5	Rab11 family-interacting protein 5	ETD	538	**TS**LSTALSSGLER	1	HexNAc@538|539	down	0.694
Q9EQZ7	Rims2	Regulating synaptic membrane exocytosis protein 2	HCD	1514	ASQSSLESSTGP**SYS**R	1	HexNAc@1526|1528	up	1.722
P25444	Rps2	40S ribosomal protein S2	ETD	285	**T**QAPAVATT	1	HexNAc@285=69	down	0.643
Q62419	Sh3gl1	Endophilin-A2	HCD	283	ITA**SSS**FR	1	HexNAc@286|287|288	down	0.539
D3YZU1	Shank1	SH3 and multiple ankyrin repeat domains protein 1	HCD	1902	GG**S**GG**ST**D**S**HHGGA**S**YIPER**TSS**LQR	1	HexNAc@1904|1907|1908|1910|1916|1922|1923|1924	up	1.944
Q80Z38	Shank2	SH3 and multiple ankyrin repeat domains protein 2	ETD	1286	SPEVMS**T**VSG**T**R	1	HexNAc@1292|1296	down	0.653
A2AQ25	Skt	Sickle tail protein	ETD	1890	AAPTT**SS**SSSPPSPASPTSLNQGAR	1	HexNAc@1895|1896	up	1.37
O55042	Snca	Alpha-synuclein	HCD	59	**T**KEQV**T**NVGGAVV**T**GV**T**AVAQK	1	HexNAc@59|64|72|75	down	0.72
Q9QXV8	Spry2	Protein sprouty homolog 2	HCD	94	LQP**S**QVH**SS**R	1	HexNAc@97|101|102	up	1.601
Q62261	Sptbn1	Spectrin beta chain, non-erythrocytic 1	ETD	2290	DDEEMNTWIQAISSAISSDKHDTSASTQSTPA**SS**R	1	Oxidation@2294;HexNAc@2322|2323	up	3.19
Q80TY4	St18	Suppression of tumorigenicity 18 protein	HCD	796	GGIKM**T**P**T**K	1	HexNAc@801|803	down	0.707
O88935	Syn1	Synapsin-1	HCD	54	A**ST**AAPVA**S**PAAP**S**PG**SS**GGGGFF**SSLS**NAVK	1	HexNAc@55|56|62|67|70|71|78|79|81	up	1.368
			ETD	508	LPSPTAAPQQ**SA**S**Q**A**T**PV**T**QGQGR	1	HexNAc@518|520|523|526	up	1.955
			ETD	508	LPSPTAAPQQSASQA**T**PV**T**QGQGR	1	HexNAc@523|526	up	1.649
F6SEU4	Syngap1	Ras/Rap GTPase-activating protein SynGAP	ETD	1133	QHSQ**TPST**LNPTMPASER	1	Oxidation@1145;HexNAc@1137|1139|1140	up	1.812
			ETD	1133	QHSQTPS**T**LNPTMPASER	1	HexNAc@1140=8	up	1.622
Q8CC35	Synpo	Synaptopodin	ETD	392	VSAPP**S**AASTFSR	1	HexNAc@397=16	down	0.66
Q9DAM7	Tmem263	Transmembrane protein 263	ETD	63	SLEVTK**T**AV**TT**VP**S**MGIGLVK	1	HexNAc@69|72|73|76	down	0.72

Table 3. Age-dependent changes in O-GlcNAcylation sites of synaptic proteins. Table 3 contains a hand-curated list of targets identified in the synaptosome with age-dependent changes in O-GlcNAcylation. Unambiguous O-GlcNAcylated sites are bolded and underlined in the peptide column, and potential O-GlcNAcylation sites are bolded in the peptide column. Potential modification sites are delineated by vertical dashes in the modification sites column. Fold change is depicted as aged/young, such that > 1 indicates an increase in O-GlcNAcylation with age and < 1 indicates a decrease in O-GlcNAcylation with age. All N-termini of peptides and Lysine residues are TMT-6 labeled and all Cysteine residues are carbamidomethylated.

detected at Threonine residue 1140 (Figure 10A,B). For this site, a relative 1.55–fold increase in O-GlcNAcylation was quantified with age using TMT reporter ions (Figure 10B). A representative schematic of the entire Syngap1 protein depicts the distribution of all O-GlcNAc sites that were detected on the protein, as well as their relative change with age (Figure 10C). Much like in the phosphoproteome, many novel un-reported modification sites were characterized in the O-GlcNAcome.

Synaptic proteins with age-dependent changes in O-GlcNAcylation are involved in glutamatergic signaling.

The aging synaptic O-GlcNAcome was then analyzed using ConsensusPathDB [25], PANTHERdb [28], and STRING [29] platforms. GO analyses identified biological processes indicative of synaptic transmission, neurotransmitter secretion, and regulation of synaptic plasticity (Figure 11A). Cellular components were similar to those identified for the phosphoproteome, in that they contained both pre- and post-synaptic components (Figure 11B). In addition, ionotropic glutamate receptor complex was an overrepresented component (Figure 11B). Two molecular functions were detected, one of which was glutamate receptor binding (Figure 11C), and glutamatergic synapse was detected as the most overrepresented pathway (Figure 11D). Functional classification of the aging synaptic O-GlcNAcome using PANTHERdb identified a distribution over 9 unique pathways, of which ionotropic glutamate receptor pathway and synaptic vesicle trafficking were the two most populated (Figure 11E). Induced network modeling by STRING analysis revealed a single cluster, with two of the most highly connected nodes being *Dlgap1*, a protein of the NMDA-receptor-associated scaffolding complex [32], and the

A

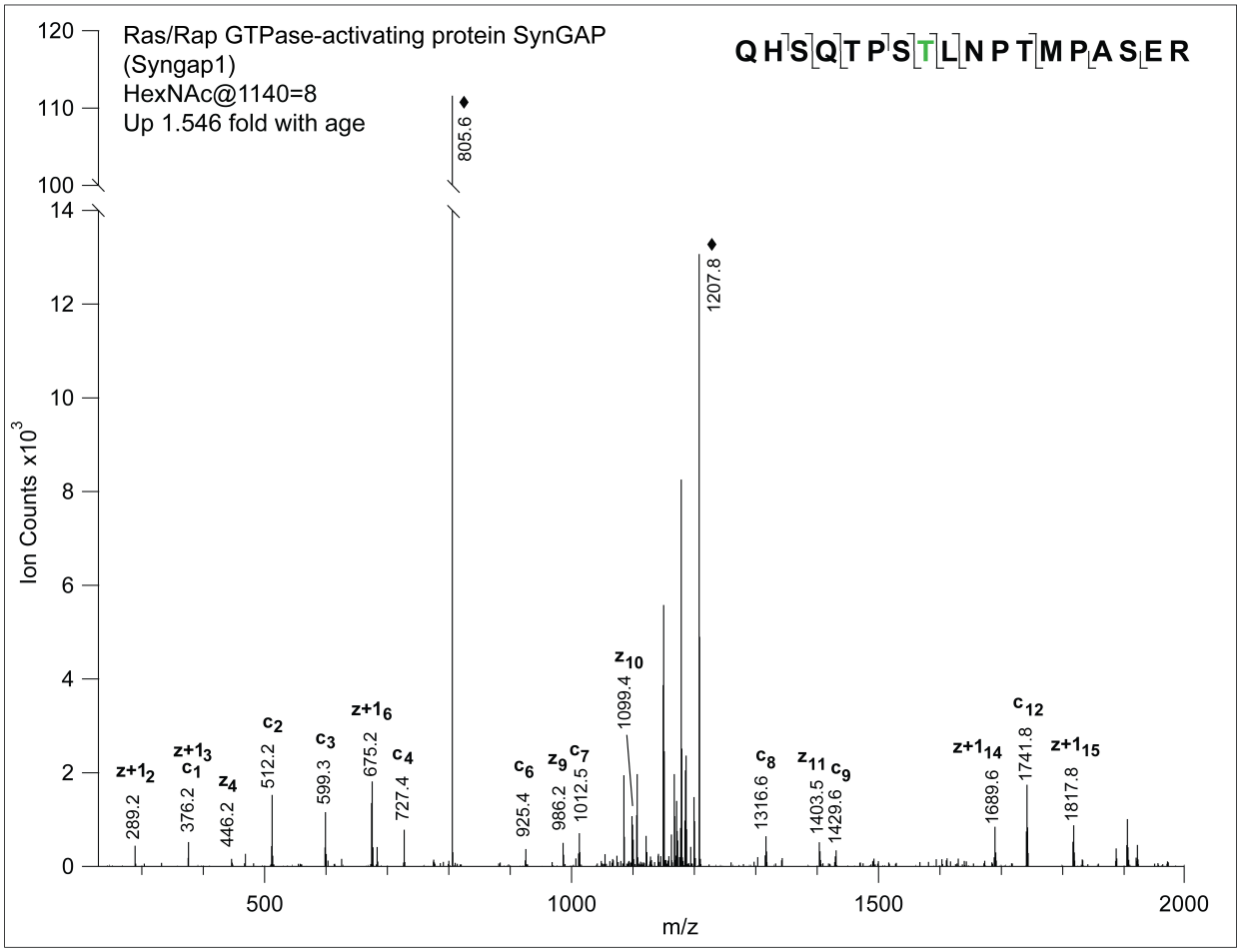
Ras/Rap GTPase-activating protein SynGAP
(Syngap1)
HexNAc@1140=8
Up 1.546 fold with age
Q H S Q T P S T L N P T M P A S E R
Ion Counts x10^3
m/z
805.6
1207.8
z+1 2
289.2
c 1
z+1 3
376.2
z 4
446.2
c 2
512.2
c 3
599.3
z+1 6
675.2
c 4
727.4
c 6
925.4
z 9
c 7
986.2
1012.5
z 10
1099.4
c 8
1316.6
z 11
c 9
1403.5
1429.6
z+1 14
1689.6
c 12
1741.8
z+1 15
1817.8

B

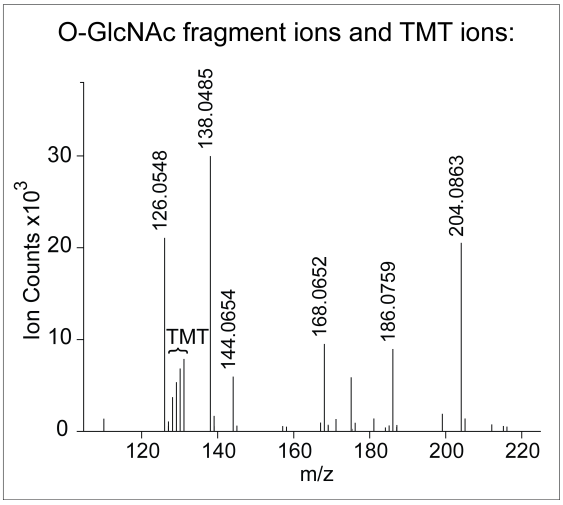
O-GlcNAc fragment ions and TMT ions:
Ion Counts x10^3
m/z
126.0548
138.0485
TMT
144.0654
168.0652
186.0759
204.0863

C

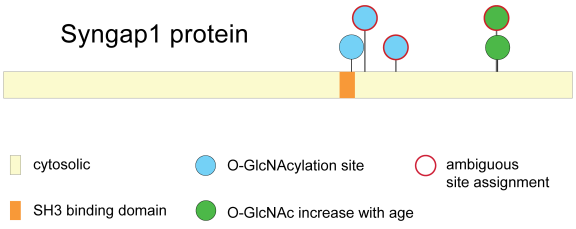
Syngap1 protein
cytosolic
SH3 binding domain
O-GlcNAcylation site
O-GlcNAc increase with age
ambiguous
site assignment

Figure 10. Representative site-specific identification and relative quantitation of synaptic protein O-GlcNAcylation. (A) Representative ETD spectra identifying an O-GlcNAc modification on the threonine residue in the eighth position of the Syngap1 peptide QHSQTPS**T**LNPTMPASER. O-GlcNAcylated Thr1140 is shown in green. (B) TMT-6plex reporter ions used for relative quantitation, and O-GlcNAc fragment ions. (C) Representative distribution of O-GlcNAcylation sites and their change with age detected on the entire Syngap1 protein. Modifications with red borders have ambiguous site assignments. Compositional features for Syngap1 that are reported on UniProt have also been included.

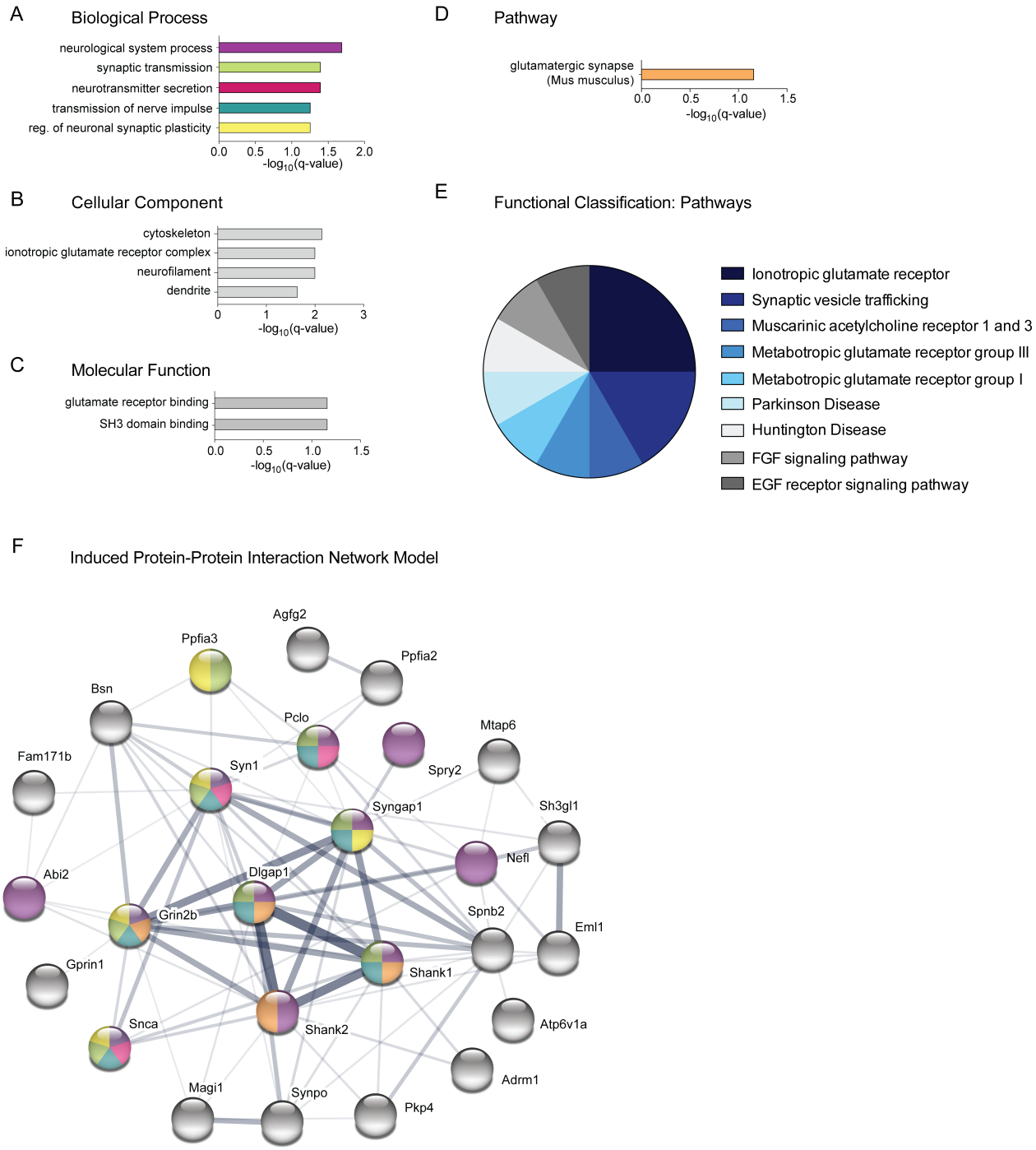
A
Biological Process
neurological system process
synaptic transmission
neurotransmitter secretion
transmission of nerve impulse
reg. of neuronal synaptic plasticity
0.0 0.5 1.0 1.5 2.0
-log10(q-value)
B
Cellular Component
cytoskeleton
ionotropic glutamate receptor complex
neurofilament
dendrite
0 1 2 3
-log10(q-value)
C
Molecular Function
glutamate receptor binding
SH3 domain binding
0.0 0.5 1.0 1.5
-log10(q-value)
D
Pathway
glutamatergic synapse
(Mus musculus)
0.0 0.5 1.0 1.5
-log10(q-value)
E
Functional Classification: Pathways
Ionotropic glutamate receptor
Synaptic vesicle trafficking
Muscarinic acetylcholine receptor 1 and 3
Metabotropic glutamate receptor group III
Metabotropic glutamate receptor group I
Parkinson Disease
Huntington Disease
FGF signaling pathway
EGF receptor signaling pathway
F
Induced Protein-Protein Interaction Network Model
Agfg2
Ppfia3
Ppfia2
Bsn
Pclo
Mtap6
Fam171b
Syn1
Spry2
Syngap1
Sh3gl1
Nefl
Abi2
Dlgap1
Grin2b
Spnb2
Eml1
Gprin1
Shank1
Snca
Shank2
Atp6v1a
Adrm1
Magi1
Synpo
Pkp4

Figure 11. Synaptic proteins with age-dependent changes in O-GlcNAcylation are involved in excitatory neuronal function.
(A-D) Gene ontology (GO) overrepresentation analyses of proteins with age-dependent alterations in O-GlcNAcylation. Calculations were done using ConsensusPathDB with the total set of proteins detected as the reference dataset, using false discovery rate (FDR) correction. (E) Functional classification of proteins with age-dependent alterations in O-GlcNAcylation was used to represent pathway distribution; performed using PANTHERdb. (F) Protein-protein interaction networks generated using STRING analysis of differentially O-GlcNAcylated proteins. Line thickness denotes relative interaction strength. Nodes are color coded according to their association with GO terms in (A) and (D).

NMDA receptor subunit Grin2B (also known as NR2B). Other highly connected nodes were Shank1 and Shank2, of the Shank family of post-synaptic scaffolding proteins (Figure 11F). In contrast to broad functional involvement of the phosphoproteome (Figure 9), the aging synaptic O-GlcNAcome suggests a more specific involvement in glutamatergic synaptic function, impairments of which in excitatory neurons are strongly linked to age-related cognitive decline [33].

Discussion

In this study, the first relative quantitation of age-dependent changes in phosphorylation and O-GlcNAcylation is characterized at the synaptic level. This proteomics approach combines high-standard PTM enrichment protocols, isobaric tandem mass tagging, and tandem mass spectrometry for optimized characterization. The present aging-associated synaptic phosphoproteome and O-GlcNAcome provide a rich dataset by which the scientific community can query synaptic proteins of interest for relative changes in site-specific PTM sites with age, and propose alterations in dynamic PTMs as a novel mechanism regulating synaptic and cognitive aging.

Prior to this study, low throughput characterization of age-dependent alterations in PTMs required targeted MS experiments or the development of site-specific antibodies. High throughput microarrays for profiling PTMs, such as phosphorylation, have been developed but remain limited in their breadth of protein detection. While proteomics studies have previously profiled age-related changes in synaptic protein abundance [10, 11] or phosphorylation and O-GlcNAcylation at the young rodent synapse [15, 34, 35], these proteomics approaches have yet to be utilized in

combination, likely owing to a number of significant technical hurdles. For example, aged mammalian tissue is not easy to obtain in quantities large enough for the detection of low-stoichiometric PTMs on a sub-cellular level. O-GlcNAcylation in particular proves a challenging modification to enrich for given its low stoichiometric abundance compared to other PTMs. This study addresses these limitations by employing LWAC to enrich for O-GlcNAcylated peptides. Unlike chemical derivatization-based approaches LWAC does not require tagging, specialized capture, and cleavage for isolation. While indirect enrichment techniques such as BEMAD exist, they often require more nuanced conditions to prevent nonspecific labeling of other more abundant O-linked PTMs [36]. An additional concern is that O-GlcNAc modifications are quite difficult to detect on a site-specific level due to their extremely labile nature during peptide fragmentation. To circumvent this, HCD fragmentation was employed for robust peptide and phosphorylation site identification, in combination with ETD fragmentation for site assignment of O-GlcNAc.

Phosphorylation mediates an enormous number of signaling pathways and cellular processes, and correspondingly, the proteomic analyses of the aging synaptic phosphoproteome identified GO terms and pathways involved in broad neuronal functions. Of note, pathways pertinent to brain aging, such as calcium signaling and glutamatergic receptor pathways were also detected. In particular, calcium signaling declines with age at glutamatergic synapses, suggesting that alterations in phosphorylation may contribute to age-related changes in excitatory neuronal signaling [37]. Functional classification identified changes in phosphorylation on proteins of the gonadotropin-releasing hormone (GnRH) receptor pathway, decline of which in the

hypothalamus promotes age-dependent cognitive impairments that are reversible by restoring GnRH signaling in the aged brain [38]. Motif analysis identified decreased phosphorylation at potential motifs corresponding to PKA and PKCs, which are strongly associated with excitatory synaptic transmission, and learning and memory, implicating dynamic PTMs in classic hallmarks of synaptic aging. Conversely, increased phosphorylation was identified on motifs corresponding to CK2. Increased activity of CK2 in neurons contributes to pathogenic hallmarks of Alzheimer's and Parkinson's disease [39, 40] – suggesting alterations in kinase activity at the aging neuronal synapse may contribute to the development of age-related neurodegenerative diseases.

In contrast to the phosphoproteome, the aging synaptic O-GlcNAcome was comprised of far fewer sites that changed with age, likely owing to the naturally lower stoichiometric abundance of O-GlcNAc. Identified GO terms and pathways point to selective involvement of age-related changes in synaptic O-GlcNAcylation in glutamatergic neuronal function, known to decline in aging-sensitive brain regions including the hippocampus. Induced network modeling of the aging synaptic O-GlcNAcome revealed that targets associated with the glutamatergic synapse pathway - Grin2b, Dlgap1, Shank1, Shank2 - are also highly connected nodes within the induced protein-protein interaction network. It is noteworthy that loss of the NMDA receptor subunit Grin2b in forebrain neurons elicits impairments in hippocampal-dependent cognition, while genetic neuronal overexpression of Grin2b prevents age-related cognitive decline [41, 42]. Of particular interest for future mechanistic investigations, these proteomic analyses identified a novel site of O-GlcNAc on Grin2b at either Ser1029 or Ser1030 that declined with age. While O-GlcNAc regulates the surface

localization and function of AMPA receptors [19, 43], its role in mediating NMDA receptor activity is unknown, with clear implications for age-related cognitive decline. Relevant to age-related neurodegenerative diseases, a decrease in O-GlcNAcylation was detected on alpha synuclein, likely at site Thr72. Interestingly, O-GlcNAcylation at this site has recently been shown to block alpha synuclein aggregation and toxicity, implicating a role for O-GlcNAc in Parkinson's disease pathology [44]. More broadly, decreased protein O-GlcNAcylation has also been implicated in Alzheimer's disease [23]. Together, these proteomics data raise the possibility that alterations in synaptic O-GlcNAcylation may both drive brain aging and increase vulnerability to age-related neurodegenerative diseases.

Collectively, this study characterizes for the first time the aging synaptic phosphoproteome and O-GlcNAcome, and proposes that investigating aging-associated changes in dynamic PTMs will prove critical to the understanding of brain aging. In particular, O-GlcNAcylation is proposed as a regulator glutamatergic synaptic function during aging, and therefore is heavily implicated as a regulator of cognitive decline. Moreover, these findings highlight dynamic PTMs as relevant to age-related neurodegenerative disorders, including Parkinson's and Alzheimer's disease. Ultimately, these data raise the possibility of targeting site-specific PTMs as potential interventions to ameliorate age-related cognitive decline and vulnerability to neurodegenerative disorders.

Materials and Methods

Animal Models. All mouse handling and use was in accordance with institutional and ethical guidelines approved by the University of California San Francisco IACUC. The following mouse lines were used: C57BL/6 young and aged mice (National Institutes of Aging; Taconic Biosciences). All studies were done in male mice. The numbers of mice used to result in statistically significant differences were calculated using standard power calculations with $\alpha = 0.05$ and a power of 0.8. We used an online tool (http://www.stat.uiowa.edu/~rlenth/Power/index.html) to calculate power and samples size based on experience with the respective tests, variability of the assays and inter-individual differences within groups. Mice were housed under specific pathogen-free conditions under a 12 h light-dark cycle. All experiments were randomized and blinded by an independent researcher. Researchers remained blinded throughout histological, molecular, and behavioral assessments. Groups were un-blinded at the end of each experiment upon statistical analysis.

Purification and Proteolytic digestion of Mouse Synaptosome. Cortical and hippocampal regions were isolated from fresh mouse brain tissue of either young (3 month) or aged (18-20 month) mice (n=8-9 mice per biological replicate; n=2 biological replicates for young, n=1 biological and 2 technical replicates for old). Synaptosome preparation was performed as previously described [15]. Frozen synaptosomal pellets were resuspended in 50mM ammonium bicarbonate containing 6M guanidine hydrochloride, 6X Phosphatase Inhibitor Cocktails II and III (Sigma-Aldrich), and 80mM

PUGNAc (Tocris Bioscience, Avonmouth, UK). Protein concentrations were estimated with bicinchoninic acid (BCA) protein assay (ThermoFisher Scientific, Rockford, IL). The mixture was reduced for 1 hour at 56ºC with 2mM Tris(2-carboxyethyl)phosphine hydrochloride and subsequently carbamidomethylated using 4.2 mM iodoacetamide for 45 min at room temperature in the dark. Lysates were diluted to 1M guanidine hydrochloride with 50 mM ammonium bicarbonate, pH 8.0, and equal amounts of each sample (7.3 mg) were digested overnight at 37°C with sequencing grade trypsin (ThermoFisher Scientific) at an enzyme to substrate ratio of 1:50 (w/w). Following digestion, samples were acidified with formic acid (FA) (Sigma-Aldrich), desalted using a 360-mg C18 Sep-Pak SPE cartridge (Waters), and dried to completeness using a SpeedVac concentrator (Thermo Electron).

Lectin Weak Affinity Chromatography. Glycopeptides were enriched as described previously [15, 45]. Briefly, desalted synaptosome tryptic peptides were resuspended in 500 µl LWAC buffer (100 mM Tris pH 7.5, 150 mM NaCl, 10 mM MgCl2, 10 mM CaCl2, 5% acetonitrile) and 100 µl were run over a 2.0 x 250mm POROS-WGA column at 100 µl/min under isocratic conditions with LWAC buffer and eluted with a 100 µl injection of 40mM GlcNAc. Glycopeptides were collected inline on a C18 column (Phenomenex, Torrance, CA). Enriched glycopeptides from 5 initial rounds of LWAC were eluted with 50% acetonitrile, 0.1% FA in a single 500 µl fraction, dried, and LWAC enrichment was repeated for a total of 3 enrichment steps.

Titanium Dioxide Phosphopeptide Enrichment. Peptides from LWAC flowthrough were acidified with FA and desalted with C18 reversed phase cartridges as above. Peptides were resuspended in 1.6 mL buffer B1 (200mM NaCl, 35% ACN, 0.4% TFA) and split into 4 aliquots. TiO_2 enrichment of phosphopeptides was performed on an AKTA Purifier (GE Heathcare) using an in-house packed 2 mm x 2 cm guard column with 5 µm TiO2 beads (GL Sciences). Peptides were loaded at 2mL/min in buffer B1, washed with 0.1% TFA, and phosphopeptides were eluted onto an online C18 microtrap peptide column (Michrom Bioresources) with 1M KH2PO4 pH 3.0. C18-bound phosphopeptides were washed with 0.5% ACN, 0.1% TFA, and eluted with 50% ACN, 0.1% TFA, pooled, and evaporated to dryness.

TMT labeling and High pH Reverse Phase Chromatography. LWAC enriched glycopeptide eluates from young1, young2, and aged1 were split into two aliquots. One aliquot of young 1 and young 2 and both aliquots of aged 1 were labeled using the TMT-6plex isobaric labeling system (ThermoFisher) according to the manufacturer's protocol. TiO_2-enriched phosphopeptide eluates from young1, young2, aged1, and aged2 and total proteins, represented by 200 µg of peptides from post-LWAC and TiO_2 enrichment flowthrough, were also TMT labeled. The glycopeptide labeling was as follows: Young1:TMT128, Young2:TMT129, Aged1-1:TMT130, Aged1-2:TMT131. The phosphopeptide labeling was as follows: Young1:TMT128, Young2:TMT129, Aged1:TMT130, Aged2:TMT131. The 'total protein' peptides were labeled as follows: Young1:TMT127, Young2:TMT128, Aged1:TMT129, Aged2:TMT130. Labeling efficiency and mixing ratios were checked on small aliquots of the labeling reaction on

an AB Sciex/ABI QSTAR Elite Q-TOF. TMT labeled peptides were mixed together at a 1:1:1:1 molar ratio and fractionated by high *p*H RP liquid chromatography. Glycopeptides were separated on a 1.0 × 100 mm Gemini 3µ C18 column (Phenomenex, Torrance, CA). Peptides were loaded onto the column in 20 mM NH_4OCH_3, *p*H 10 and subjected to a gradient from 1% to 21% 20mM NH_4OCH_3, *p*H10 in 50% acetonitrile over 1.1 ml, up to 62% 20mM NH_4OCH_3, *p*H10 in 50% acetonitrile over 5.4 ml with a flow rate of 80 µl/min while collecting 24 fractions. TMT-labeled phosphopeptides were separated by high pH reverse phase chromatography on the AKTA purifier with a 1 x 100mm Gemini 3um C18 column (Phenomenex). Peptides were loaded onto the column in 20mM NH_4OCH_3, pH 10 and eluted off the column over a gradient from 2% to 70% 20mM NH_4OCH_3, pH 10 in 90% ACN.TMT labeled-peptides from total proteins were fractionated on a 4.6 × 150 mm Gemini 5µ C18 column (Phenomenex) with a gradient from 1% to 9% 20mM NH_4OCH_3, *p*H10 in 90% acetonitrile over 2 min, then to 49% over 20 min and finally to 70% over 1.5 min. Forty-five fractions were collected and dried. Every other fraction was resuspended in 0.1% FA for mass spectrometry analysis.

Mass Spectrometry Analysis. All samples were analyzed on an Orbitrap Velos (Thermo Scientific, San Jose, CA) equipped with a nano-Acquity UPLC (Waters, Milford, MA). Peptides were fractionated on a 15cm x 75 µm ID 3µm C18 EASY-Spray column using a linear gradient from 2-35% solvent B over 60 min. Survey mass measurements were performed in the Orbitrap, scanning from m/z 350-2000. The 3 most abundant multiply charged ions were computer-selected for analysis by both HCD

and ETD with supplemental activation. The trigger intensity was set to 2000. Supplemental activation was enabled. The ETD fragments were measured in the linear trap, whereas HCD fragments were measured in the Orbitrap. Each LWAC enriched sample was injected twice; the first analysis selected only 2+ precursor ions and in the second analysis 2+ precursor ions were excluded. Peaklists were extracted using Proteome Discoverer 1.4. ETD data was searched against the UniProt Mus musculus database (downloaded December 1, 2015) (and concatenated with a randomized sequence for each entry) using Protein (v5.10.15). Cleavage specificity was set as tryptic, allowing for 2 missed cleavages. Carbamidomethylation of Cys and TMT6plex on lysine and the N-terminus were set as constant modifications. The required mass accuracy was 10 ppm for precursor ions and 0.8 Da for ETD fragments. Variable modifications included acetylation of protein N-termini, oxidation of Met, cyclization of N-terminal Gln, and HexNAc modification of Ser, Thr, and Asn as variable modifications. The following extended O-linked glycans on Ser or Thr: HexNAc2, HexNAcFuc, HexNAcHexFuc, HexNAcHexSA, HexNAcHexSA2, HexNAcHexSAAc, HexNAcHexSAAc2, HexNAcSA and the following extended N-linked glycans on Asn; HexNAc2, HexNAc2Fuc, HexNAc2Hex, HexNAc2Hex10, HexNAc2Hex2, HexNAc2Hex2Fuc, HexNAc2Hex3, HexNAc2Hex3Fuc, HexNAc2Hex4, HexNAc2Hex4Fuc, HexNAc2Hex5, HexNAc2Hex5Fuc, HexNAc2Hex6, HexNAc2Hex7, HexNAc2Hex8, HexNAc2Hex9, HexNAc2HexFuc, HexNAc3Hex3, HexNAc3Hex3Fuc, HexNAc3Hex4, HexNAc3Hex5, HexNAc3Hex6, HexNAc3Hex7, HexNAc4Hex3, HexNAc4Hex3Fuc, HexNAc4Hex4, HexNAc4Hex5, HexNAc4Hex5SA2, HexNAc4Hex6Fuc, HexNAc4Hex6SA, HexNAc5Hex3, HexNAc5Hex3Fuc,

HexNAc5Hex4, HexNAc5Hex4Fuc, HexNAc5Hex4NeuAc, HexNAcFuc, were set as rare variable modifications. Those modifications on Asn were permitted only within the N-linked consensus motif NX(S/T) were X cannot be Pro [46]. Three modifications per peptide were permitted. Unambiguous PTMs were determined using a minimum SLIP score of six, which corresponds to a 5% local FLR. HCD data were searched with the same parameters except that fragment ion mass accuracy was 30 ppm and the only glycans set as variable modifications were HexNAc on Asn (set as rare within the NX(S/T) motif), Ser, Thr, and as a neutral loss. Modified peptides were identified with a protein and peptide false discovery rate of 1%. O-GlcNAc and O-GalNAc modifications were differentiated based on known protein subcellular localization and HexNAc oxonium ion fragment ratios [47]. TiO_2-enriched peptides and non-enriched peptides were run and analyzed as above with the following differences. The 6 most abundant multiply charged ions were selected for HCD fragmentation and measurement in the Orbitrap. The variable modifications were the same as for the glycopeptide searches except that no glycosylation was considered and Phospho on S, T, and Y was chosen for the TiO_2-enriched samples.

TMT Mass Spectrometry Data Analysis. Data was filtered to only include peptides unique to a single protein. Quantitation of TMT data was performed by calculating ratios of reporter ion peak intensities between conditions along with variance for each ratio, and median normalized. Reporter ion peak intensities were obtained from HCD spectra. For glycopeptide analysis, when a peptide was identified by ETD only, the reporter ion peak intensities were used from the preceding HCD scan of the same precursor ion.

Peptide abundances were normalized by the median of ratio distributions. The significant age-dependent changes in the phosphorylation and O-GlcNAcylation datasets were determined using a normalized median Log_2 aged/young ratio of at least 0.5, corresponding to a 1.4 fold change with age. This cutoff corresponded to 3 times the average standard deviation of the median Log_2 aged/young ratio of all peptides with more than one data point.

Gene Ontology, Pathway, Induced Network, and Motif-x Analyses. The online PANTHER [28] platform was used to calculate gene ontology (GO) overrepresentation analyses and functional classification of pathways for the phosphorylation and O-GlcNAcylation datasets. The entire detected MS/MS dataset was used as a reference dataset for statistical overrepresentation analyses. Cutoff was $P<0.05$, and Bonferroni correction for multiple testing was used. Pathway overrepresentation analyses were calculated using ConsensusPathDB [25]. The entire detected MS/MS dataset used as a reference in both phosphorylation and O-GlcNAcylation dataset analyses. Cutoff was $P<0.05$, and p-values were corrected for multiple testing using the false discovery rate method. Sources used for pathway overrepresentation were Reactome, Wikipathways, Kegg, and Mousecyc databases. Induced network models were represented using the STRING [29] platform, and generated using curated databases, experimentally determined co-expression, text mining, gene neighborhood, gene co-occurrence, gene fusions, and protein homology. The O-GlcNAcylation network was calculated using all proteins with significant changes in O-GlcNAcylation. The representative induced network model for the phosphorylation dataset was produced using targets from the

highest overrepresented pathway and the highest confidence interaction score, given the size of the dataset. An increase in line thickness between nodes denotes an increase in relative interaction confidence, as represented by the STRING platform. Phosphorylation motifs were calculated using motif-x [26, 27]. Analysis was performed on sequences 11 amino acids in length centered on unambiguous sites of phosphorylation (S, T, or Y). Peptides were separated into mini datasets for analysis by phosphorylated amino acid type, and by direction of change with age. The background dataset for each run included all single unambiguous phosphorylation sites in the synaptosome for S, T, or Y, extended from the mouse IPI database, with occurrences set to 20 and significance cutoff set to 0.000001.

Data and statistical analysis. Graphed data are expressed as mean ± SEM. Statistical analysis was performed with Prism 5.0 software (GraphPad Software). Means between two groups were compared with two-tailed, unpaired Student's t-test. Comparisons of means from multiple groups with each other or against one control group were analyzed with 2-way ANOVA and Bonferroni post hoc tests. All histology, electrophysiology and behavior experiments conducted were done in a randomized and blinded fashion. For each experiment, the overall size of the experimental groups corresponded to distinct animals. Unique samples were not measured repeatedly within the same characterization of a given cohort.

References

1. Geinisman, Y., *Structural synaptic modifications associated with hippocampal LTP and behavioral learning.* Cereb Cortex, 2000. **10**(10): p. 952-62.
2. Oh, M.M., et al., *Altered calcium metabolism in aging CA1 hippocampal pyramidal neurons.* J Neurosci, 2013. **33**(18): p. 7905-11.
3. Jurado, S., *AMPA Receptor Trafficking in Natural and Pathological Aging.* Front Mol Neurosci, 2017. **10**: p. 446.
4. Hara, Y., et al., *Synaptic distributions of GluA2 and PKMzeta in the monkey dentate gyrus and their relationships with aging and memory.* J Neurosci, 2012. **32**(21): p. 7336-44.
5. Yang, Y.J., et al., *Cognitive decline is associated with reduced surface GluR1 expression in the hippocampus of aged rats.* Neurosci Lett, 2015. **591**: p. 176-81.
6. Geinisman, Y., L. de Toledo-Morrell, and F. Morrell, *Loss of perforated synapses in the dentate gyrus: morphological substrate of memory deficit in aged rats.* Proc Natl Acad Sci U S A, 1986. **83**(9): p. 3027-31.
7. Nicholson, D.A., et al., *Reduction in size of perforated postsynaptic densities in hippocampal axospinous synapses and age-related spatial learning impairments.* J Neurosci, 2004. **24**(35): p. 7648-53.
8. Markham, J.A., et al., *Sexually dimorphic aging of dendritic morphology in CA1 of hippocampus.* Hippocampus, 2005. **15**(1): p. 97-103.
9. Bloss, E.B., et al., *Evidence for reduced experience-dependent dendritic spine plasticity in the aging prefrontal cortex.* J Neurosci, 2011. **31**(21): p. 7831-9.

10. VanGuilder, H.D., et al., *Aging alters the expression of neurotransmission-regulating proteins in the hippocampal synaptoproteome.* J Neurochem, 2010. **113**(6): p. 1577-88.

11. Sato, Y., et al., *Comparison of hippocampal synaptosome proteins in young-adult and aged rats.* Neurosci Lett, 2005. **382**(1-2): p. 22-6.

12. Vegh, M.J., et al., *Hippocampal extracellular matrix levels and stochasticity in synaptic protein expression increase with age and are associated with age-dependent cognitive decline.* Mol Cell Proteomics, 2014. **13**(11): p. 2975-85.

13. Norris, C.M., S. Halpain, and T.C. Foster, *Alterations in the balance of protein kinase/phosphatase activities parallel reduced synaptic strength during aging.* J Neurophysiol, 1998. **80**(3): p. 1567-70.

14. Kempsell, A.T. and L.A. Fieber, *Age-related deficits in synaptic plasticity rescued by activating PKA or PKC in sensory neurons of Aplysia californica.* Front Aging Neurosci, 2015. **7**: p. 173.

15. Trinidad, J.C., et al., *Global identification and characterization of both O-GlcNAcylation and phosphorylation at the murine synapse.* Mol Cell Proteomics, 2012. **11**(8): p. 215-29.

16. Milanesi, L., et al., *Systematic analysis of human kinase genes: a large number of genes and alternative splicing events result in functional and structural diversity.* BMC Bioinformatics, 2005. **6 Suppl 4**: p. S20.

17. Esteban, J.A., et al., *PKA phosphorylation of AMPA receptor subunits controls synaptic trafficking underlying plasticity.* Nat Neurosci, 2003. **6**(2): p. 136-43.

18. Verstegen, A.M., et al., *Phosphorylation of synapsin I by cyclin-dependent kinase-5 sets the ratio between the resting and recycling pools of synaptic vesicles at hippocampal synapses.* J Neurosci, 2014. **34**(21): p. 7266-80.

19. Kanno, T., et al., *Regulation of AMPA receptor trafficking by O-glycosylation.* Neurochem Res, 2010. **35**(5): p. 782-8.

20. Skorobogatko, Y., et al., *O-linked beta-N-acetylglucosamine (O-GlcNAc) site thr-87 regulates synapsin I localization to synapses and size of the reserve pool of synaptic vesicles.* J Biol Chem, 2014. **289**(6): p. 3602-12.

21. Lagerlof, O., G.W. Hart, and R.L. Huganir, *O-GlcNAc transferase regulates excitatory synapse maturity.* Proc Natl Acad Sci U S A, 2017. **114**(7): p. 1684-1689.

22. Tallent, M.K., et al., *In vivo modulation of O-GlcNAc levels regulates hippocampal synaptic plasticity through interplay with phosphorylation.* J Biol Chem, 2009. **284**(1): p. 174-81.

23. Wang, A.C., et al., *Loss of O-GlcNAc glycosylation in forebrain excitatory neurons induces neurodegeneration.* Proc Natl Acad Sci U S A, 2016. **113**(52): p. 15120-15125.

24. Su, C. and T.L. Schwarz, *O-GlcNAc Transferase Is Essential for Sensory Neuron Survival and Maintenance.* J Neurosci, 2017. **37**(8): p. 2125-2136.

25. Kamburov, A., et al., *ConsensusPathDB: toward a more complete picture of cell biology.* Nucleic Acids Res, 2011. **39**(Database issue): p. D712-7.

26. Schwartz, D. and S.P. Gygi, *An iterative statistical approach to the identification of protein phosphorylation motifs from large-scale data sets.* Nat Biotechnol, 2005. **23**(11): p. 1391-8.

27. Chou, M.F. and D. Schwartz, *Biological sequence motif discovery using motif-x.* Curr Protoc Bioinformatics, 2011. **Chapter 13**: p. Unit 13 15-24.

28. Mi, H., et al., *PANTHER version 11: expanded annotation data from Gene Ontology and Reactome pathways, and data analysis tool enhancements.* Nucleic Acids Res, 2017. **45**(D1): p. D183-D189.

29. Szklarczyk, D., et al., *The STRING database in 2017: quality-controlled protein-protein association networks, made broadly accessible.* Nucleic Acids Res, 2017. **45**(D1): p. D362-D368.

30. Amanchy, R., et al., *A curated compendium of phosphorylation motifs.* Nat Biotechnol, 2007. **25**(3): p. 285-6.

31. Warsow, G., et al., *PodNet, a protein-protein interaction network of the podocyte.* Kidney Int, 2013. **84**(1): p. 104-15.

32. Moutin, E., et al., *The stoichiometry of scaffold complexes in living neurons - DLC2 functions as a dimerization engine for GKAP.* J Cell Sci, 2014. **127**(Pt 16): p. 3451-62.

33. Stephens, M.L., et al., *Age-related changes in glutamate release in the CA3 and dentate gyrus of the rat hippocampus.* Neurobiol Aging, 2011. **32**(5): p. 811-20.

34. Chalkley, R.J., et al., *Identification of protein O-GlcNAcylation sites using electron transfer dissociation mass spectrometry on native peptides.* Proc Natl Acad Sci U S A, 2009. **106**(22): p. 8894-9.

35. Vosseller, K., et al., *O-linked N-acetylglucosamine proteomics of postsynaptic density preparations using lectin weak affinity chromatography and mass spectrometry.* Mol Cell Proteomics, 2006. **5**(5): p. 923-34.

36. Wells, L., et al., *Mapping sites of O-GlcNAc modification using affinity tags for serine and threonine post-translational modifications.* Mol Cell Proteomics, 2002. **1**(10): p. 791-804.

37. Foster, T.C. and C.M. Norris, *Age-associated changes in Ca(2+)-dependent processes: relation to hippocampal synaptic plasticity.* Hippocampus, 1997. **7**(6): p. 602-12.

38. Zhang, G., et al., *Hypothalamic programming of systemic ageing involving IKK-beta, NF-kappaB and GnRH.* Nature, 2013. **497**(7448): p. 211-6.

39. Pigino, G., et al., *Disruption of fast axonal transport is a pathogenic mechanism for intraneuronal amyloid beta.* Proc Natl Acad Sci U S A, 2009. **106**(14): p. 5907-12.

40. Lee, G., et al., *Casein kinase II-mediated phosphorylation regulates alpha-synuclein/synphilin-1 interaction and inclusion body formation.* J Biol Chem, 2004. **279**(8): p. 6834-9.

41. Clayton, D.A., et al., *A hippocampal NR2B deficit can mimic age-related changes in long-term potentiation and spatial learning in the Fischer 344 rat.* J Neurosci, 2002. **22**(9): p. 3628-37.

42. Cao, X., et al., *Maintenance of superior learning and memory function in NR2B transgenic mice during ageing.* Eur J Neurosci, 2007. **25**(6): p. 1815-22.

43. Taylor, E.W., et al., *O-GlcNAcylation of AMPA receptor GluA2 is associated with a novel form of long-term depression at hippocampal synapses.* J Neurosci, 2014. **34**(1): p. 10-21.

44. Marotta, N.P., et al., *O-GlcNAc modification blocks the aggregation and toxicity of the protein alpha-synuclein associated with Parkinson's disease.* Nat Chem, 2015. **7**(11): p. 913-20.

45. Kim, S., et al., *Schwann Cell O-GlcNAc Glycosylation Is Required for Myelin Maintenance and Axon Integrity.* J Neurosci, 2016. **36**(37): p. 9633-46.

46. Pless, D.D. and W.J. Lennarz, *Enzymatic conversion of proteins to glycoproteins.* Proc Natl Acad Sci U S A, 1977. **74**(1): p. 134-8.

47. Halim, A., et al., *Assignment of saccharide identities through analysis of oxonium ion fragmentation profiles in LC-MS/MS of glycopeptides.* J Proteome Res, 2014. **13**(12): p. 6024-32.

Chapter 3

Loss of excitatory neuronal Ogt reduces hippocampal O-GlcNAcylation and recapitulates cellular and cognitive hallmarks of aging

Elizabeth G. Wheatley[1,2], Eddy Albarran[3,4], Cedric E. Snethlage[1], Gregor Bieri[1,3], Jun B. Ding[3,4], Saul A. Villeda[1,2,5,6]

1. Department of Anatomy, University of California San Francisco, San Francisco, California 94143, USA
2. Developmental and Stem Cell Biology Graduate Program, University of California San Francisco, San Francisco, California 94143, USA
3. Neuroscience IDP Program, Stanford University School of Medicine, Stanford, California 94305, USA
4. Department of Neurosurgery, Stanford University School of Medicine, Palo Alto, CA 94304, USA
5. Department of Physical Therapy and Rehabilitation Science, University of California San Francisco, San Francisco, California 94143, USA
6. The Eli and Edythe Broad Center for Regeneration Medicine and Stem Cell Research, San Francisco, California 94143, USA

Author contributions:

E.G.W. and S.A.V. developed concept and designed experiments. E.G.W. collected and analyzed data. E.G.W. performed histological and biochemical studies. E.A. and J.B.D performed electrophysiological studies. E.G.W., C.E.S. and S.A.V. performed cognitive studies. E.G.W. and G.B. generated viral constructs. E.G.W. and G.B generated schematics. S.A.V supervised all aspects of this project.

Abstract

Aging elicits impairments in learning and memory, largely attributed to age-related changes in excitatory neurons of brain regions such as the hippocampus. Recent work has identified a dynamic form of intracellular protein glycosylation called O-linked N-Acetylglucosamine (O-GlcNAc) as a regulator of excitatory neuronal function. It has remained unclear, however, how O-GlcNAc may regulate aspects of neuronal and cognitive aging. A decrease in O-GlcNAc and O-GlcNAc Transferase (Ogt), the enzyme that adds O-GlcNAc to proteins, was detected in the hippocampus of aging mice. To investigate a role for O-GlcNAc in regulating phenotypes of hippocampal aging, a temporally controlled conditional knockout mouse was generated to ablate Ogt in adult excitatory forebrain neurons. The findings indicate that loss of Ogt and reduced O-GlcNAcylation elicit alterations in neuronal molecular, synaptic, and cognitive function, many of which are reminiscent of phenotypes observed during aging. Furthermore, this study proposes that reduced hippocampal O-GlcNAc during aging is a driver of hallmarks like synaptic loss and impaired learning and memory.

Introduction

Recent work has highlighted O-linked N-Acetylglucosamine (O-GlcNAc), a uniquely dynamic form of intracellular post-translational glycosylation, as an attractive target for regulating neuronal function during aging. The addition of O-GlcNAc to serine or threonine residue of proteins is catalyzed by an enzyme called O-GlcNAc Transferase (Ogt), and is removed from proteins by an enzyme called O-GlcNAcase (Oga). O-GlcNAc has been linked to lifespan in *C. elegans*, with loss of Ogt shortening lifespan and promoting early aging phenotypes [1, 2]. In excitatory neurons, Ogt knockout during early post-natal development elicits neuronal cell death, neurodegenerative phenotypes, and impaired contextual memory in mice [3, 4]. At the synaptic level, O-GlcNAc has been attributed a role for mediating the structure and formation of excitatory neuronal synapses *in vitro* [5]. Additionally, loss of Ogt in hypothalamic neurons elicits a decrease in post-synaptic current, suggesting O-GlcNAc plays a role in mediating synaptic function [6]. In support of this, pharmacological approaches have linked O-GlcNAc to long-term potentiation (LTP) and long term depression (LTD), to two counteracting synaptic processes both critical for proper memory formation [7, 8].

Collectively, the literature supports a role for O-GlcNAc in mediating features of excitatory neuronal and synaptic function. Studies involving the hippocampus demonstrate robust neurodegenerative phenotypes upon loss of Ogt, but have utilized a non-temporally inducible knockout model that may not exclude contributions from early post-natal development [3, 4]. To date, roles for O-GlcNAc in regulating excitatory neuronal and cognitive function in the developmentally mature hippocampus, and in the context of aging, have not been investigated.

Thus, in this study, Ogt and O-GlcNAc are investigated in the adult and aging hippocampus, given this brain region demonstrates stereotypic alterations in neuronal and synaptic function that coincide with age-related cognitive decline (see Chapter 1). This study demonstrates necessary roles for Ogt and O-GlcNAc in maintaining mature adult excitatory neuronal, synaptic, and cognitive functions. Furthermore, loss of excitatory neuronal Ogt and reduction of O-GlcNAc recapitulate many aging-related phenotypes *in vivo*. These findings propose that alterations in neuronal O-GlcNAcylation promote synaptic and cognitive impairments in the aging brain.

Results

Aging elicits a decrease in hippocampal protein O-GlcNAcylation

To begin this investigation, protein O-GlcNAcylation and Ogt expression were profiled in the hippocampus during aging. Hippocampal tissue was isolated from young (3 month old) or aged (18-24 month old) wild type mice and profiled using western blot analysis. A decrease in global protein O-GlcNAcylation, as well as a decrease in Ogt protein levels were both observed in aged hippocampi (Figure 1A,B). Collectively, the literature supports a role for O-GlcNAc in regulating excitatory neuronal function, and the data herein demonstrate aging elicits decreased O-GlcNAcylation and Ogt, in addition to hippocampal impairments (Chapter 1). Therefore, the question was raised as to whether reducing O-GlcNAcylation, specifically in excitatory neurons of the adult hippocampus, could elicit features of brain aging in a young mouse.

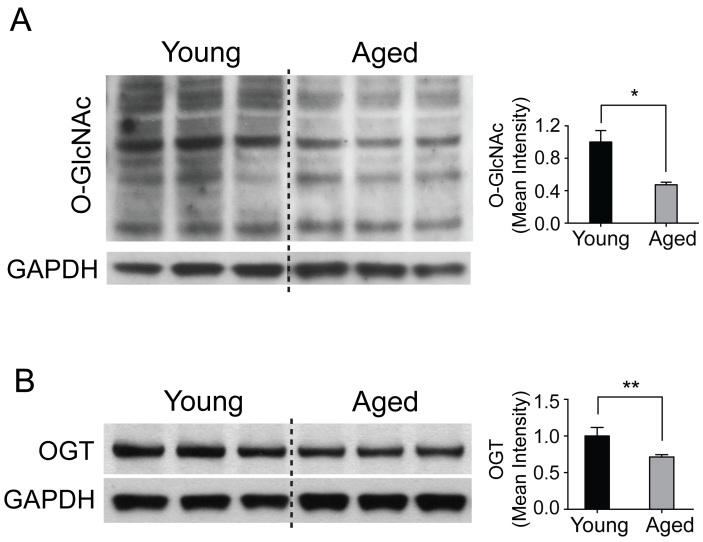

Figure 1. Aging elicits a decrease in O-GlcNAcylation and Ogt protein levels in the hippocampus. (A) Representative bands showing global protein O-GlcNAcylation, assessed in whole hippocampal lysates from young (3 month old) and aged (24 month old) mice. Quantification of global protein O-GlcNAcylation mean intensity, normalized to GAPDH as a loading control and shown as fold change from young. *n* = 3-4 mice per group. (B) Representative bands of Ogt protein, assessed in whole hippocampal lysates from young (3 month old) and aged (18 month old) mice. Quantification of Ogt mean intensity, normalized to GAPDH as a loading control and shown as fold change from young. *n* = 4 mice per group. Data represented as mean ± SEM *P<0.05; **P<0.01; t-test.

Decreased excitatory neuronal O-GlcNAcylation elicits aging-associated neuronal phenotypes *in vivo*

In order to investigate the effects of decreased neuronal O-GlcNAcylation, an *Ogt*$^{flox/y}$ mouse model was generated, carrying an inducible *CamK2a-Cre-ER*^{T2} gene in which *Ogt* is excised specifically in young adult excitatory forebrain neurons upon tamoxifen administration (Ogt-cKO mouse) (Figure 2A). Decreased Ogt and global protein O-GlcNAcylation were confirmed in hippocampal lysates of Ogt-cKO mice when compared to *Ogt*$^{flox/y}$ littermate controls (Figure 2B,C). As expected, no significant changes in Ogt and O-GlcNAc expression were detected outside of the forebrain region in the cerebellum (Figure 2D,E).

Previous work using a non-inducible mouse model, in which Ogt is excised in CamK2a-expressing neurons during early postnatal development, reports neuronal loss and increased apoptosis in the hippocampi of knockout mice during late adulthood [3, 4]. Here, hippocampal cell loss was assessed in Ogt-cKO mice using Cresyl violet staining for Nissl bodies and immunohistological staining for the apoptosis marker cleaved caspase 3. By contrast, no changes in widespread cell loss or apoptosis were detected in either CA1 or DG neuronal sub-regions upon acute conditional loss of Ogt (Figure 3A-D), in line with what is also observed in aging wild type mice (Figure 1C,D).

Next, molecular and structural changes were profiled in hippocampal neurons of Ogt-cKO and control mice by immunohistochemistry and Golgi analysis, employing the same characterizations performed on young and aged mice in Chapter 1. Phosphorylation was profiled at site Ser133 on the transcription factor Creb (pCreb), which promotes synaptic plasticity and immediate early gene (IEG) expression, and

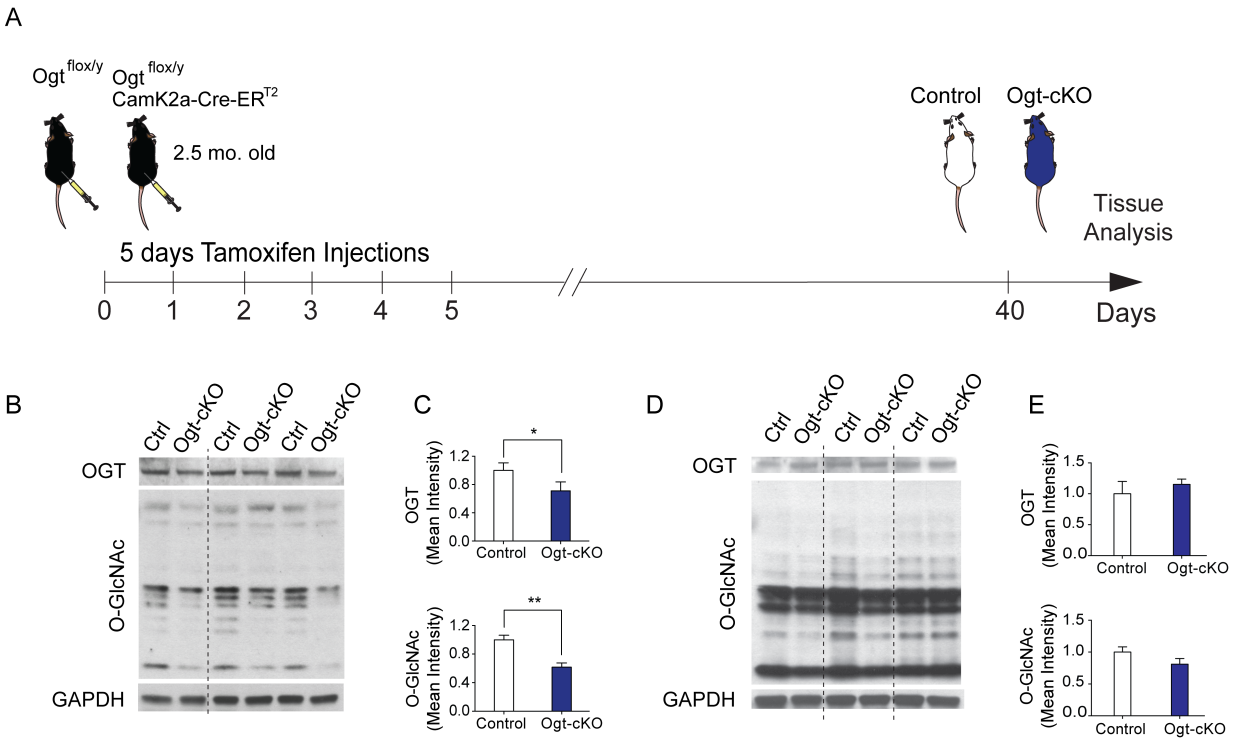

Figure 2. Generation of the Ogt-cKO mouse model. (A) Schematic depicting the timeline for the generation of and subsequent experiments using the young adult (4 month old) conditional excitatory neuron Ogt knockout mouse (Ogt-cKO). (B) Western blot of O-GlcNAc modifications and Ogt protein levels from whole hippocampal lysates of control and Ogt-cKO mice. (C) Quantification of (B) normalized to GAPDH and represented as fold change normalized to control. (D) Western blot of O-GlcNAc modifications and Ogt protein levels from whole cerebellar lysates of control and Ogt-cKO mice. (E) Quantification of (D) normalized to GAPDH and represented as fold change normalized to control. *n*=3 mice per group. Data represented as mean ± SEM *P<0.05; t-test.

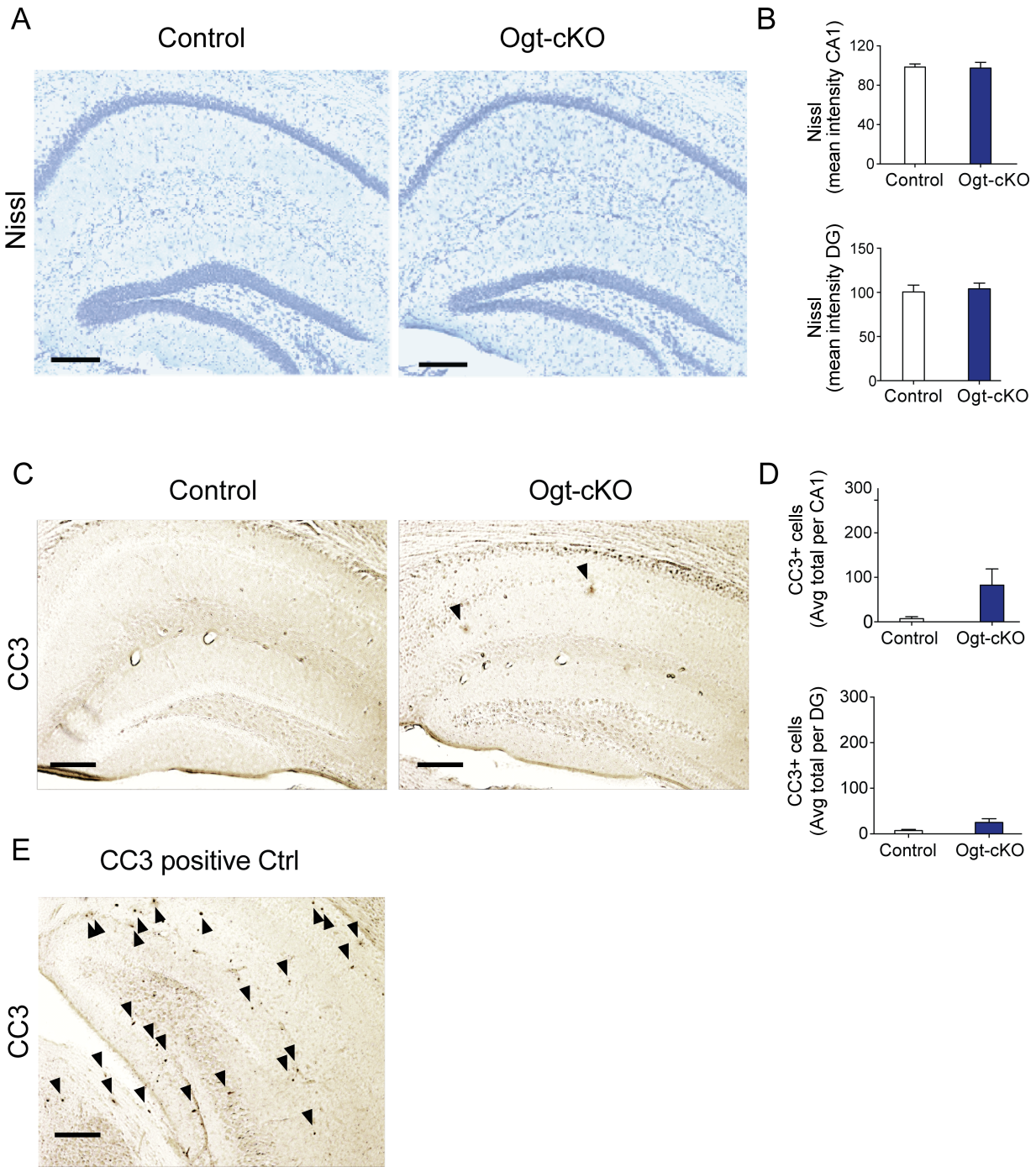
A
Control
Ogt-cKO
Nissl
B
Nissl (mean intensity CA1)
120
80
40
0
Control
Ogt-cKO
Nissl (mean intensity DG)
150
100
50
0
Control
Ogt-cKO
C
Control
Ogt-cKO
CC3
D
CC3+ cells (Avg total per CA1)
300
200
100
0
Control
Ogt-cKO
CC3+ cells (Avg total per DG)
300
200
100
0
Control
Ogt-cKO
E
CC3 positive Ctrl
CC3

Figure 3. Ogt-cKO mice do not display increased cell loss or apoptosis in the hippocampus. (A) Representative field of Nissl stain in the hippocampus of young Ogt-cKO and control mice. (B) Quantification of Nissl stain mean intensity in CA1 region of the hippocampus. (C) Representative immunohistochemical DAB stain of cleaved caspase 3 (CC3) in hippocampal regions of young control and Ogt-cKO mice. **(**D) Quantification of average total CC3+ cells in CA1 and DG neuronal sub-regions; *n* = 4 mice per group. Data represented as mean ± SEM; t-test. (E) A positive control known to have CC3+ brain cells was included to ensure the staining was accurate. Scale bars = 200 μm.

decreases with age in the hippocampus (Chapter 1; Figure 2C,D) [9, 10]. Similarly to what is observed during aging, a reduction in pCreb mean intensity was detected in neurons of both the CA1 and DG sub-regions in Ogt-cKO compared to control mice (Figure 4A,B). Additionally, cFos was profiled in the hippocampi of Ogt-cKO and control mice. cFos is an IEG downstream of Creb, a marker of neuronal activity, and also declines with age in hippocampal neurons (Chapter 1; Figure 2E,F) [11, 12]. A reduction in the number of cFos-positive activated neurons was also detected in the CA1 region of Ogt-cKO mice (Figure 4C,D). Given that pCreb and cFos regulate synaptic plasticity, the question was raised as to whether Ogt-cKO mice displayed alterations in neuronal structure at the synaptic level.

A second cohort of young Ogt-cKO and control mice was then characterized with a Golgi stain, to label the cell body and synaptic structures of mature neurons. Ogt-cKO mice displayed a reduction in the number of tertiary dendritic spines on CA1 pyramidal neurons when compared to controls (Figure 5A,B), reminiscent of CA1 neurons in the hippocampi of aging mice (Chapter 1, Figure 3A,B). Taken together these *in vivo* data indicate that decreased O-GlcNAcylation in adult excitatory neurons recapitulates certain hallmarks of neuronal molecular and synaptic aging in the adult hippocampus.

Decreased excitatory neuronal O-GlcNAcylation alters hippocampal synaptic protein expression and function

Given that histological and Golgi analyses were indicative of alterations in synaptic structure and plasticity, synaptic proteins were next assessed using western

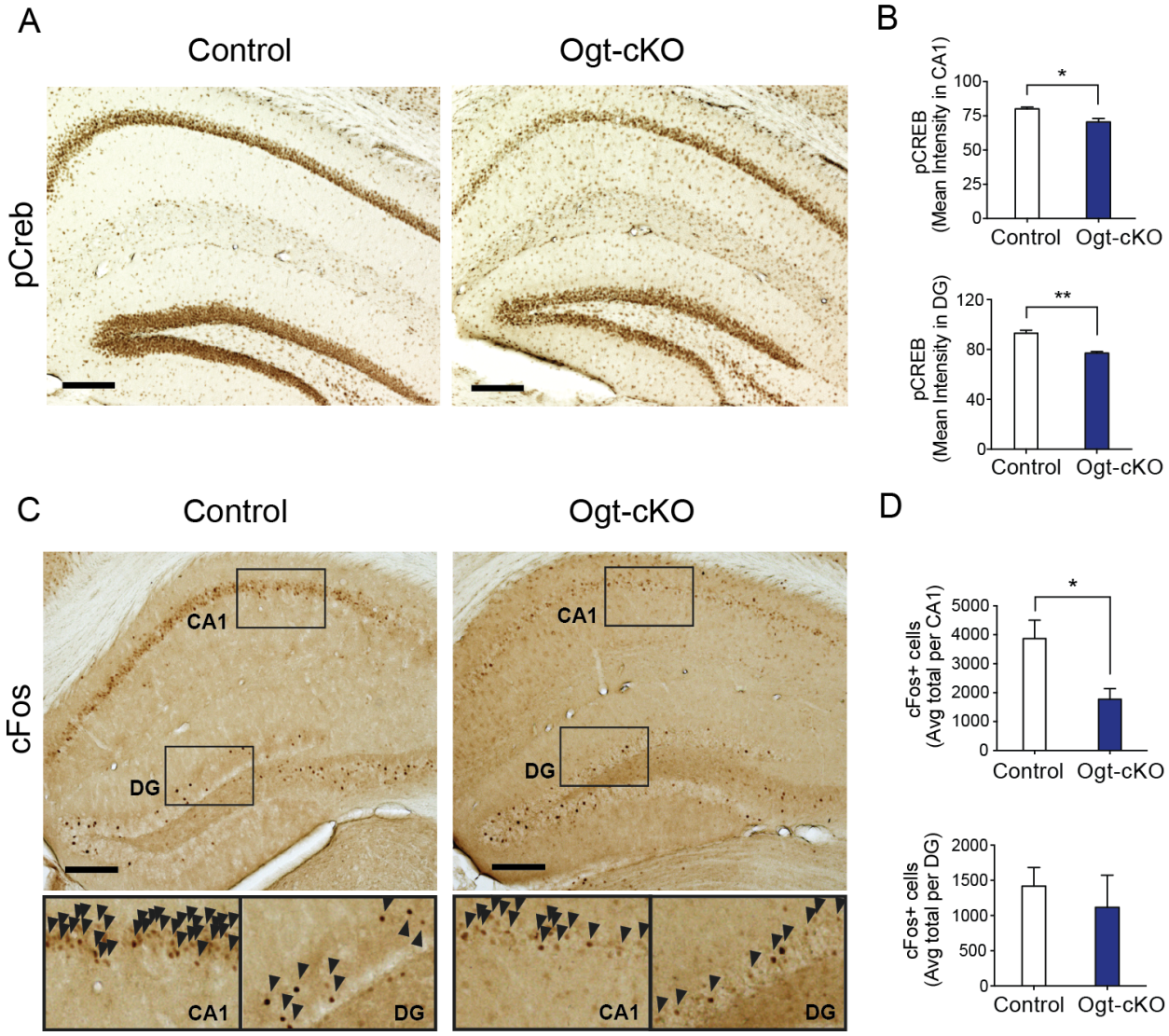

Figure 4. Decreased O-GlcNAcylation in excitatory neurons elicits aging-associated molecular changes. (A) Representative field of pCreb immunostain in the hippocampus of young Ogt-cKO and control mice. Scale bar = 200 µm. (B) Quantification of pCreb mean intensity in the DG or CA1 region, *n = 3* mice per group. (C) Representative field of cFos immunostaining in the hippocampus of young Ogt-cKO and control mice. Scale bar = 200 µm. (D) Quantification of cFos-positive cells in the CA1 region of the hippocampus of young Ogt-cKO and control mice, *n* = 4 mice per group. Data represented as mean ± SEM *P<0.05; **P<0.01; t-test (B,D).

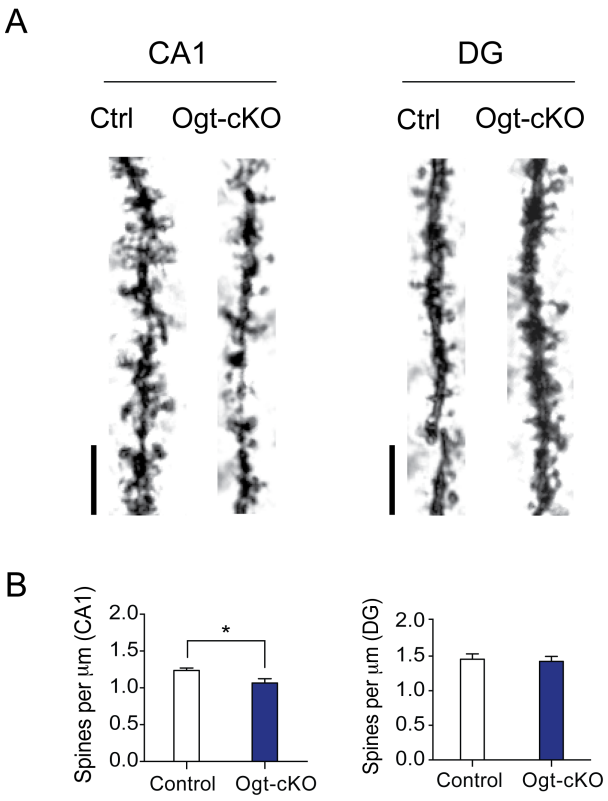

Figure 5. Decreased O-GlcNAcylation elicits reduced dendritic spine density in CA1 pyramidal neurons of Ogt-cKO mice. (A) Representative field of Golgi stain from DG granule cell neurons and CA1 pyramidal neurons in young Ogt-cKO and control mice. (B) Quantification of spine number from tertiary dendrites of DG granule cell neurons and CA1 pyramidal neurons in Ogt-cKO and control mice, *n* = 5 mice per group, *n* = 10 neurons per mouse. Data represented as mean ± SEM *P<0.05; **P<0.01; t-test.

blot analyses. Several synaptic markers that have been reported to change with age were characterized in hippocampal lysates from Ogt-cKO versus control mice. The post-synaptic scaffolding protein PSD-95, pre-synaptic vesicle endocytosis protein Synaptophysin, and vesicle release regulating protein Synapsin1 all have been reported to decline in the hippocampus with age [13, 14]. Indeed, Ogt-cKO mice displayed reduced hippocampal levels of these three proteins when compared to controls (Figure 6A,B). In addition, subunits 2A and 2B of the post-synaptic Glutamate receptor *N*-methyl-D-aspartate receptor (NMDAR) were profiled by western blot as well. A change in the ratio of NR2A/NR2B often used as an indicator for potential alterations in synaptic function [15]. A decrease the protein levels of both NR2A and NR2B, and a modest decrease in the NR2A/NR2B ratio was observed in the hippocampi of Ogt-cKO versus control mice (Figure 6A,B). Hippocampal NR2B protein does selectively decline with age, although the ratio of NR2A/NR2B typically increases with age alongside increased LTD and decreased LTP [16, 17]. Overall, Ogt-cKO mice display some changes in synaptic protein expression that are reminiscent of aging, as well as changes that collectively are suggestive of altered synaptic function.

To expand upon these findings, extracellular electrophysiological recordings were performed to measure synaptic function in hippocampal slices in a third cohort of Ogt-cKO and control mice. Electrophysiological recordings were performed specifically on Schaffer collateral projections from the CA3 to CA1 region (Figure 7A), given the CA1 demonstrated increased sensitivity to the effects of the Ogt knockout. The input-output relationship was calculated by plotting the amplitude of presynaptic volleys with the resulting slope of the evoked field excitatory post synaptic potential (fEPSP). No

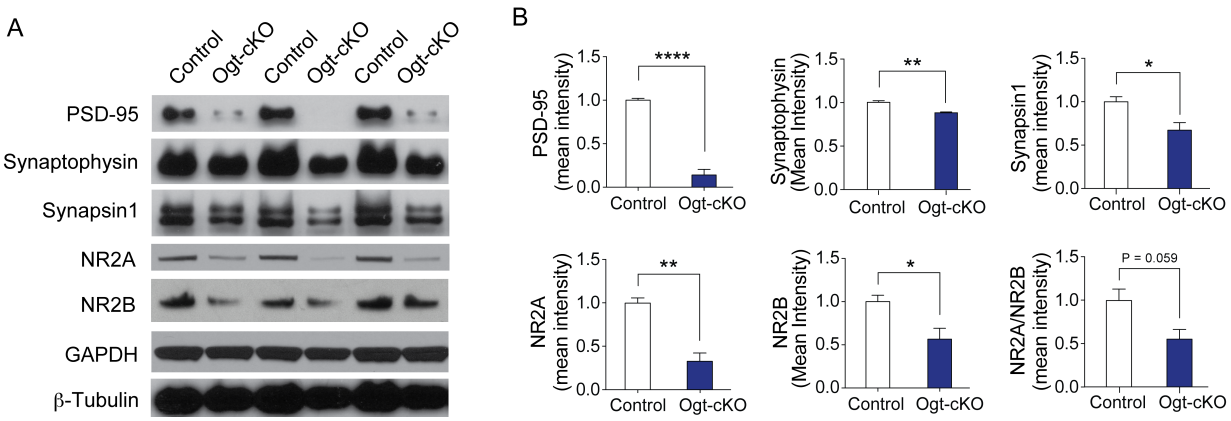

Figure 6. Decreased O-GlcNAcylation in excitatory neurons alters hippocampal synaptic protein expression. (A) Representative Western blot of synaptic proteins PSD-95, Synaptophysin, Synapsin-1, NR2A, and NR2B from whole hippocampal lysates of young Ogt-cKO and control mice. (B) Quantification of synaptic proteins, represented as fold change from control group. GAPDH and β-Tubulin used as loading controls, with PSD-95, Synapsin-1, NR2A, and NR2B normalized to GAPDH and Synaptophysin normalized to β-Tubulin. *n* = 3 mice per group. Data represented as mean ± SEM *P<0.05; **P<0.01; ****P<0.0001; t-test (B).

difference was detected, indicating there was no overall change in synaptic strength between Ogt-cKO and control mice (Figure 7B). Next, paired-pulse ratio (PPR) was measured to assess presynaptic release probability. Similarly, no significant difference was detected between control and Ogt-cKO mice (Figure 7C). These results suggest Ogt-cKO mice exhibit normal basal synaptic transmission from CA3 to CA1 compared to controls. In order to investigate long-term changes in synaptic function in response to a stimulus, LTP and LTD were measured as well. No difference was observed in LTD (Figure 7D,E), however, a modest but significant increase in LTP was detected in Ogt-cKO compared to control mice (Figure 7F,G). There was also a moderate inverse correlation between LTP and hippocampal Ogt protein expression (Figure 7H). Additionally, the increased LTP observed in Ogt-cKO mice logically follows the decrease observed in the NR2A/NR2B ratio (Figure 6A,B) [18]. These data indicate that decreased neuronal O-GlcNAcylation alters hippocampal LTP, an excitatory synaptic process that is strongly associated with memory regulation [19, 20].

Ogt-cKO mice display impaired hippocampal-dependent learning and memory

Given that alterations in synaptic structure, composition, and function were observed in Ogt-cKO mice, cognitive testing was performed to investigate the consequences of these alterations. In particular, forms of learning and memory sensitive to the effects of hippocampal aging were assessed in a separate large cohort of Ogt-cKO and control mice. Anxiety and general motor function were profiled using open field, as well as hippocampal-dependent learning and memory using RAWM and fear conditioning paradigms (Figure 8A).

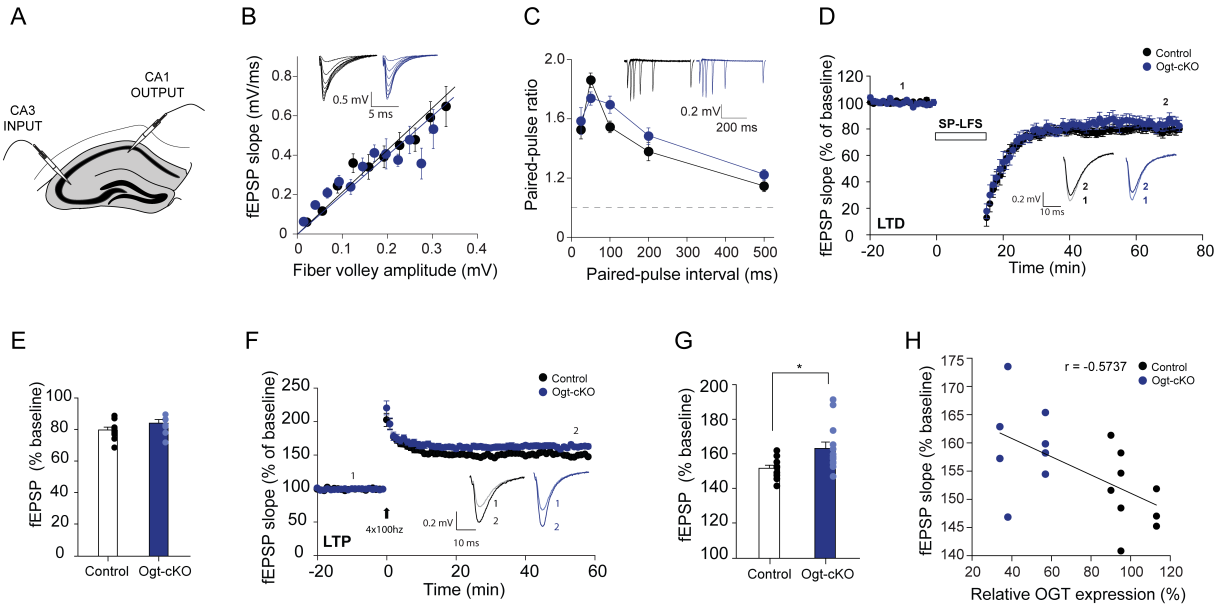

Figure 7. Decreased O-GlcNAcylation in hippocampal excitatory neurons alters long-term potentiation at CA3-CA1 Schaffer collateral projections.
(A) Schematic for electrophysiological recordings in CA3-CA1 neuronal projections, performed in *ex vivo* hippocampal slices from young adult Ogt-cKO or control mice. (B) Basal transmission of CA3-CA1 measured as the Input-output relationship between presynaptic fiber volley amplitude and the slope of the resulting fEPSP. in acute hippocampal slices from 8-10-week-old control and Ogt-cKO mice, *n* = 10 slices / 7 animals, *n* = 7 slices / 3 animals, respectively.(C) Paired-pulse facilitation measured at various timing delays. (D) LTD recordings in the CA1 region of the hippocampus. fEPSP slope is plotted as percentage of baseline average. Recordings were performed in acute hippocampal slices from 8-10-week-old control and Ogt-cKO mice, *n* = 10 slices / 7 animals, *n* = 7 slices / 3 animals, respectively) induced via 15 min single-pulse low-frequency stimulation (SP-LFS) (1hz). (E) Bar graphs summarizing the average fEPSP slopes as a percentage of baseline, measured in the last 5 min of recording. (F) LTP recordings in the CA1 region of the hippocampus of Ogt-cKO and control mice. fEPSP slope is plotted as percentage of baseline average. Electrophysiological recordings were performed in acute slices from 8-10-week-old control and OGT-cKO mice *n* = 10 slices / 6 animals, *n* = 13 slices / 7 animals, respectively, LTP was induced via 4 trains of 100hz stimulation. (G) Bar graphs summarizing the average fEPSP slopes as a percentage of baseline, measured in the last 5 min of recording. (H) LTP magnitude shows a moderate correlation with levels of Ogt protein. Ogt levels measured via western blot and plotted against average magnitude of LTP during last 5 min of recording. Data represented as mean ± SEM; *P<0.05; t-test (E,G).

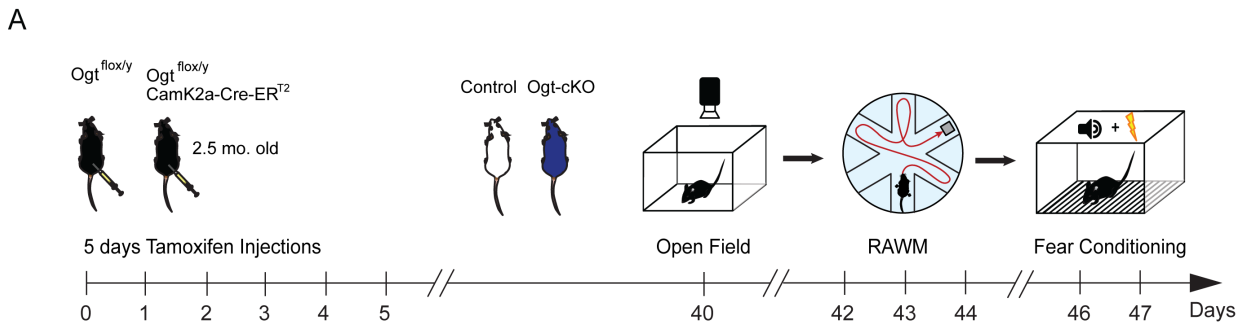
A
Ogt flox/y
Ogt flox/y CamK2a-Cre-ER T2
2.5 mo. old
Control Ogt-cKO
5 days Tamoxifen Injections
Open Field
RAWM
Fear Conditioning
0 1 2 3 4 5 40 42 43 44 46 47 Days

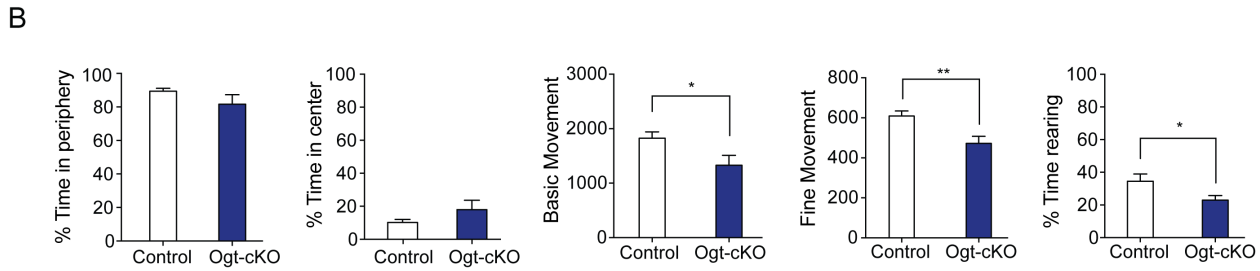
B
% Time in periphery
% Time in center
Basic Movement
Fine Movement
% Time rearing
Control Ogt-cKO

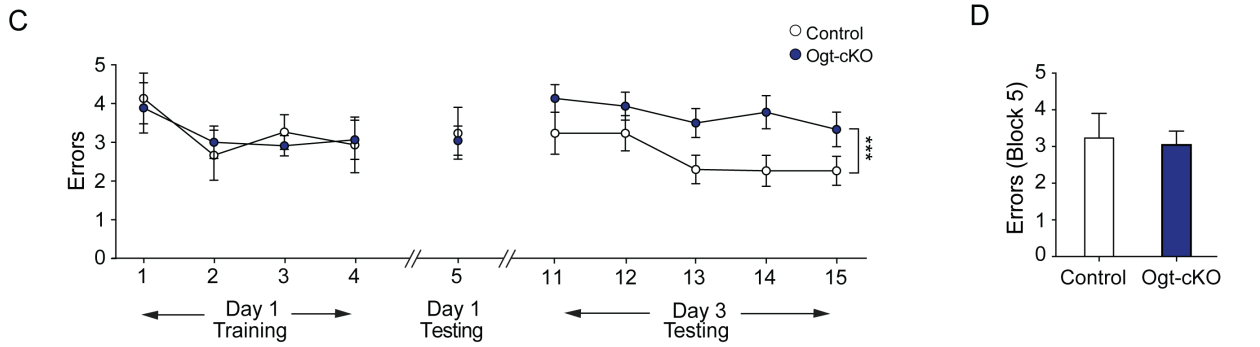
C
Control
Ogt-cKO
Errors
***
Day 1 Training
Day 1 Testing
Day 3 Testing
D
Errors (Block 5)
Control Ogt-cKO

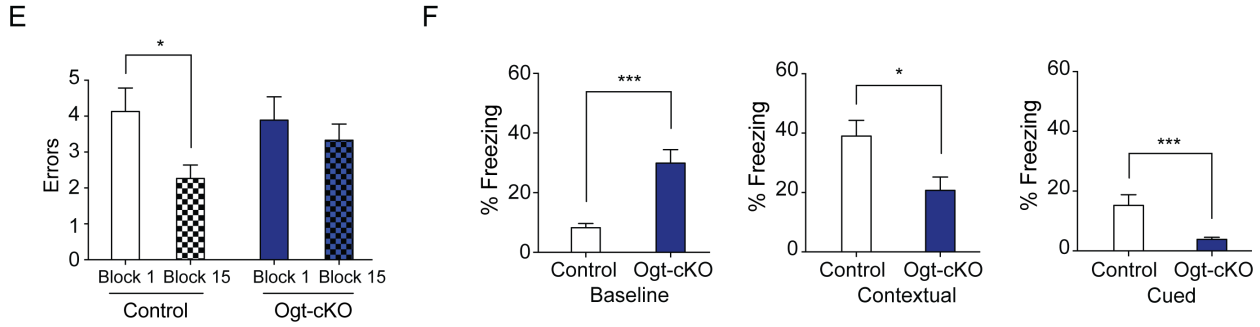
E
Errors
Block 1 Block 15 Block 1 Block 15
Control
Ogt-cKO
F
% Freezing
Control Ogt-cKO
Baseline
Contextual
Cued

Figure 8. Ogt-cKO mice display impairments in hippocampal learning and memory. (A) Schematic depicting generation of Ogt-cKO mice and subsequent cognitive testing using open field, radial arm water maze (RAWM), and fear conditioning behavioral paradigms. (B) Data from the open field paradigm depicting percent time spend in periphery and center of the field, as well as basic movements, fine movements, and rearing behavior of Ogt-cKO and control mice. Data shown are cumulative from ten minutes of testing, measured using the MotorMonitor software. (C-E) Hippocampal-dependent spatial learning and memory was assessed in Ogt-cKO and control mice using RAWM. Quantification of the number of entry errors during RAWM training and testing (C), short-term memory testing (D) and long-term learning and memory testing (E), *n* =10-15 mice per group. (F) Baseline, contextual, and cued fear memory was assessed in Ogt-cKO and control mice using fear conditioning. Baseline freezing was measured during the first two minutes of training. Freezing in contextual and cued conditions was measured 24 hours after training, *n* = 10-15 mice per group. Data represented as mean ± SEM; *P<0.05; **P<0.01; ***P<0.001; repeated measures ANOVA, column factor (C); t-test (B,D,E,F).

Ogt-cKO mice did not spend significantly more time in the periphery or center of the open field during testing, indicative of no differences in general anxiety between groups (Figure 8B). However, Ogt-cKO mice did display decreased basic and fine movements during the open field test, as well as decreased rearing (Figure 8B).

When testing spatial learning and memory using RAWM, all mice showed similar learning capacity during the training phase (Figure 8C), and no difference in short-term memory during the testing phase on day 1 (Figure 8D). However, Ogt-cKO mice committed more errors as a whole in locating the target platform during long-term memory testing compared to control animals, similarly to what is observed in aging mice (Figure 8C; Chapter 1, Figure 4C,D). In addition, Ogt-cKO mice failed to learn the task overall when comparing average errors between the first and last block (Figure 8E).

During fear conditioning, OGT-cKO mice exhibited elevated baseline freezing levels, consistent with the reduction in overall movement without increased anxiety that was observed during open field analyses (Figure 8B,F). When controlling for baseline freezing, Ogt-cKO mice displayed decreased freezing during contextual testing compared to controls, indicative of impairments in hippocampal dependent memory also observed in aging mice (Figure 8F; Chapter 1, Figure 4G). While not classically associated with aging, Ogt-cKO mice displayed impairments in amygdala-dependent cued fear memory as well, indicated by decreased freezing during cued testing (Figure 8F). These behavioral data demonstrate that Ogt and O-GlcNAc are necessary for maintaining hippocampal-dependent spatial and contextual learning and memory in young adult mice, and that their conditional loss elicits phenotypes that are reminiscent of hippocampal cognitive aging.

Discussion

In this study a novel investigation is performed of the role of O-GlcNAc in regulating adult excitatory neuronal function and cognition in the hippocampus. A cell-type specific and temporally controlled genetic mouse model (Ogt-cKO) is employed to mimic the age-related decline in hippocampal Ogt and O-GlcNAcylation, specifically in neurons where Ogt and O-GlcNAc are highly expressed [4]. A surprising number of aging-associated impairments were identified that are mediated by acute reduction of neuronal O-GlcNAcylation, including plasticity-related molecular impairments, decreased synaptic density, altered synaptic protein composition, and impaired spatial and contextual memory. These results reinforce the notion that alterations in neuronal function may lie at the heart of age-related cognitive decline, and propose changes in O-GlcNAcylation as a driver of synaptic and cognitive impairments in the aging brain.

O-GlcNAcylation has been linked to neurodegenerative conditions like Alzheimer's disease [21], yet has not been attributed a role in regulating physiological aging until now. Furthermore, contradictory reports indicate that constitutive loss of Ogt in post-natal excitatory neurons elicits widespread neurodegeneration in the adult brain [4], while acute loss of adult neuronal Ogt does not affect cell death [6]. Here the role of Ogt in adult hippocampal neurons is resolved, demonstrating loss of Ogt elicits alterations reminiscent of aging-associated impairments in the absence of widespread neuronal cell death. Nevertheless, both these results and previous work frame O-GlcNAc as a neuroprotective molecule, suggesting age-related declines in O-GlcNAc may increase the susceptibility of the brain to neurodegenerative conditions.

Interestingly, some alterations in Ogt-cKO mice not classically associated with

aging were observed [22], such as a modest increase in LTP in the hippocampal CA1 region. While increased LTP is often assumed to be a correlate for cognitive enhancement, it has also been reported by independent groups in the presence of cognitive impairments, suggesting the relationship between LTP and memory regulation is more complex than previously believed [19, 20]. Notwithstanding, a more indicative measure of hippocampal function is the result of cognitive testing for spatial and contextual memory.

Impairments were observed in two distinct hippocampal-dependent tasks, indicating maintenance of excitatory neuronal Ogt and O-GlcNAc are necessary for proper hippocampal cognition. These data support the notion that age-related reduction of hippocampal Ogt and O-GlcNAc drive impairments in cognition that are observed during aging. The impairments we observed in movement, baseline, and cued freezing behavior in Ogt-cKO mice are likely due to the fact the CamK2a gene is driving Cre expression in additional forebrain regions that govern such behaviors, including the substantia nigra and amygdala [3]. While impaired movement and cued freezing behavior are not observed in normal aging mice, it is not clear how Ogt and O-GlcNAc change in these brain regions with age. These behavioral results, alongside reports in the hypothalamus [6], suggest Ogt and O-GlcNAc are necessary for excitatory neuronal function in several brain regions, and that age-related changes occurring in sensitive regions like the hippocampus manifest as cognitive impairments.

The question remains for future studies as to whether O-GlcNAcylation may be targeted to prevent or reverse cognitive decline in the aging brain. Reports exist that indicate enhancement of O-GlcNAcylation can rescue impairments in

neurodegenerative mouse models [23], though it is not known whether O-GlcNAc can promote enhancements outside of neurodegenerative conditions. Taken together, the *in vivo* data included in this study demonstrate that loss of Ogt in excitatory forebrain neurons elicits features of neuronal and synaptic aging, and demonstrates that Ogt and O-GlcNAc are necessary for maintaining aging-sensitive forms of hippocampal cognition in adult mice. These findings suggest that age-dependent alterations in hippocampal O-GlcNAcylation promote impairments in learning and memory that occur during normal aging.

Materials and methods

Animal Models. All mouse handling and use was in accordance with institutional and ethical guidelines approved by the University of California San Francisco IACUC. The following mouse lines were used: C57BL/6 young mice (The Jackson Laboratory), C57BL/6 young and aged mice (National Institutes of Aging; Taconic Biosciences), OGTfloxed (The Jackson Laboratory line 004860) CamK2a-CreERT2 (The Jackson Laboratory line 012362). All studies were done in male mice. The numbers of mice used to result in statistically significant differences were calculated using standard power calculations with $\alpha = 0.05$ and a power of 0.8. We used an online tool (http://www.stat.uiowa.edu/~rlenth/Power/index.html) to calculate power and samples size based on experience with the respective tests, variability of the assays and inter-individual differences within groups. Mice were housed under specific pathogen-free conditions under a 12 h light-dark cycle. All experiments were randomized and blinded by an independent researcher. Researchers remained blinded throughout histological, molecular, and behavioral assessments. Groups were un-blinded at the end of each experiment upon statistical analysis.

Tamoxifen injections. Animals were injected via intraperitoneal injection with 180mg/kg of tamoxifen or vehicle once every 24 hours for a total of 5 injections per animal. Animals were monitored after recovery and five weeks were allowed to pass after the final injection before any analyses were performed.

Nissl Staining. Sections were cut to 40μm and mounted on superfrost plus microscope slides (ThermoFisher) and allowed to dry overnight. Slides were then soaked in 100% ethanol 3x2min each, and then immersed in cresyl violet working solution for 10 min. Slides were then dipped in 95% ethanol, soaked in 100% ethanol 2x2min, then in Citrasolv 2x2min before being cover slipped with Entellan. Mean intensity was quantified using FIJI software (Version 1.0).

Immunohistochemistry. Tissue processing and immunohistochemistry was performed on free-floating sections following standard published techniques [24]. Mice were anesthetized with ketamine, transcardially perfused with 0.9% saline, and brains removed and fixed in phosphate-buffered 4% paraformaldehyde for 48h before cryoprotection with 30% sucrose. Free floating coronal sections (40 μm) were incubated overnight with either rabbit anti-Cleaved Caspase-3 (Asp175) antibody #9661 (1:400; CS Technology) or rabbit anti-c-Fos (Ab-5) (4-17) (1:10,000; Calbiochem) primary antibodies, and staining was revealed using biotinylated secondary antibodies and the ABC kit (Vector) with Diaminobenzidine (DAB, Sigma-Aldrich). Sections were mounted in phosphate buffer on superfrost plus microscope slides (ThermoFisher), allowed to dry overnight, briefly soaked in Citrasolv and cover slipped with Entellan. Individual cell number was quantified for c-Fos or cleaved caspase 3 using FIJI software (Version 1.0).

Golgi Staining. After brain removal, hemispheres were immersed in 10 ml of A+B solution from FD Rapid GolgiStain™ Kit, which was prepared 24 hours prior. Solution was then changed after the initial 12 hours, and left for 10 days at room temperature in

the dark. Brains were then transferred to solution C, which was changed after the initial 24 hours, and then left for 3 days at room temperature in the dark. Brains were cut into 100 µm sections using a vibratome and were mounted onto slides coated with 0.3% gelatin in solution C. Slides were then air-dried for 24 hours in the dark. Slides were immersed into Milli-Q H_2O, 2 x 4 min with gentle shaking, then transferred to a developing solution (Solution D, E, and Milli-Q H_2O) for 10 min. Slides were then rinsed 2x4 min in Milli-Q H_2O, dehydrated through graded ethanol, immersed in Xylenes 3x4 min, and then coverslipped using Permount. All slides were then blinded and neurons imaged using a 63X oil immersion objective. Tertiary dendritic spine density was quantified using FIJI software (Version 1.0) for dendritic tracing and spine count, and results were un-blinded just prior to statistical analyses.

Western Blot Analysis. Mouse brain tissues were dissected after perfusion of animal and snap frozen and lysed in RIPA lysis buffer (500 mM Tris, pH 7.4, 150 mM NaCl, 0.5% Na deoxycholate, 1% NP40, 0.1% SDS, complete protease inhibitors 2X; Roche, and PUGNAc 100uM; Sigma). Tissue lysates were mixed with 4x NuPage LDS loading buffer (Invitrogen), loaded on a 4-12% SDS polyacrylamide gradient gel (Invitrogen), and subsequently transferred onto a nitrocellulose membrane. The blots were blocked in 5% milk in Tris-Buffered Saline with Tween (TBST) and incubated with mouse anti-O-GlcNAc antibody (CTD110.6) sc-59623 (1:500, SC Biotech), rabbit anti-OGT antibody (H-300) sc-32921 (1:1000, SC Biotech), rabbit anti-PSD-95 antibody #2507 (1:300; CS Technology), rabbit anti-NR2B ab65783 (1:1000, Abcam), rabbit anti-synapsin-1 ab18814 (1:1000, Abcam), mouse anti-synaptophysin (SY38) MAB5258 (1:1000, EMD

Millipore), mouse anti-GAPDH (6C5) ab8245 (1:10,000, Abcam), and mouse anti-β-tubulin (TUJ1) 801201 (1:1000, BioLegend). For cell culture experiments, cells were gently washed 2x with cold PBS and then lysed directly in RIPA lysis buffer. Horseradish peroxidase-conjugated secondary antibodies and an ECL kit (GE Healthcare/Amersham Pharmacia Biotech) were used to detect protein signals. Multiple exposures were taken to select images within the dynamic range of the film (GE Healthcare Amersham HyperfilmTM ECL). Selected films were scanned (300 dpi) and quantified using FIJI software (Version 1.0). GAPDH or β-tubulin bands were used for normalization.

Slice Electrophysiology. Coronal brain slices (300 μm) containing hippocampus were prepared from 8-10 week old WT and OGT cKO littermate mice. Mice were anesthetized with isoflurane, decapitated, and the brain was quickly removed and transferred to ice-cold artificial cerebrospinal fluid (ACSF) containing 125 mM NaCl, 2.5 mM KCl, 1.25 mM NaH2PO4, 25 mM NaHCO3, 15 mM glucose, 2 mM CaCl2, and 1 mM MgCl2, oxygenated with 95% O2 and 5% CO2 (300-305 mOsm, pH 7.4). Acute brain slices containing hippocampus were cut with a vibratome (VT1200S, Leica) and transferred to an incubation chamber containing ACSF at 34 °C for 30 min and then to a recovery chamber containing ACSF at room temperature for 30 min. Before recording, coronal slices were hemisected and hippocampi dissected before being transferred to a submerged recording chamber perfused with ACSF at a rate of 2~3 ml/min at 30 °C. Brain slices were recorded within 4 hours after recovery. CA1 field potential were evoked by Schaffer collateral electrical stimulation, recorded using broken tip

borosilicate glass pipettes filled with ACSF. Signals were acquired using a Multiclamp 700B, filtered at 2kHz, and digitized at 10 kHz. After recording a stable baseline for at least 20 min, LTP was induced by 20 hz presentation of 4 trains (each consisting of 10 pulses at 100 hz), and LTD by a single-pulse, low-frequency stimulation (SP-LFS) (900 pulses at 1 hz). Recorded data were monitored online using WinLTP and WinWCP and analyzed offline using MATLAB and Prism.

Radial Arm Water Maze. Paradigm followed previously described protocol [25]. The goal arm location containing a platform remains constant throughout the training and testing phase, while the start arm is changed during each trial. Entry into an incorrect arm is scored as an error, and errors are averaged over training blocks (three consecutive trials). On day one during the training phase, mice are trained for 15 trials, with trials alternating between a visible and hidden platform. Every 3 trials are counted as one block of training. Prior to the final 3 trials of day 1 (block 5), the mice are given an extended break, and short-term memory is then tested using three consecutive hidden platform trials. On subsequent days during the testing phase, mice are tested for 15 trials per day with a hidden platform. All behavior is performed double blinded.

Contextual Fear Conditioning. Paradigm follows previously published techniques [26]. Mice learned to associate the environmental context (fear conditioning chamber) with an aversive stimulus (mild foot shock; unconditioned stimulus, US) enabling testing for hippocampal-dependent contextual fear conditioning. The mild foot shock was paired with a light and tone cue (conditioned stimulus, CS) in order to also assess amygdala-

dependent cued fear conditioning. Conditioned fear was displayed as freezing behavior. Specific training parameters are as follows: tone duration is 30 seconds; level is 70 dB, 2 kHz; shock duration is 2 seconds; intensity is 0.6 mA. On day 1 each mouse was placed in a fear-conditioning chamber and allowed to explore for 2 minutes before delivery of a 30-second tone (70 dB) ending with a 2-second foot shock (0.6mA). Two minutes later, a second CS-US pair was delivered. On day 2 each mouse was first place in the fear- conditioning chamber containing the same exact context, but with no administration of a CS or foot shock. Freezing was analyzed for 1-3 minutes. One hour later, the mice were placed in a new context containing a different odor, cleaning solution, floor texture, chamber walls and shape. Animals were allowed to explore for 2 minutes before being re-exposed to the CS. Freezing was analyzed for 1-3 minutes. Freezing was measured using a FreezeScan video tracking system and software (Cleversys, Inc). All behavior is performed double blinded.

Data and statistical analysis. Graphed data are expressed as mean ± SEM. Statistical analysis was performed with Prism 5.0 software (GraphPad Software). Means between two groups were compared with two-tailed, unpaired Student's t-test. Comparisons of means from multiple groups with each other or against one control group were analyzed with 2-way ANOVA and Bonferroni post hoc tests. All histology, electrophysiology and behavior experiments conducted were done in a randomized and blinded fashion. For each experiment, the overall size of the experimental groups corresponded to distinct animals. Unique samples were not measured repeatedly within the same characterization of a given cohort.

References

1. Love, D.C., et al., *Dynamic O-GlcNAc cycling at promoters of Caenorhabditis elegans genes regulating longevity, stress, and immunity.* Proceedings of the National Academy of Sciences of the United States of America, 2010. **107**(16): p. 7413-7418.
2. Wang, P., et al., *O-GlcNAc cycling mutants modulate proteotoxicity in Caenorhabditis elegans models of human neurodegenerative diseases.* Proc Natl Acad Sci U S A, 2012. **109**(43): p. 17669-74.
3. Wang, X., et al., *Distribution of CaMKIIalpha expression in the brain in vivo, studied by CaMKIIalpha-GFP mice.* Brain Res, 2013. **1518**: p. 9-25.
4. Wang, A.C., et al., *Loss of O-GlcNAc glycosylation in forebrain excitatory neurons induces neurodegeneration.* Proc Natl Acad Sci U S A, 2016. **113**(52): p. 15120-15125.
5. Lagerlof, O., G.W. Hart, and R.L. Huganir, *O-GlcNAc transferase regulates excitatory synapse maturity.* Proc Natl Acad Sci U S A, 2017. **114**(7): p. 1684-1689.
6. Lagerlof, O., et al., *The nutrient sensor OGT in PVN neurons regulates feeding.* Science, 2016. **351**(6279): p. 1293-6.
7. Tallent, M.K., et al., *In vivo modulation of O-GlcNAc levels regulates hippocampal synaptic plasticity through interplay with phosphorylation.* J Biol Chem, 2009. **284**(1): p. 174-81.

8. Taylor, E.W., et al., *O-GlcNAcylation of AMPA receptor GluA2 is associated with a novel form of long-term depression at hippocampal synapses.* J Neurosci, 2014. **34**(1): p. 10-21.

9. Sakamoto, K., K. Karelina, and K. Obrietan, *CREB: a multifaceted regulator of neuronal plasticity and protection.* J Neurochem, 2011. **116**(1): p. 1-9.

10. Villeda, S.A., et al., *Young blood reverses age-related impairments in cognitive function and synaptic plasticity in mice.* Nat Med, 2014.

11. Gandolfi, D., et al., *Activation of the CREB/c-Fos Pathway during Long-Term Synaptic Plasticity in the Cerebellum Granular Layer.* Front Cell Neurosci, 2017. **11**: p. 184.

12. Castellano, J.M., et al., *Human umbilical cord plasma proteins revitalize hippocampal function in aged mice.* Nature, 2017. **544**(7651): p. 488-492.

13. VanGuilder, H.D., et al., *Aging alters the expression of neurotransmission-regulating proteins in the hippocampal synaptoproteome.* J Neurochem, 2010. **113**(6): p. 1577-88.

14. Zhao, X., et al., *The effects of aging on N-methyl-D-aspartate receptor subunits in the synaptic membrane and relationships to long-term spatial memory.* Neuroscience, 2009. **162**(4): p. 933-45.

15. Massey, P.V., et al., *Differential roles of NR2A and NR2B-containing NMDA receptors in cortical long-term potentiation and long-term depression.* J Neurosci, 2004. **24**(36): p. 7821-8.

16. Cui, Z., et al., *Increased NR2A:NR2B ratio compresses long-term depression range and constrains long-term memory.* Sci Rep, 2013. **3**: p. 1036.

17. Norris, C.M., D.L. Korol, and T.C. Foster, *Increased susceptibility to induction of long-term depression and long-term potentiation reversal during aging.* J Neurosci, 1996. **16**(17): p. 5382-92.

18. Philpot, B.D., K.K. Cho, and M.F. Bear, *Obligatory role of NR2A for metaplasticity in visual cortex.* Neuron, 2007. **53**(4): p. 495-502.

19. Migaud, M., et al., *Enhanced long-term potentiation and impaired learning in mice with mutant postsynaptic density-95 protein.* Nature, 1998. **396**(6710): p. 433-9.

20. Gu, Y., et al., *Impaired conditioned fear and enhanced long-term potentiation in Fmr2 knock-out mice.* J Neurosci, 2002. **22**(7): p. 2753-63.

21. Akan, I., et al., *Nutrient-driven O-GlcNAc in proteostasis and neurodegeneration.* J Neurochem, 2018. **144**(1): p. 7-34.

22. Boric, K., et al., *Potential adaptive function for altered long-term potentiation mechanisms in aging hippocampus.* J Neurosci, 2008. **28**(32): p. 8034-9.

23. Yuzwa, S.A., et al., *Pharmacological inhibition of O-GlcNAcase (OGA) prevents cognitive decline and amyloid plaque formation in bigenic tau/APP mutant mice.* Mol Neurodegener, 2014. **9**: p. 42.

24. Luo, J., et al., *Glia-dependent TGF-beta signaling, acting independently of the TH17 pathway, is critical for initiation of murine autoimmune encephalomyelitis.* J Clin Invest, 2007. **117**(11): p. 3306-15.

25. Alamed, J., et al., *Two-day radial-arm water maze learning and memory task; robust resolution of amyloid-related memory deficits in transgenic mice.* Nat Protoc, 2006. **1**(4): p. 1671-9.

26. Raber, J., et al., *Irradiation enhances hippocampus-dependent cognition in mice deficient in extracellular superoxide dismutase.* Hippocampus, 2011. **21**(1): p. 72-80.

Chapter 4

Investigating the role of O-GlcNAc in enhancing cognitive function

Elizabeth G. Wheatley[1,2], Gregor Bieri[1,3], Saul A. Villeda[1,2,4]

1. Department of Anatomy, University of California San Francisco, San Francisco, California 94143, USA
2. Developmental and Stem Cell Biology Graduate Program, University of California San Francisco, San Francisco, California 94143, USA
3. Neuroscience IDP Program, Stanford University School of Medicine, Stanford, California 94305, USA
4. The Eli and Edythe Broad Center for Regeneration Medicine and Stem Cell Research, San Francisco, California 94143, USA

Author contributions:

E.G.W. and S.A.V. developed concept and designed experiments. E.G.W. collected and analyzed data. E.G.W. performed histological and biochemical studies. E.G.W. performed all surgeries and cognitive studies. E.G.W. and G.B. generated viral constructs. E.G.W. and G.B generated schematics. S.A.V supervised all aspects of this project.

Abstract

Impairments in learning and memory that occur during aging are becoming an increasing concern, given that the aging population is expanding rapidly. The scientific community has recently demonstrated it is possible to slow, or even reverse certain aspects of brain aging – a phenomenon known as rejuvenation. There is a demand for mechanistic insights into processes that govern aging and rejuvenation, which hold significant translational potential for increasing quality of life in the elderly and aging populations. The dynamic post-translational modification O-GlcNAc is a regulator of learning and memory, and declines with age in brain regions associated with cognitive impairments like the hippocampus. In this study, O-GlcNAc levels are increased in the brains of adult and aging mice using viral and pharmacologically-mediated approaches, and the effects on learning and memory are assessed. The findings indicate increased O-GlcNAcylation is associated with enhanced hippocampal-dependent learning and memory in young mice, with a mild beneficial effect observed in aged mice. These results suggest O-GlcNAc is capable of promoting cognitive enhancements in the adult hippocampus, although more extensive investigation is required to determine whether O-GlcNAcylation can be employed to promote rejuvenation.

Introduction

Aging steadily drives cognitive impairments and remains the single most dominant risk factor for dementia-related neurodegenerative diseases, such as Alzheimer's disease (AD) [1-3]. When considering the rate at which the human population is aging, it becomes imperative to identify means by which to maintain cognitive integrity by counteracting or reversing the effects of aging, through a process known as rejuvenation.

Previous work using systemic interventions like exercise [4], caloric restriction [5, 6], and exposure to young blood by parabiosis and plasma treatments [7, 8], have demonstrated aspects of brain rejuvenation in rodents. Although these interventions demonstrate potential, such demanding alterations in lifestyle are not feasible on a global level in elderly humans. Therefore, elucidating the cellular mechanisms that can promote rejuvenation is vital for expanding the translational potential of the field of brain rejuvenation. Indeed, some mechanistic insight has been gained thus far, particularly in aging-sensitive brain regions like the hippocampus (See Chapter 1 for a summary of hippocampal aging). Upon exposure to young blood, aged mice experience a restoration of phosphorylation at Ser133 on the transcription factor Creb, which is known to promote neuronal synaptic plasticity, learning, and memory [9]. During caloric restriction, widespread alterations occur in many forms, including alterations in the insulin signaling pathway, and inhibition of mTOR signaling [5]. There is also a well characterized connection between exercise, cognitive enhancement, and BDNF expression in the adult and aging hippocampus [4].

As an additional approach for rejuvenation, factors that change with age in the

hippocampus have been characterized, and subsequently manipulated for more mechanistically targeted studies. Despite widespread changes occurring with age, only a handful of factors including Dnmt3a2, Rbap48, Creb, and NR2B have been able to rescue cognitive impairments when their expression is restored in aged mice [7, 10-13]. Despite these findings, the field of rejuvenation is still very much in its early pioneering phase. Significant mechanistic insight is still needed, highlighting the urgency for identifying novel factors that may serve as targets for future cognitive rejuvenation studies.

O-GlcNAcylation declines with age in the hippocampus, a brain region that displays numerous stereotypic impairments and cognitive deficits during aging (Chapter 3, Figure 1A,B; Chapter 1). Reduction of hippocampal neuronal O-GlcNAc recapitulates features of cellular and cognitive aging in young adult mice (Chapter 3), demonstrating that O-GlcNAc is necessary to maintain integrity in the young adult hippocampus, and proposing O-GlcNAc as a functional driver of age-related impairments. Furthermore, in the context of neurodegeneration, O-GlcNAc has been proposed as a neuroprotective molecule [14]. Protein O-GlcNAcylation is lower in the brains of AD patients [15], as well as in animal models of AD and related disorders. Furthermore, loss of neuronal O-GlcNAc elicits Tau hyperphosphorylation in adult mice [16, 17]. Pharmacologically-mediated inhibition of Oga, the enzyme that removes O-GlcNAc from proteins, increases brain O-GlcNAcylation and rescues cognitive and synaptic impairments in a mouse model of AD [18]. Given that aging is the number one risk factor for neurodegenerative diseases like AD, changes in O-GlcNAcylation could reside at the interface between aging and disease, representing a mechanism by which aging promotes impairments and susceptibility to the onset of neurodegeneration. Thus, the

question was raised as to whether increasing O-GlcNAcylation could have a beneficial impact on cognitive function not only in the context of disease, but in adult and aging wild type mice.

Results

Increased O-GlcNAcylation in the adult hippocampus enhances cognitive function

To test this possibility, an *in vivo* viral-mediated RNA interference approach was employed to knock down expression of the enzyme that removes O-GlcNAc from proteins, O-GlcNAcase (Oga). A lentivirus construct was generated encoding either an shRNA targeting Oga (sh-Oga), or a scrambled shRNA sequence as a control (Scramble), with GFP included as a reporter to mark transfected or infected cells (Figure 1A). The lentiviral constructs were initially tested by transfection of a mouse Neuro2A cell line (Figure 1B), which had been confirmed to express Oga and O-GlcNAcylated proteins. Western blot analysis of whole cell lysates taken 48 hours post-transfection revealed reduction of Oga protein as well as an increase in global protein O-GlcNAcylation in sh-Oga transfected cells when compared to Scramble controls (Figure 1C,D).

Infectious lentiviral particles were then generated, and titered to a concentration of 10^9 particles per ml. Using stereotactic (STX) surgery, infectious lentiviral particles were delivered directly into the hippocampi of young adult wild type mice (Figure 2A). Oga knockdown was confirmed by western blot analysis in lysates of GFP+ sub-dissected hippocampal tissue, 4 weeks post-injection (Figure 2B,C).

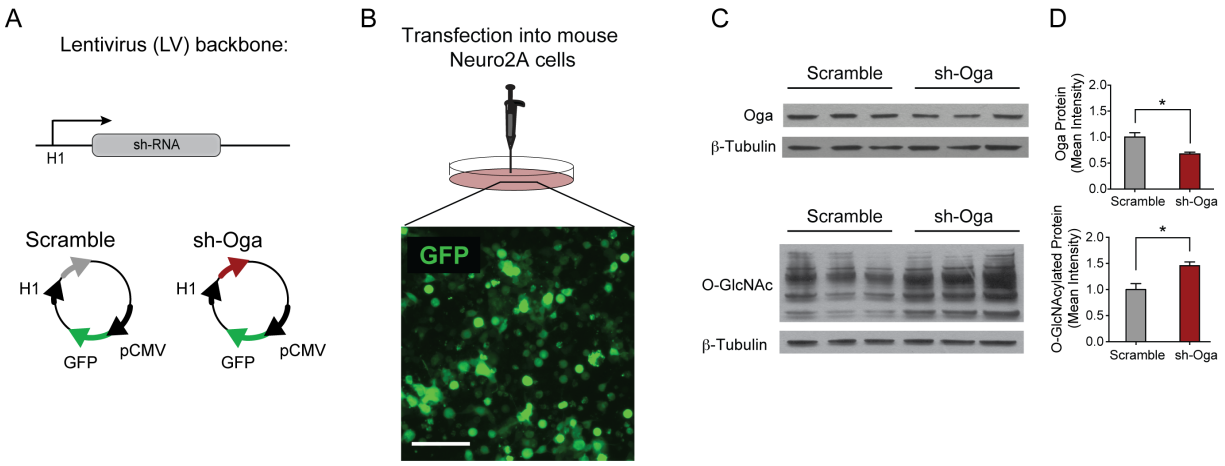

Figure 1. Generation of a lentiviral construct targeting Oga. (A) Schematic depiction of a lentiviral backbone encoding Scramble (control) or sh-Oga (shRNA targeting mouse Oga) sequences, driven by the H1 promoter. The construct also encodes GFP, driven by the CMV promoter. (B) Representative field of mouse Neuro2A cells transfected by the lentiviral construct. Scale bar = 25μm. (C) Western blot analysis of whole cell lysates from Neuro2A cells transfected with either Scramble or sh-Oga, harvested 48 hours post-transfection. (D) Quantification of (C) normalized to β-Tubulin and represented as fold change from Scramble. *n* = 3 transfected wells per group. Data represented as mean ± SEM *P<0.05; t-test.

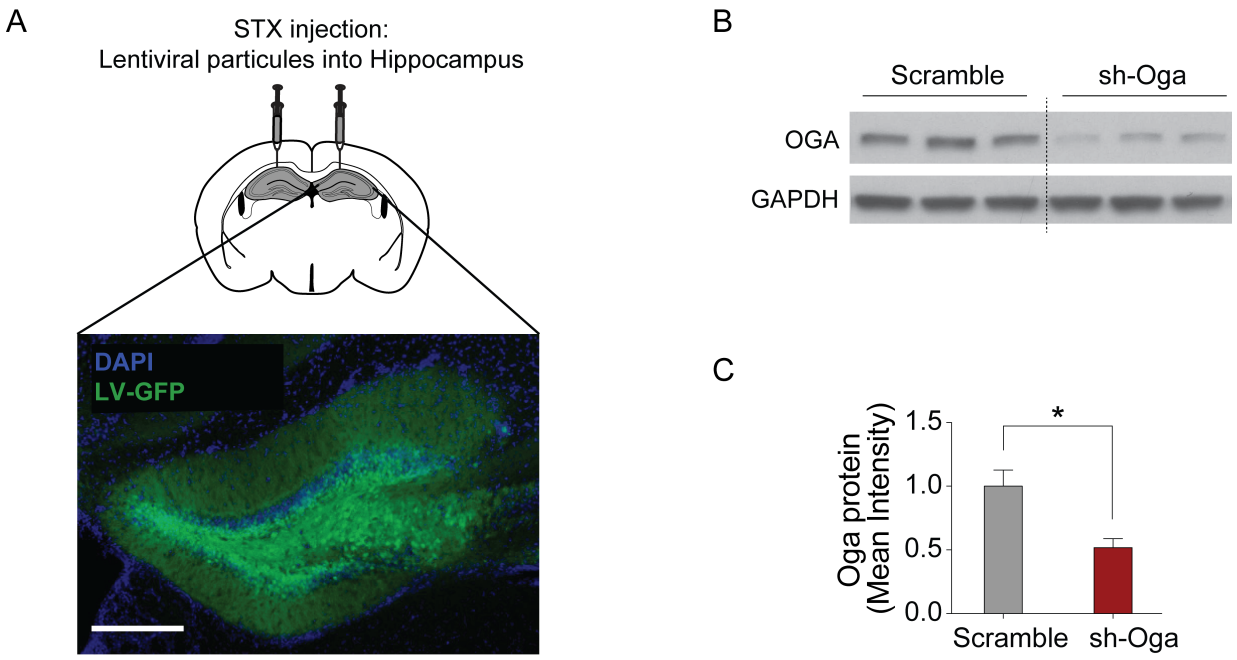

Figure 2. *In vivo* validation of lentiviral construct targeting mouse Oga. (A) Schematic depiction of a stereotactic (STX) injection of lentiviral particles into the hippocampi of an adult mouse brain. A representative image of a slice from a STX-injected hippocampus is shown, with GFP+ infected cells shown in green. (B) Representative bands from western blot analysis of whole tissue lysates from GFP+ hippocampi infected with either Scramble or sh-Oga lentivirus, harvested 4 weeks after injection. (C) Quantification of (B) normalized to GAPDH and represented as fold change from Scramble. *n* = 5 per group. Data represented as mean ± SEM *P<0.05; t-test.

A large cohort of adult wild type mice were then given STX injections into the hippocampi, of high-titer infectious lentivirus encoding either sh-Oga or Scramble sequences (Figure 3A). Following recovery, anxiety and general motor function was assessed using the open field behavioral paradigm, and two forms of hippocampal-dependent memory were tested using the radial arm water maze (RAWM) and fear conditioning paradigms (Figure 3A). As expected, no difference was observed between groups in time spent in the periphery or center, basic and fine movements, or rearing behavior in the open field task (Figure 3B). This result is indicative of no change in anxiety or motor function as a function of Oga knockdown in the hippocampus. All mice showed similar learning capacity during the training phase of the RAWM (Figure 3C), but Oga knockdown resulted in fewer errors in locating the target platform during short-term memory testing (Figure 3D). Additionally, long-term memory and overall learning were slightly enhanced in mice with knockdown of hippocampal Oga (Figure 3C,E). During fear conditioning training, as expected no differences in baseline freezing time were detected between groups (Figure 3F). However, mice injected with sh-Oga virus exhibited increased freezing time during contextual memory testing, indicative of enhanced hippocampal-dependent memory (Figure 3F). As expected, given the viral manipulation was specific to the hippocampus, no difference was observed between groups during cued memory testing- which is more dependent on the amygdala region of the brain (Figure 3F), Collectively, these behavioral data and findings that loss of O-GlcNAc elicits cognitive impairments (Chapter 3, Figure 7), indicate that modulation of O-GlcNAc can bi-directionally regulate hippocampal–dependent cognitive function. O-GlcNAcylation is therefore considered as molecular target for investigating the reversal

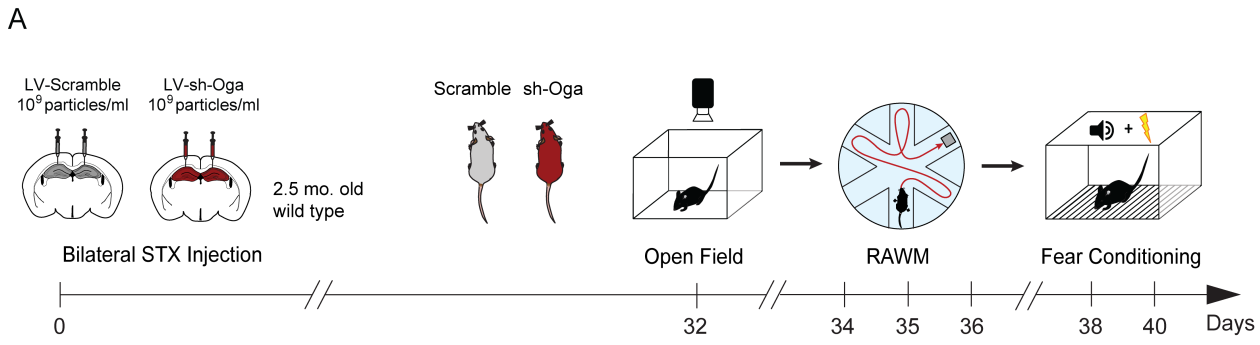
A
LV-Scramble
10^9 particles/ml
LV-sh-Oga
10^9 particles/ml
2.5 mo. old
wild type
Bilateral STX Injection
Scramble
sh-Oga
Open Field
RAWM
Fear Conditioning
0
32
34
35
36
38
40
Days

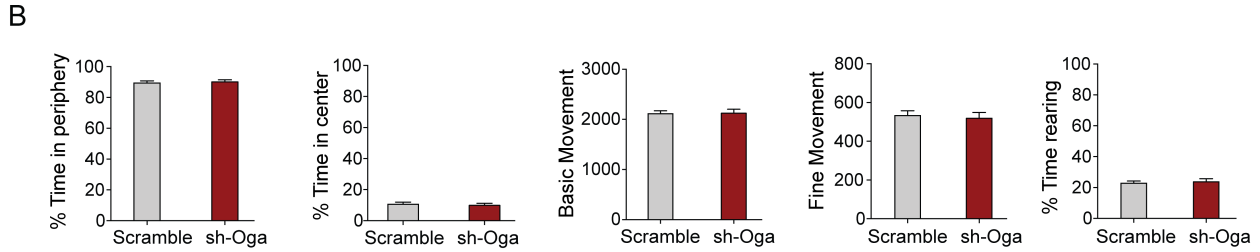
B
% Time in periphery
% Time in center
Basic Movement
Fine Movement
% Time rearing
Scramble
sh-Oga

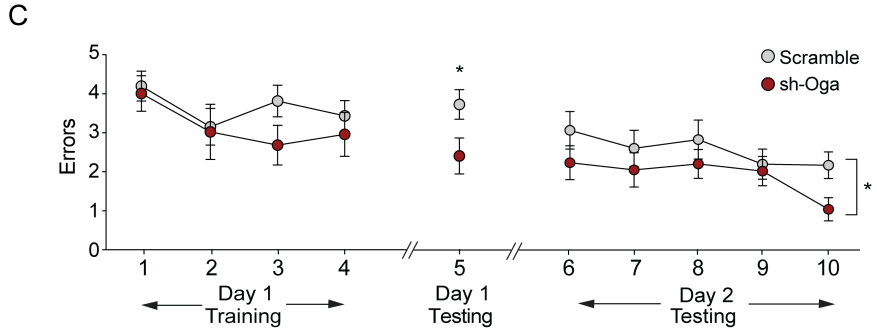
C
Errors
Scramble
sh-Oga
Day 1
Training
Day 1
Testing
Day 2
Testing

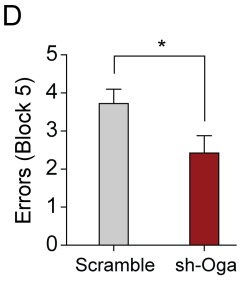
D
Errors (Block 5)
Scramble
sh-Oga

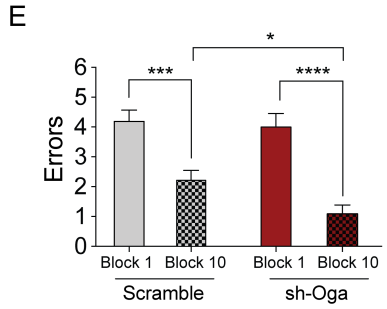
E
Errors
Block 1
Block 10
Scramble
sh-Oga

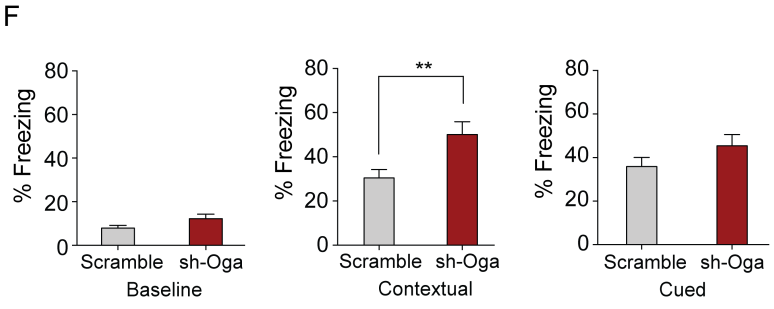
F
% Freezing
Baseline
Contextual
Cued

Figure 3. sh-Oga injected mice display enhanced spatial and contextual hippocampal memory.
(A) Learning and memory testing in adult mice with increased level of O-GlcNAcylation in the hippocampus. Schematic depicting the generation of Scramble and sh-Oga mice and subsequent cognitive testing using open field, radial arm water maze (RAWM), and fear conditioning behavioral paradigms. (B) Data from the open field paradigm depicting percent time spend in periphery and center of the field, as well as basic movements, fine movements, and time rearing of Scramble and sh-Oga injected mice. Data shown are cumulative from ten minutes of testing, measured using the MotorMonitor software. (C-E) Hippocampal-dependent spatial learning and memory was assessed using RAWM. Quantification of the number of entry errors during RAWM training and testing (C), short-term memory testing (D) and long-term learning and memory testing (E). (F) Baseline, contextual, and cued fear memory was assessed using fear conditioning. Baseline freezing was measured during the first two minutes of training. Freezing in contextual and cued conditions was measured 24 hours after training. *n* = 12-24 mice per group. Data represented as mean ± SEM; *P<0.05; **P<0.01; ***P<0.001; ****P<0.0001; repeated measures ANOVA, column factor (C); t-test (B-F).

of aging-associated cognitive impairments.

Investigating the potential for neuronal O-GlcNAc in restoring cognitive capacity in the aged brain

Given that increasing O-GlcNAcylation in the young hippocampus can improve cognitive function, the question was raised as to whether increasing O-GlcNAc in the aged brain could rescue cognitive deficits. As an initial approach, and to gain cell-type specificity for the role of O-GlcNAc in regulating neuronal aging, lentiviral constructs were generated encoding a Synapsin promoter to drive gene over expression (OE) specifically in neurons. A construct expressing the mouse Ogt gene was generated, as well as a construct expressing GFP alone (Figure 4A). Due to the size of the Ogt gene, a plasmid containing both Ogt and GFP yielded a poor lentiviral titer, so a construct without GFP was used. Primary neurons isolated from E16.5 embryos were grown and subsequently infected with lentiviral particles containing either Synapsin-GFP or Synapsin-Ogt-OE constructs (Figure 4B). Western blot of whole neuronal cell lysates confirmed overexpression of the Ogt protein *in vitro* (Figure 4C).

Aged wild type mice (17 months old) were then injected with high-titer lentiviral particles, directly into their hippocampi using STX surgery (Figure 5A). In order to label the injected regions of the hippocampus in Synapsin-Ogt-OE mice, infectious particles containing the Synapsin-Ogt-OE construct were mixed with a small aliquot containing control particles expressing GFP prior to injection. Mice were then bilaterally injected with either Synapsin-GFP (Control) or Synapsin-Ogt-OE + Synapsin-GFP (Ogt-OE), and were allowed to age and recover for a further 2 months post-surgery. Brains were sectioned to

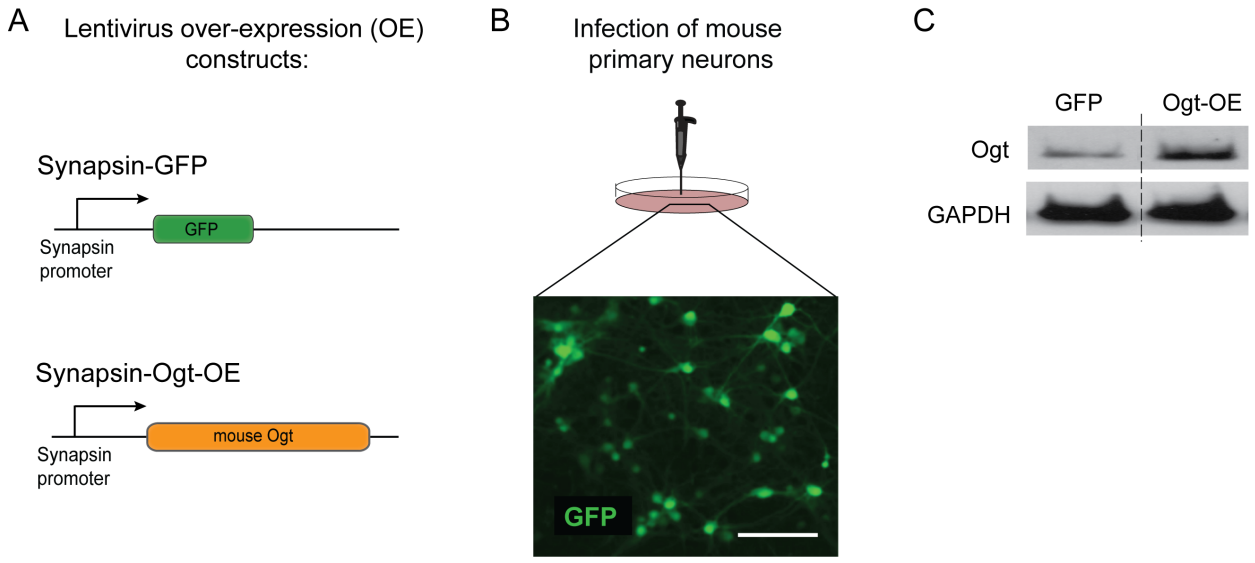

Figure 4. Generation of neuronal-specific lentiviral Ogt overexpression construct. (A) Schematic depiction of lentiviral constructs encoding GFP or Ogt for overexpression (OE) driven by the Synapsin promoter. (B) Representative field of primary mouse neurons infected by the Synapsin-GFP lentiviral construct. Scale bar = 25μm. (C) Representative bands from western blot analysis of whole cell lysates from infected neurons showing increased Ogt protein expression, with GAPDH as a loading control.

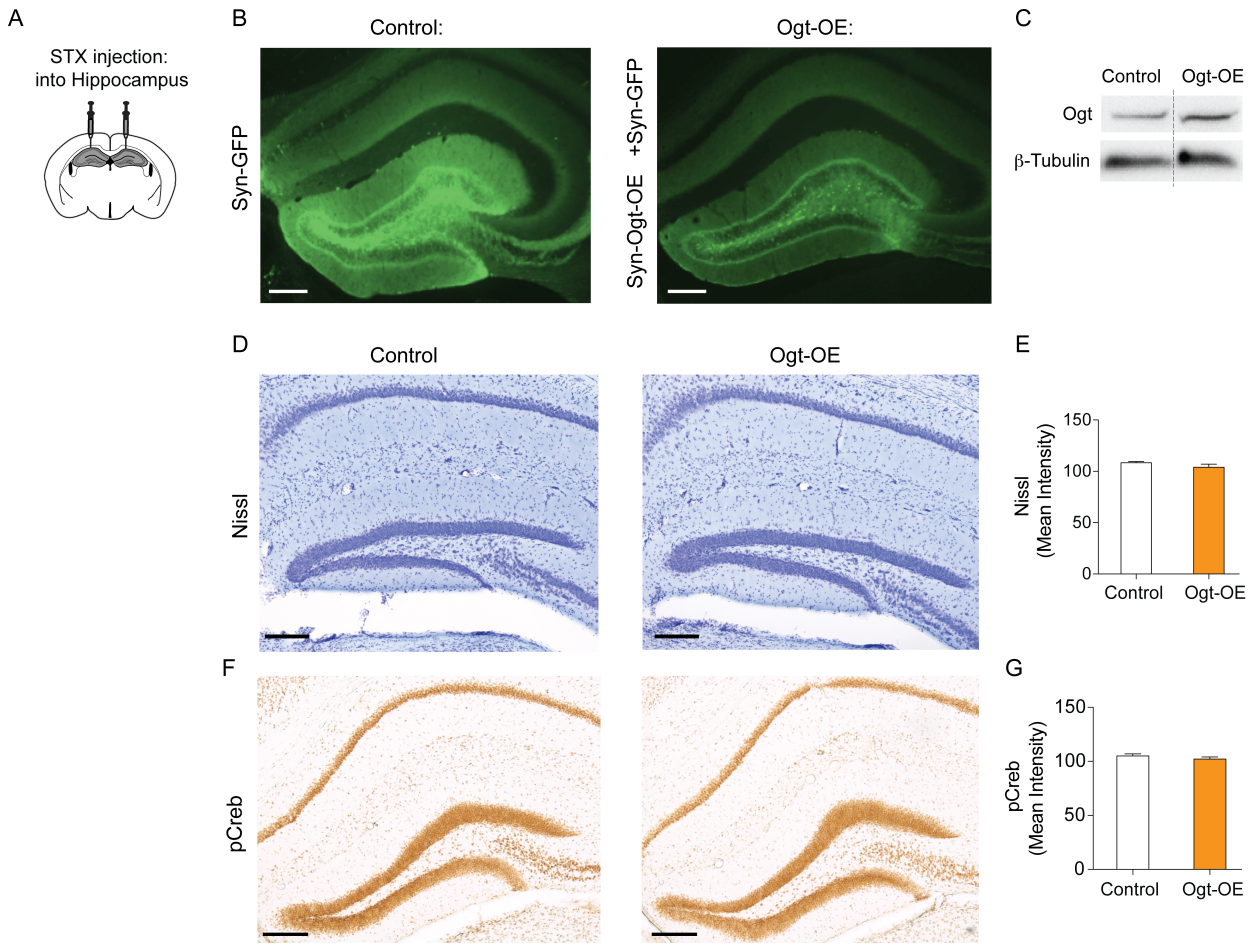

Figure 5. *In vivo* validation of stereotaxic injection of the Ogt-OE construct into the aged hippocampus. (A) Schematic depiction of stereotaxic (STX) injections into the mouse hippocampus. (B) Aged mice (17 months old) were injected with either control (Syn-GFP) or Ogt-OE (Syn-Ogt-OE + Syn-GFP) lentiviral constructs. Representative fluorescent images of GFP+ hippocampi taken following STX surgery confirm the injection site is accurate. Scale bar = 200μm (C) Representative bands from western blot analysis of lysates from GFP+ infected hippocampal tissue. (D) Representative field of Cresyl violet staining for Nissl bodies in control and Ogt-OE mice. Scale bar = 200μm. (E) Quantification of Nissl mean intensity in neuronal sub-regions. (F) Representative field of immunohistological staining for pCreb in control and Ogt-OE mice. Scale bar = 200μm. (G) Quantification of pCreb mean intensity in neuronal sub-regions. *n* = 7 per group; t-test.

confirm GFP+ tissue was found in the hippocampal region (Figure 5B) and GFP+ tissue lysate was profiled by western blot to confirm Ogt overexpression (Figure 5C). A cresyl violet stain for Nissl bodies confirmed there were no gross changes in hippocampal architecture or neuronal cell loss in Control versus Ogt-OE mice (Figure 5D,E). To investigate whether overexpression of Ogt may have restored molecular hallmarks of aging, hippocampal tissue from Control and Ogt-OE mice was profiled for pCreb expression, which declines with age in hippocampal neurons (Chapter 1, Figure 2C,D). Ogt-OE mice did not display increased pCreb in the hippocampus when compared to Control mice (Figure 5F,G).

Cognitive function of control and Ogt-OE mice was also assessed, using the open field paradigm to measure anxiety and motor function, and the RAWM to measure hippocampal-dependent learning and memory (Figure 6A). No difference was observed in time spent in the periphery versus center, or in basic and fine movements was between groups, indicative of no increased anxiety or impairments in motor function (Figure 6B). In RAWM testing, aside from one point of separation during the learning phase, there were no significant enhancements in short or long-term spatial memory, or overall learning ability in Ogt-OE versus Control mice (Figure 6C,D). Collectively, these data indicate that overexpression of Ogt in 17 month old mouse hippocampal neurons is not sufficient to enhance spatial memory in an aged brain.

Investigating the potential for Oga inhibitors to rescue cognitive decline under normal aging conditions.

An additional approach was employed to increase brain O-GlcNAcylation, by using a

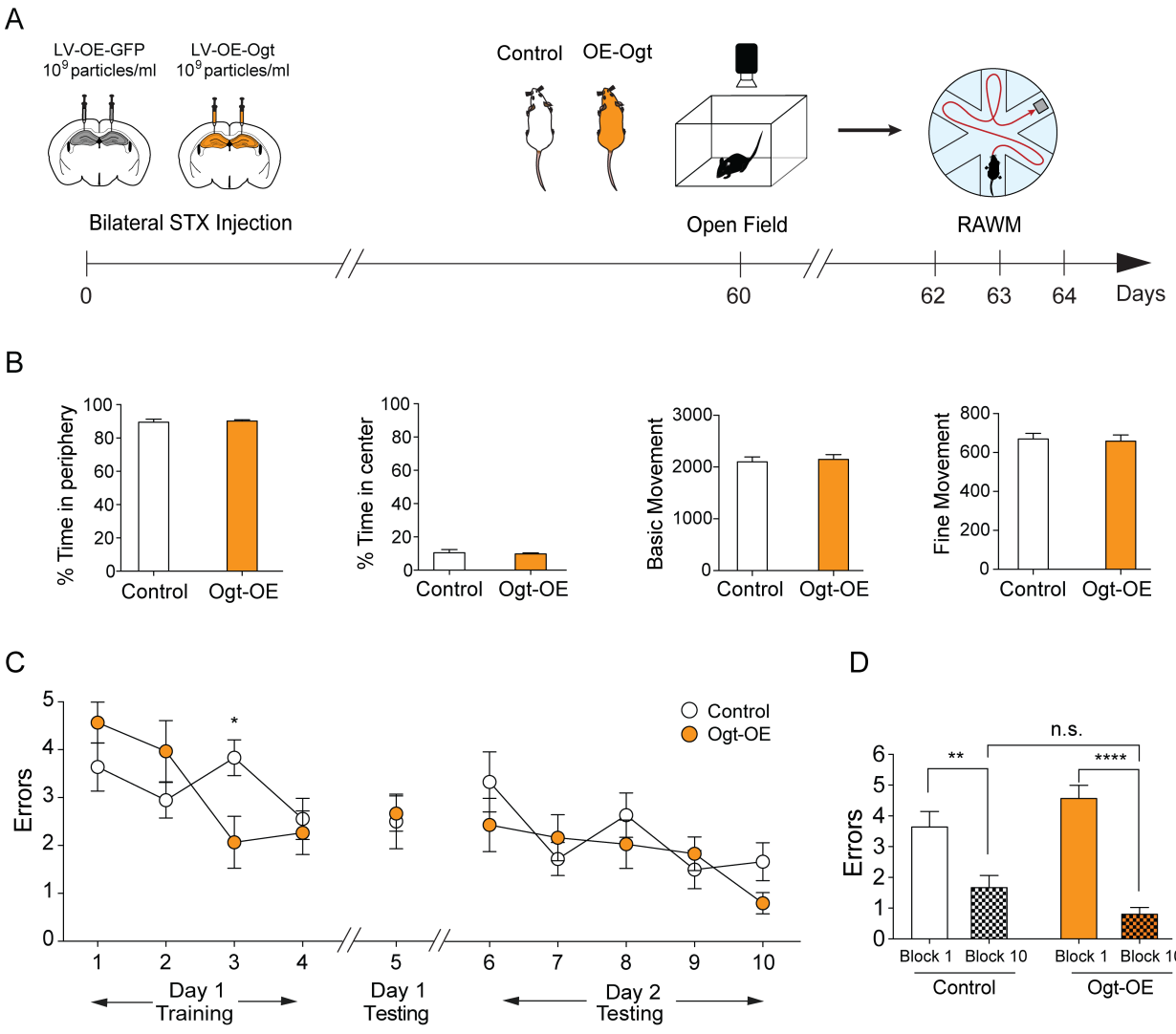

Figure 6. Ogt-OE does not sufficiently enhance cognitive function in aged mice. (A) Learning and memory testing in aged mice with increased level of O-GlcNAcylation in the hippocampus. Schematic depicting generation of Control and Ogt-OE mice and subsequent cognitive testing using open field and radial arm water maze (RAWM). (B) Data from the open field paradigm depicting percent time spend in periphery and center of the field, as well as basic and fine movements. Data shown are cumulative from ten minutes of testing, measured using the MotorMonitor software. (C,D) Hippocampal-dependent spatial learning and memory was assessed using RAWM. Quantification of the number of entry errors during RAWM training and testing were assessed in (C), and overall memory assessed in (D). *n* = 10-12 mice per group. Data represented as mean ± SEM; *P<0.05; **P<0.01; ****P<0.0001; repeated measures ANOVA (C); t-test (B,D).

selective Oga inhibitor called Thiamet G (THG). THG has previously been shown to robustly increase brain O-GlcNAcylation in mice, and rescue cognitive deficits in neurodegenerative mouse models of disease [18]. Aged mice (18 month old) were injected with either vehicle (Saline) or THG (500mg/kg) every other day for one month, followed by RAWM testing to assess spatial learning and memory (Figure 7A). THG treatment did not elicit differences in learning or short term memory, but during the long-term testing phase there was a separation between the two treatment groups as a whole (Figure 7B). Additionally, there was a slight advantage in overall learning observed in THG-injected mice (Figure 7C). Overall, THG treatment had a very mild but beneficial effect on spatial memory in aged mice.

Discussion

In this study, the role of O-GlcNAcylation was investigated as a regulator of cognitive enhancements, in both the adult and aging brain. An *in vivo* viral-mediated RNAi approach was employed to inhibit Oga expression in the adult mouse hippocampus, demonstrating that increased O-GlcNAcylation is sufficient to enhance cognitive function, even in the young adult hippocampus. This result is exciting, given it demonstrates O-GlcNAc is capable of eliciting enhancements even in the absence of impairments or disease.

As an extension of this experiment, O-GlcNAcylation was enhanced in the brains of aged mice, both on a cell-type and region-specific level, as well as globally. Overexpression of Ogt in aged hippocampal neurons did not elicit any notable changes, either at the molecular level by Creb phosphorylation, or at the cognitive level using

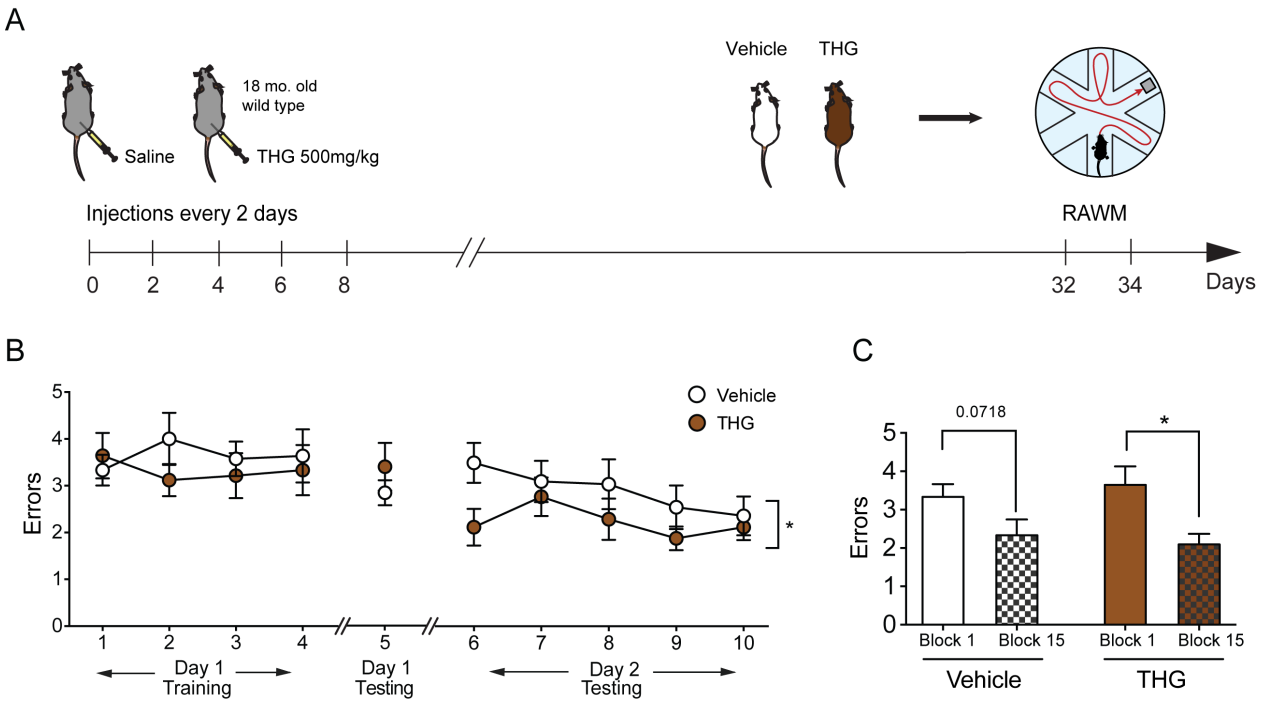

Figure 7. THG treatment produces a mild beneficial effect on spatial memory in aged mice.
(A) Learning and memory testing in aged mice treated with vehicle or Thiamet-G (THG). Schematic depicting intraperitoneal injections in aged mice and subsequent cognitive testing using radial arm water maze (RAWM). (B,C) Hippocampal-dependent spatial learning and memory was assessed using RAWM. Quantification of the number of entry errors during RAWM training and testing were assessed in (B), and overall memory assessed in (C). *n* = 11-14 mice per group. Data represented as mean ± SEM; *P<0.05; repeated measures ANOVA column factor (B); t-test (C).

RAWM testing. In a secondary approach, systemic treatment with a selective Oga inhibitor, THG, produced a mild cognitive improvement in aged mice. In summary, loss of O-GlcNAcylation drives aging-related cognitive phenotypes in the brain, and increased O-GlcNAcylation is beneficial for cognitive function- however it still remains to be determined whether restoring O-GlcNAc can rejuvenate the aged brain and ameliorate cognitive impairments (Figure 8).

In order to further investigate a role for O-GlcNAc in cognitive rejuvenation during aging, these experiments should be repeated with some notable alterations. The viral-mediated approach of Ogt overexpression should likely be initiated closer to the equivalent of middle age (12 months old) and the mice left until 18-20 months before cognitive testing. An additional approach could be to employ injections of sh-Oga in middle aged or aged mice as well. Regarding pharmacological manipulations, the duration and route of administration could be altered in order to investigate more brain-specific effects. Osmotic mini-pumps for delivery of THG directly in to the brain have been piloted in-house with success, and could provide proof-of-principle that increasing O-GlcNAcylation is sufficient to restore cognitive decline in the aged brain. Collectively, these *in vivo* data do raise significant translational potential, highlighting O-GlcNAcylation as a molecular target for eliciting cognitive enhancements, which warrants further pursuit in the context of aging.

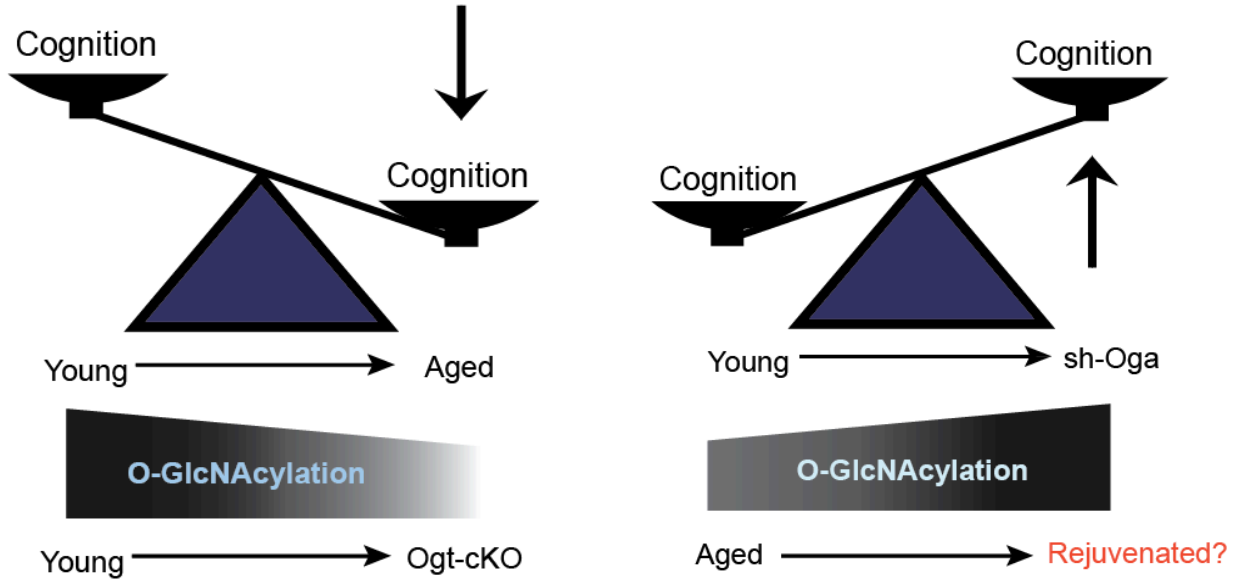

Figure 8. Working model for the role of O-GlcNAcylation in regulating age-related cognitive function.
Model depicting that loss of O-GlcNAc drives impairments in young Ogt-cKO mice and aged mice, and increased O-GlcNAc drives enhancements in sh-Oga injected young mice. The question still remains as to how O-GlcNAc may be employed to promote brain rejuvenation in aged mice.

Materials and methods

Animal Models. All mouse handling and use was in accordance with institutional and ethical guidelines approved by the University of California San Francisco IACUC. The following mouse lines were used: C57BL/6 young mice (The Jackson Laboratory), C57BL/6 young and aged mice (National Institutes of Aging; Taconic Biosciences). All studies were done in male mice. The numbers of mice used to result in statistically significant differences were calculated using standard power calculations with $\alpha = 0.05$ and a power of 0.8. We used an online tool (http://www.stat.uiowa.edu/~rlenth/Power/index.html) to calculate power and samples size based on experience with the respective tests, variability of the assays and inter-individual differences within groups. Mice were housed under specific pathogen-free conditions under a 12 h light-dark cycle. All experiments were randomized and blinded by an independent researcher. Researchers remained blinded throughout histological, molecular, and behavioral assessments. Groups were un-blinded at the end of each experiment upon statistical analysis.

Radial Arm Water Maze. Paradigm followed previously described protocol [19]. The goal arm location containing a platform remains constant throughout the training and testing phase, while the start arm is changed during each trial. Entry into an incorrect arm is scored as an error, and errors are averaged over training blocks (three consecutive trials). On day one during the training phase, mice are trained for 15 trials, with trials alternating between a visible and hidden platform. Every 3 trials are counted

as one block of training. Prior to the final 3 trials of day 1 (block 5), the mice are given an extended break, and short-term memory is then tested using three consecutive hidden platform trials. On subsequent days during the testing phase, mice are tested for 15 trials per day with a hidden platform. All behavior is performed double blinded.

Contextual Fear Conditioning. Paradigm follows previously published techniques [20]. Mice learned to associate the environmental context (fear conditioning chamber) with an aversive stimulus (mild foot shock; unconditioned stimulus, US) enabling testing for hippocampal-dependent contextual fear conditioning. The mild foot shock was paired with a light and tone cue (conditioned stimulus, CS) in order to also assess amygdala-dependent cued fear conditioning. Conditioned fear was displayed as freezing behavior. Specific training parameters are as follows: tone duration is 30 seconds; level is 70 dB, 2 kHz; shock duration is 2 seconds; intensity is 0.6 mA. On day 1 each mouse was placed in a fear-conditioning chamber and allowed to explore for 2 minutes before delivery of a 30-second tone (70 dB) ending with a 2-second foot shock (0.6mA). Two minutes later, a second CS-US pair was delivered. On day 2 each mouse was first place in the fear- conditioning chamber containing the same exact context, but with no administration of a CS or foot shock. Freezing was analyzed for 1-3 minutes. One hour later, the mice were placed in a new context containing a different odor, cleaning solution, floor texture, chamber walls and shape. Animals were allowed to explore for 2 minutes before being re-exposed to the CS. Freezing was analyzed for 1-3 minutes. Freezing was measured using a FreezeScan video tracking system and software (Cleversys, Inc). All behavior is performed double blinded.

Stereotaxic injections. Animals were placed in a stereotaxic frame and anesthetized with 2% isoflurane (2L/min oxygen flow rate) delivered through an anesthesia nose cone. Ophthalmic eye ointment was applied to the cornea to prevent desiccation during surgery. The area around the incision was trimmed. Viral solutions were injected bilaterally into the dorsal hippocampi using the following coordinates: (from bregma) anterior = -2mm, lateral = 1.5mm, (from skull surface) height = -2.1mm. 2µl volume was injected stereotaxically over 10 minutes (injection speed: 0.20µl/min) using a 10µl 26s gauge Hamilton syringe. To limit reflux along the injection track, the needle was maintained in situ for three minutes, slowly pulled out half way and kept in position for an additional two minutes. The skin was closed using silk suture. Each mouse was injected subcutaneously with the analgesic Bupranex. Mice were single-housed and monitored during recovery.

Western Blot Analysis. Mouse brain tissues were dissected after perfusion of animal and further sub-dissected for GFP+ tissue on a fluorescent dissection microscope. Tissue was then snap frozen and lysed in RIPA lysis buffer (500 mM Tris, pH 7.4, 150 mM NaCl, 0.5% Na deoxycholate, 1% NP40, 0.1% SDS, complete protease inhibitors 2X; Roche, and PUGNAc 100uM; Sigma). Tissue lysates were mixed with 4x NuPage LDS loading buffer (Invitrogen), loaded on a 4-12% SDS polyacrylamide gradient gel (Invitrogen), and subsequently transferred onto a nitrocellulose membrane. The blots were blocked in 5% milk in Tris-Buffered Saline with Tween (TBST) and incubated with mouse anti-O-GlcNAc antibody (CTD110.6) sc-59623 (1:500, SC Biotech), rabbit anti-OGT antibody (H-300) sc-32921 (1:1000, SC Biotech), rabbit anti-OGA ab124807

(1:600, Abcam), mouse anti-GAPDH (6C5) ab8245 (1:10,000, Abcam), and mouse anti-β-tubulin (TUJ1) 801201 (1:1000, BioLegend). For cell culture experiments, cells were gently washed 2x with cold PBS and then lysed directly in RIPA lysis buffer. Horseradish peroxidase-conjugated secondary antibodies and an ECL kit (GE Healthcare/Amersham Pharmacia Biotech) were used to detect protein signals. Multiple exposures were taken to select images within the dynamic range of the film (GE Healthcare Amersham HyperfilmTM ECL). Selected films were scanned (300 dpi) and quantified using FIJI software (Version 1.0). GAPDH or β-tubulin bands were used for normalization.

Thiamet-G injections. Animals were treated via intraperitoneal injection with 500mg/kg of Thiamet G (THG) or vehicle (Saline) once every 48 hours for a total of 4 weeks. Animals were monitored continuously throughout and were allowed to recover for 3 days after their last injection before cognitive testing began.

Nissl Staining. Sections were cut to 40μm and mounted on superfrost plus microscope slides (ThermoFisher) and allowed to dry overnight. Slides were then soaked in 100% ethanol 3x2min each, and then immersed in cresyl violet working solution for 10 min. Slides were then dipped in 95% ethanol, soaked in 100% ethanol 2x2min, then in Citrasolv 2x2min before being cover slipped with Entellan. Mean intensity was quantified using FIJI software (Version 1.0).

Immunohistochemistry. Tissue processing and immunohistochemistry was performed

on free-floating sections following standard published techniques [21]. Mice were anesthetized with ketamine, transcardially perfused with 0.9% saline, and brains removed and fixed in phosphate-buffered 4% paraformaldehyde for 48h before cryoprotection with 30% sucrose. Free floating coronal sections (40 µm) were incubated overnight with rabbit anti-phospho-Creb (Ser133) (1:2,500; CST) and staining was revealed using biotinylated secondary antibodies and the ABC kit (Vector) with Diaminobenzidine (DAB, Sigma-Aldrich). Sections were mounted in phosphate buffer on superfrost plus microscope slides (ThermoFisher), allowed to dry overnight, briefly soaked in Citrasolv and cover slipped with Entellan. Mean intensity was quantified using FIJI software (Version 1.0).

Viral plasmids and generation of lentiviral particles. A lentivirus encoding small hairpin RNAs (shRNA) targeting endogenous OGA were generated using a lentiviral shRNA expression system (pGreenPuro shRNA, System Biosciences) according to the manufacturer's instructions. The OGA-targeted [22] and luciferase targeted [23] scramble sequences (OGA, 5′-AAGTATACCAAGCCAAATGGT-3′; Scramble, 5′-GCCATTCTATCCTCTAGAGGA-3′) were cloned into the pGreenPuro vector. In addition, overexpression lentivirus encoding a Synapsin promoter to drive expression of Ogt (CloneId: 6830845, Thermofisher) or GFP alone (hrGFP) was generated as well. Construct quality was tested with Western blot analysis and sequencing. Preparation of non-replicative lentiviral particles was performed using the UCSF Viracore, and titered to $1.0x10^9$ viral particles/ml.

Cell culture experiments. An N2A neuronal cell line was used for confirming the

effectiveness of the shRNA in vitro. Cells were plated at a confluency of 85-90 percent for transfection experiments. Lipofectamine 3000 (Invitrogen) was used as transfection reagent. Culture media (DMEM + 10% FBS) was exchanged after 6h to reduce toxicity caused by the transfection reagent. Transfection was assessed with the help of GFP reporters and fluorescence microscopy. Cells were lysed 48 hours following transfection in the same RIPA buffer used for tissue lysis. Experiments were performed in triplicates. For validation of infectious lentiviral particles, primary neurons were harvested from the brains of E16.5 embryos following the protocol outlined in the Worthington papain dissociation system kit (Cat no. LK0003150). Neurons were infected for 48 hours and harvested in the same RIPA buffer used for tissue lysis.

Data and statistical analysis. Graphed data are expressed as mean ± SEM. Statistical analysis was performed with Prism 5.0 software (GraphPad Software). Means between two groups were compared with two-tailed, unpaired Student's t-test. Comparisons of means from multiple groups with each other or against one control group were analyzed with 2-way ANOVA and Bonferroni post hoc tests. All histology and behavior experiments conducted were done in a randomized and blinded fashion. For each experiment, the overall size of the experimental groups corresponded to distinct animals. Unique samples were not measured repeatedly within the same characterization of a given cohort.

References

1. Bishop, N.A., T. Lu, and B.A. Yankner, *Neural mechanisms of ageing and cognitive decline.* Nature, 2010. **464**(7288): p. 529-35.
2. Hedden, T. and J.D. Gabrieli, *Insights into the ageing mind: a view from cognitive neuroscience.* Nat Rev Neurosci, 2004. **5**(2): p. 87-96.
3. Mattson, M.P. and T. Magnus, *Ageing and neuronal vulnerability.* Nat Rev Neurosci, 2006. **7**(4): p. 278-94.
4. Intlekofer, K.A. and C.W. Cotman, *Exercise counteracts declining hippocampal function in aging and Alzheimer's disease.* Neurobiol Dis, 2013. **57**: p. 47-55.
5. Van Cauwenberghe, C., et al., *Caloric restriction: beneficial effects on brain aging and Alzheimer's disease.* Mamm Genome, 2016. **27**(7-8): p. 300-19.
6. Kuhla, A., et al., *Lifelong caloric restriction increases working memory in mice.* PLoS One, 2013. **8**(7): p. e68778.
7. Villeda, S.A., et al., *Young blood reverses age-related impairments in cognitive function and synaptic plasticity in mice.* Nat Med, 2014.
8. Castellano, J.M., et al., *Human umbilical cord plasma proteins revitalize hippocampal function in aged mice.* Nature, 2017. **544**(7651): p. 488-492.
9. Sakamoto, K., K. Karelina, and K. Obrietan, *CREB: a multifaceted regulator of neuronal plasticity and protection.* J Neurochem, 2011. **116**(1): p. 1-9.
10. Oliveira, A.M., T.J. Hemstedt, and H. Bading, *Rescue of aging-associated decline in Dnmt3a2 expression restores cognitive abilities.* Nat Neurosci, 2012. **15**(8): p. 1111-3.

11. Pavlopoulos, E., et al., *Molecular mechanism for age-related memory loss: the histone-binding protein RbAp48.* Sci Transl Med, 2013. **5**(200): p. 200ra115.

12. Yu, X.W., et al., *CREB overexpression in dorsal CA1 ameliorates long-term memory deficits in aged rats.* Elife, 2017. **6**.

13. Cao, X., et al., *Maintenance of superior learning and memory function in NR2B transgenic mice during ageing.* Eur J Neurosci, 2007. **25**(6): p. 1815-22.

14. Hanover, J.A. and P. Wang, *O-GlcNAc cycling shows neuroprotective potential in C. elegans models of neurodegenerative disease.* Worm, 2013. **2**(4): p. e27043.

15. Liu, F., et al., *O-GlcNAcylation regulates phosphorylation of tau: a mechanism involved in Alzheimer's disease.* Proc Natl Acad Sci U S A, 2004. **101**(29): p. 10804-9.

16. Wang, A.C., et al., *Loss of O-GlcNAc glycosylation in forebrain excitatory neurons induces neurodegeneration.* Proc Natl Acad Sci U S A, 2016. **113**(52): p. 15120-15125.

17. O'Donnell, N., et al., *Ogt-dependent X-chromosome-linked protein glycosylation is a requisite modification in somatic cell function and embryo viability.* Mol Cell Biol, 2004. **24**(4): p. 1680-90.

18. Yuzwa, S.A., et al., *Pharmacological inhibition of O-GlcNAcase (OGA) prevents cognitive decline and amyloid plaque formation in bigenic tau/APP mutant mice.* Mol Neurodegener, 2014. **9**: p. 42.

19. Alamed, J., et al., *Two-day radial-arm water maze learning and memory task; robust resolution of amyloid-related memory deficits in transgenic mice.* Nat Protoc, 2006. **1**(4): p. 1671-9.

20. Raber, J., et al., *Irradiation enhances hippocampus-dependent cognition in mice deficient in extracellular superoxide dismutase.* Hippocampus, 2011. **21**(1): p. 72-80.

21. Luo, J., et al., *Glia-dependent TGF-beta signaling, acting independently of the TH17 pathway, is critical for initiation of murine autoimmune encephalomyelitis.* J Clin Invest, 2007. **117**(11): p. 3306-15.

22. Keembiyehetty, C.N., et al., *A lipid-droplet-targeted O-GlcNAcase isoform is a key regulator of the proteasome.* J Cell Sci, 2011. **124**(Pt 16): p. 2851-60.

23. Cheng, J.C., et al., *CREB is a critical regulator of normal hematopoiesis and leukemogenesis.* Blood, 2008. **111**(3): p. 1182-92.

Publishing Agreement

It is the policy of the University to encourage the distribution of all theses, dissertations, and manuscripts. Copies of all UCSF theses, dissertations, and manuscripts will be routed to the library via the Graduate Division. The library will make all theses, dissertations, and manuscripts accessible to the public and will preserve these to the best of their abilities, in perpetuity.

Please sign the following statement:

I hereby grant permission to the Graduate Division of the University of California, San Francisco to release copies of my thesis, dissertation, or manuscript to the Campus Library to provide access and preservation, in whole or in part, in perpetuity.

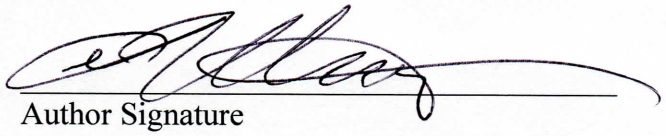

Author Signature

4/27/18

Date